Solid State Photochemistry of Uranyl Carboxylate and 1,3-Diketonate Complexes: Photochemical Patterning of Uranium Oxide Lines via Uranyl Complex Thin Film Precursors

by

Meihua Gao

B.Sc., Xiamen University, 1982

THESIS SUBMITTED IN PARTIAL FULFILLMENT OF

THE REQUIREMENTS FOR THE DEGREE OF

MASTER OF SCIENCE

in the Department

of

Chemistry

© MEIHUA GAO 1995

SIMON FRASER UNIVERSITY

May 1995

All rights reserved. This work may not be
reproduced in whole or in part, by photocopy
or other means, without permission of the author.

Approval

Name: Meihua Gao

Degree: Master of Science

Title of thesis: Solid State Photochemistry of Uranyl Carboxylate and 1,3-Diketonate Complexes: Photochemical Patterning of Uranium Oxide Lines via Uranyl Complex Thin Film Precursors

Examining Committee:

Chair: Dr. Steven Holdcroft, Associate Professor

Dr. Ross H. Hill
Associate Professor
Senior Supervisor

Dr. Ian D. Gay
Professor
Supervisory Committee

Dr. F. W. B. Einstein
Professor
Supervisory Committee

Dr. Gary W. Leach
Assistant Professor, Internal Examiner
Department of Chemistry, Simon Fraser University

Date Approved: May 23, 1995

PARTIAL COPYRIGHT LICENSE

I hereby grant to Simon Fraser University the right to lend my thesis, project or extended essay (the title of which is shown below) to users of the Simon Fraser University Library, and to make partial or single copies only for such users or in response to a request from the library of any other university, or other educational institution, on its own behalf or for one of its users. I further agree that permission for multiple copying of this work for scholarly purposes may be granted by me or the Dean of Graduate Studies. It is understood that copying or publication of this work for financial gain shall not be allowed without my written permission.

Title of Thesis/Project/Extended Essay:

Solid State Photochemistry of Uranyl Carboxylate and 1,3- Diketonate Complexes: Photochemical Patterning of Uranium Oxide Lines via Uranyl Complex Thin Film Precursors.

Author: ______________________
(signature)

____
(name)

May 29, 1995
(date)

MSFOHWSPARTIAL_CPY

Abstract

Uranium oxide is a potential X-ray lithography mask material due to its high X-ray absorption cross-section. An investigation into the solid state photochemistry of uranyl carboxylate and 1,3-diketonate complexes has been carried out to develop methods for the deposition of uranium oxide films.

A series of uranyl carboxylate complexes, $UO_2(OOCR)_2$, (R = i-C_3H_7, C_5H_{11}, $CH_2C_6H_5$, $C_2H_5OCH_2$, $C_2H_5OC_2H_4$, $C_2H_5OC_6H_4$) and 1,3-diketonate complexes, $UO_2(RCOCHCOR)_2$ (R = CH_3 and t-C_4H_9), have been synthesized and characterized. The thin films of these precursors were prepared by a spin-coating technique and the quality of these precursor films was examined. The photoproducts of these complexes were different depending on the R group, but a common product, UO_3, was obtained in each case.

The mechanism of photochemically activated reactions of $UO_2(OOCR)_2$ has been investigated. It has been found that the energy resulting from absorption of a photon leads to a decarboxylation via a ligand to metal charge transfer excitation. The resultant CO_2 is ejected from the film. The other resultant species, alkyl radical, not only underwent radical coupling and disproportionation to generate organic products, but also reacted with the starting material $UO_2(OOCR)_2$ in a radical chain reaction in some of the cases. This was demonstrated by the quantum yield measurements in which some of the quantum yields exceeded one. The initiation of the decomposition of $UO_2(OOCR)_2$ by a radical initiator, azo-isobutyro nitrile, is also indicative of a radical chain process.

The photochemistry of $UO_2(RCOCHCOR)_2$ as thin films on Si surfaces was also studied. The photoextrusion of all the ligands was indicated in both complexes (R = CH_3 and t-C_4H_9) due to the disappearance of all of the IR absorption bands associated with diketonate ligands. A single photon process was indicated by linear plots of ln[Ao/At]

versus photolysis time. The quantum yields, less than 1, were consistent with a non-chain process.

Irradiation of thin films of uranyl complexes through a photolithographic mask produced resolvable uranium oxide patterns with sub-micron resolution. Electron-beams were used to expose uranyl complex thin films for the generation of uranium oxide lines. The investigation has shown that electron-beam lithography easily produces 0.2 μm resolution depositions. These results indicate the feasibility of using uranyl complexes for the production of X-ray lithography mask materials.

Dedication

To my parents

Acknowledgments

I wish to express my sincere appreciation and gratitude to Dr. Ross H. Hill. He, being a busy boss, always found time to guide and encourage me with his characteristic patience during the whole course.

I would like to thank my groupmates for their valuable help and friendship. Special thanks are given to Ms. Sharon L. Blair for running Auger samples.

I would also like to thank Dr. Vic Brett, of the Department of Biological Science, for teaching me and allowing me to play with the SEM. Mr. Greg L. Owen, for running MS samples, and Mr. M. K. Yang, for C, H analysis, are also gratefully acknowledged. The Surface Physics Laboratory at SFU is also acknowledged.

I sincerely thank my husband, Dr. Weibin Wang, for his understanding, encouragement and patience.

My special appreciation goes to my son, Rui Wang, who had to understand and support a busy Mom by making less trouble when he was six-years old.

The generous financial support from Dr. Ross H. Hill, NSERC, the Chemistry Department and Simon Fraser University is greatly acknowledged.

Table of Contents

Approval ii

Abstract iii

Dedication v

Acknowledgments vi

Table of Contents vii

List of Tables xi

List of Figures xii

List of abbreviations xiv

Chapter 1. Introduction

1.1 Techniques of Thin Film deposition 1

1.2 The Film Deposition Technique Developed in Our Laboratory: Photochemical Deposition From Surface Films (PDSF) 7

1.3 A Comparison of CVD with PDSF 7

1.4 The Laws of Photochemistry and Quantum Yields 9

1.4.1 First law of photochemistry 9

1.4.2 Quantum yields 9

1.4.3 Second law of photochemistry 11

1.5 Auger Electron Spectroscopy—An Sensitive Surface Analysis Technique 11

1.6 Reasons of Studying Uranium 13

1.7 Research Objectives 14

Chapter 2. Synthesis of Uranium Oxide Film

2.1 Introduction 15

2.2 Results and Discussion 16
2.2.1 The choice of precursor molecules 16
2.2.2 Synthesis of uranyl 1,3-diketonate complexes and uranyl carboxylate complexes 19
2.2.3 Characterization of uranyl 1,3- diketonate complexes 20
2.2.4 Characterization of uranyl carboxylate complexes 24
2.2.5 The quality of thin precursor films 30
2.2.6 Photochemical deposition and characterization of uranium oxide films 32
2.3 Conclusion 37
2.4 Experimental section 38
2.4.1 Synthesis of uranyl complexes 38
2.4.2 Calibration of IR absorption on Si surfaces 40
2.4.3 Preparation of thin films of uranyl complex precursors 43
2.4.4 Extinction coefficient of UV bands 44
2.4.5 Photolysis experiments 44
2.4.6 Auger electron spectroscopy 45

Chapter 3. Mechanistic Study of Photochemistry of Uranyl 1,3-diketonate Complexes and Uranyl Carboxylate Complexes as Thin Films on Silicon Surfaces
3.1 Introduction 47
3.2 Results 47
3.2.1 Photolysis of uranyl 1,3-diketonate complexes as thin films on silicon surfaces: quantum yields 47
3.2.2 Photolysis of $UO_2(OOCC_5H_{11})_2$, $UO_2(OOCC_2H_4OC_2H_5)_2$ and $UO_2(OOCCH_2OC_2H_5)_2$ as thin films on silicon surfaces: quantum yields 51

3.2.3 Photolysis of $UO_2(OOCCH_3)_2$, $UO_2(OOC(i)\text{-}C_3H_7)_2$ and $UO_2(OOCCH_2C_6H_5)_2$ as thin films on silicon surfaces: quantum yields 57
3.2.4 Photolysis of $UO_2(OOCC_2H_4OC_6H_5)_2$ as thin films on silicon surfaces: quantum yields 58
3.2.5 Summary of quantum yields 58
3.2.6 Radical initiation experiments 59
3.2.7 Mass spectrometric analyses of organic photoproducts 62
3.3 Discussion
3.3.1 Mechanism of the photolysis of 1,3-diketonate complexes 68
3.3.2 Phochemistry of uranyl carboxylate complexes as thin films on silicon surfaces 71
3.4 Conclusion 74
3.5 Experimental Section 75
3.5.1 Quantum yield measurements and calculations 75
3.5.2 Mass spectrometric analyses of volatile products 78
3.5.3 Radical initiation experiments 79

Chapter 4. Photolithography and Electron Beam Lithography of Uranium Oxide Patterns on Silicon Substrates
4.1 Introduction 81
4.2 Results 85
4.2.1 Photolithography with uranyl 1,3-diketonate complexes 85
4.2.2 Photolithography with uranyl carboxylate complexes 87
4.2.3 Comparison of the photolysis time needed for different uranyl complexes to form stable patterns by means of PDSF 89
4.2.4 Electron beam lithography with uranyl complexes 89
4.3 Discussion 92

4.4 Conclusion 94

4.5 Experimental Section 94

4.5.1 Photolithography 94

4.5.2 Electron beam lithography 96

References 97

List of Tables

1-1 A summary of electrolytic thin film deposition techniques 2

1-2 Vacuum deposition methods of thin films 3

1-3 Deposition techniques in the environments of plasma, liquid and solid phase 4

1-4 Chemical vapour deposition techniques 5

1-5 Requirements of CVD and PDSF 8

2-1 Thickness required to stop X-rays for U and UO_3 16

2-2 A comparison of IR absorption data of uranyl diketonate complexes in crystalline states and as films on Si surface 20

2-3 UV-Vis data of uranyl 1,3-diketonate complexes as films on Si surfaces 23

2-4 FTIR spectroscopic data of $UO_2(OOCR)_2$ and RCOOH on Si(111) 25

2-5 UV-Vis data of uranyl carboxylate complexes 29

2-6 Elemental analysis result of uranyl complexes 30

2-7 Auger electron spectroscopic analysis result 37

2-8 Calibration of IR absorption on Si surface 42

3-1 Decomposition quantum yields of uranyl complexes upon photolysis 59

3-2 Reduction ratio of the intensities of $\nu_{as}(COO)$ and $\nu_s(COO)$ bands upon radical initiation for 24 hrs. 62

3-3 MS analysis results of volatile products resulting from the photolysis of uranyl 1,3-diketonate complexes 63

3-4 Results of MS analysis of volatile products from photolysis 67

4-1 Progress of lithography and a rough relationship between minimum feature size and capacity of DRAM 81

4-2 A comparison of stability of photolithographic patterns 89

List of Figures

1-1 An illustration of PDSF 7

1-2 One of the simplest thermal activated CVD processes 8

1-3 An Auger process 11

2-1 Structure of $UO_2(OH_2)$(t-butylacac)$_2$ 18

2-2 Structure of uranyl carboxylate complexes 18

2-3 a) FTIR spectra of $UO_2(OH_2)$(t-butylacac)$_2$ for 2.0, 4.0, 6.0, 8.0 and 10.0 molecules per $Å^2$ on a Si surface

b) Plot of the absorbance of 1351 cm^{-1} band of $UO_2(OH_2)$(t-butylacac)$_2$ versus coverage 21

2-4 a) FTIR spectra of $UO_2(OOCC_5H_{11})_2$ for 5.9, 11.8, 17.7, 23.6 and 29.5 molecules per $Å^2$ on a Si surface

b) Plot of the absorbance of ν_{as}(O=U=O) of $UO_2(OOCC_5H_{11})_2$ versus coverage 26

2-5 Plots of the absorbances of ν_{as}(O=U=O) versus coverage for uranyl complexes on silicon surfaces 27

2-6 Plots of the absorbances of ν_{as}(O=U=O) versus coverage for uranyl complexes on silicon surfaces 28

2-7 FTIR spectra of $UO_2(OOCC_5H_{11})_2$ upon photolysis at 334 nm 33

2-8 a) Auger electron spectrum of UO_2 pellet

b) Auger electron spectrum of a film resulted from the photolysis of $UO_2(OOCC_5H_{11})_2$ 36

2-9 a) FTIR spectra of $UO_2(OOCCH_2OC_2H_5)_2$ for 2.4, 4.8, 7.2, 9.6, 12.0 and 29.5 molecules per $Å^2$ on a Si surface

b) Plot of the absorbance of ν_{as}(O=U=O) of $UO_2(OOCCH_2OC_2H_5)_2$ versus coverage 41

2-10 An illustration of a spin coating process 43

2-11 Photolysis experiment 45

3-1 Changes in FTIR spectra of $UO_2(OH_2)$(t-butylacac)$_2$ thin film upon photolysis at 254 nm 48

3-2 Logarithmic plot of absorbances versus photolysis time for $UO_2(OH_2)$(t-butylacac)$_2$ thin film upon photolysis at 254 nm 50

3-3 Logarithmic plot of absorbances versus photolysis time for $UO_2(OH_2)(acac)_2$ thin film upon photolysis at 254 nm 50

3-4 FTIR spectroscopic changes in $\nu_{as}(O{=}U{=}O)$ of a thin film of $UO_2(OOCC_5H_{11})_2$ on a Si surface upon photolysis 52

3-5 Logarithmic plot of Ao/At versus photolysis time 53

3-6 Logarithmic plot of $(Ao-A\infty)/(At-A\infty)$ versus photolysis time 53

3-7 FTIR spectroscopic changes in $\nu_{as}(O{=}U{=}O)$ of a thin film of $UO_2(OOCC_2H_4OC_2H_5)_2$ on a Si surface upon photolysis 55

3-8 FTIR spectroscopic changes in the dark of a film with $UO_2(OOCC_5H_{11})_2$ and radical initiator AIBN 60

3-9 A designed tube for MS sample collection 79

4-1 Major steps in a photolithography process 82

4-2 The lithographic technique used in our laboratory 83

4-3 An uranium oxide pattern with 0.8 μm resolution on silicon surface resulting from the contact printing of a $UO_2(OH_2)$(t-butylacac)$_2$ film 86

4-4 SEM image of an uranium oxide pattern from the photolithography of $UO_2(OOCC_5H_{11})_2$ 88

4-5 0.2 μm Electron-beam lithographic lines 91

4-6 An illustration of the photolysis time comparison experiments 95

List of Abbreviations

acac: $CH_3COCHCOCH_3$

acacH: $CH_3COCH_2COCH_3$

AES: Auger electron spectroscopy

AIBN: azo-isobutyro nitrile

CVD: chemical vapour deposition

DRAM: dynamic random access memory

FTIR: Fourier transform infrared

IC: integrated circuit

IR: infrared

L: ligand

M: metal

PDSF: photochemical deposition from surface films

R: alkyl group

RF: radio frequency

SD: semiconductor device

SEM: scanning electron microscope

t-butylacac: (t)-$C_4H_9COCHCO$(t)-C_4H_9

t-butylacacH: (t)-$C_4H_9COCH_2CO$(t)-C_4H_9

TIC: total ion current

Chapter 1. Introduction

Presented in this thesis is the photochemistry of uranyl 1,3-diketonate complexes and uranyl carboxylate complexes as amorphous thin films on Si surfaces and an investigation of lithographing uranium oxide patterns. In order to help the readers to understand the project, a brief introduction to thin film deposition methods will be given. Photochemical deposition from surface films (PDSF), a method that we developed in our laboratory, will be introduced. This is followed by a comparison of PDSF with the current major deposition method, chemical vapour deposition (CVD). Some of the pertinent laws of photochemistry will then be described. The definition and derivation of photoreaction quantum yield will also be given. The sensitive surface analysis technique, Auger electron spectroscopy (AES) will also be introduced. Next I will present the reasons for choosing uranium compounds for study. Finally, my research goals will be described.

1.1 The Techniques of Thin Film Deposition

Thin films of the noble metals have been used for decorating glass and ceramics for over a thousand years.[1] As early as the 17th century, a method for the conversion from a layer of suspended silver salt to metallic silver film was known. The beating of gold to form "gold leaves" was another thin film formation method. In the last quarter century, thin film techniques have become important in the field of semiconductor electronics.[2] Current film formation techniques include: electrolytic deposition, vacuum evaporation, liquid and solid phase epitaxy, and chemical vapour deposition according to the film formation environment. Below, a brief introduction to each technique is summarized in Tables 1-1, 1-2, 1-3 and 1-4. CVD is one of the major techniques for preparing various kinds of films. It is useful in the fabrication of semiconductor devices and integrated circuits.[3] A comparison of CVD and PDSF will also be given.

Table 1-1 A summary of electrolytic thin film deposition techniques[4]

Deposition process	Short description of the process	Process parameters	Advantages	Limitations	Typical films formed and applications
Electro-plating[5]	Obtaining films by reducing the metallic ions by external electrons at the cathode.	concentration of ions current density cathode morphology nature of electrolyte	high deposition rate simple equipment	limited materials only on conductive substrates. low uniformity	Cu, Ni. conducting layers
Electroless plating[6]	Without an external current, a metallic layer formed by the chemical reduction occurring in plating solution.	temperature concentration of metallic & reducing ions pH	denser coating relatively uniform	conducting substrate. (limited No of non-conducting substrate.)	Ni conducting layers
Electrolytic anodization[7,8]	An oxide coating by means of the electro-chemical oxidation of an anode.	current density temperature pH	precise control of thickness	limited substrate contaminated film not very dense	Al_2O_3, Ta_2O_3, SiO_2 Passivation layers

Table 1-2 Vacuum deposition methods of thin films[4]

Deposition process	Short description of the process	Process parameters	Advantages	Limitations	Typical films formed and applications
Vacuum evaporation[9]	Vaporizing the source material in vacuum, followed by its vapour recondensation as a thin film.	temperature of source & substrate source-substrate separation gas background pressure	any substrates	limited substrate temperature (300-400°C) undesired impurities crystalline defect non-uniform film thickness	Al, Au, Ni-Cr Metallization or resistive layers
Ion beam deposition[10,11]	Thin layer deposition by bombarding the target materials with a beam of ions.	energy of impinging ions temperature target material	pure film	high vacuum low rate	Si, GaAs, Si_3N_4 semiconductor and dielectric layers
Molecular beam epitaxy[12]	Epitaxy by the interaction of a crystalline substrate and molecular beams	nature of effusing species beam energy source-substrate distance	precise control of thickness, composition, crystallinity	low rate UHV expensive system	GaAs, $Al_{1-x}Ga_xAs$ semiconductors for microwave & optoelectronic device.

Table 1-3 Deposition techniques in the environments of plasma, liquid and solid phase[4]

Deposition process	Short description of the process	Process parameters	Advantages	Limitations	Typical films formed and applications
Sputter deposition[13,14]	Neutral atom release from a cathodic target bombarded with positive ionized gas, subsequently deposit on substrates.	target material substrate bias concentration of sputtering gas shape+size of electrode	unheated sources conformal coating on irregular substrate	low rate contamination from target damaged film structure expensive equipment	W, Mo, WSi_2, $MoSi_2$, Si_3N_4 conductor & insulators for SD & IC superconductors
Ion plating[15,16]	A combination of vacuum evaporation with RF sputtering.	nature of evaporation source, substrate & reactive gas pressure RF power	higher rate good adhesion on 3-d substrate suitable substrate cleaning	contamination from target damaged film structure expensive equipment	Si_3N_4 dielectric material on SD
Liquid-phase epitaxy[17]	Precipitating a material from a cooling solution on to a heated substrate.	purity of carrier gas & solution material growth temperature cooling rate dopant additives	simple equipment. high rate incorporate dopants elimination of chemical hazards	not easy to adjust stoichiometry reproducibility is not very good	$Al_y Ga_{1-x}As$, $R_3 Fe_5O_{12}$ semiconductors for microwave & opto-electronic devices magnetic material
Solid-phase epitaxy[18]	Conversion of a deposited layer by thermal annealing to obtain a layer similar to the substrate in structure.	ambient temperature	good thickness control high purity+quality simple equipment	require highly clean substrate	Si potentially useful for obtaining epitaxial Si

Table 1-4 Chemical vapour deposition techniques[4]

Deposition process	Short description of the process	Process parameters	Advantages	Limitations	Typical films formed and applications
Chemical vapour conversion of substrate[19-24]	Oxidation or nitration of substrates by thermal or laser excitation or plasma anodization.	pressure anodization current laser irradiance	reproducible highest quality of grown SiO_2	not thick enough low rate p-n junction movement	SiO_2 , Si_3N_4, GaAs passivation layers, masks in SD & IC
Thermally-activated CVD[25]	Formation of thin films resulting from Gas-phase reactions activated by thermal energy.	pressure temperature reactant ratio pumping rate	high rate simple equipment reproducible	hard to control film thickness, composition & uniformity undesired secondary reaction	Si, SiO_2, Si_3N_4, GaAs polycrystalline semiconductor layers; dielectric material on SD and IC.
Plasma-enhanced CVD[26]	Uses of RF plasma to stimulate a reaction and subsequently deposit a layer on the substrates.	RF energy pressure temperature mole fraction of reactant	low temperature conformal films amorphous films on heat-sensitive substrate	low rate difficult to control film composition +thickness and uniformity	SiO_2, Si_3N_4, polymers Passivation layers for SD & IC.

Table 1-4 continued

UV-enhanced CVD[27]	Obtaining coatings from the decomposition of reactant gases promoted by UV light.	light intensity pressure	low temperature overcomes all disadvantages resulting from high temperature	low rate uniformity low throughput	SiO_2, Si_3N_4, polymers passivation layers in solid-state technology.
Laser-induced CVD[28,29]	Deposition from pyrolytic or photolytic decomposition of gaseous phase molecules.	laser irradiance temperature scanning velocity	high rate one step	short life time of continuous laser limited variation of process parameters	SiO_2, Si_3N_4, metals passivation or metal layers in solid-state technology
E-beam-assisted CVD[30]	Deposition on a heated substrate by confined plasma reaction generated from e-beam.	beam energy temperature pressure	high rate low temperature conformal coatings on uneven surface patternable	film contamination	SiO_2, Si_3N_4 passivation layers in solid-state technology
Ion-beam-assisted CVD[31]	Deposition from a suitable ambient gas by inducing a focused beam of ions.	beam current beam diameter gas flow rate	obtaining patterns with high resolution high rate low temperature	C or O contamination	Al, Au, W, C metal layers in solid-state technology

1.2 The Film Deposition Technique Developed in Our Laboratory: Photochemical Deposition From Surface Films (PDSF)

The deposition method developed in our laboratory is a photochemical process. The deposition of various materials is achieved by the direct photolysis of thin amorphous films of precursor molecules prepared by spin coating from organic solvents.

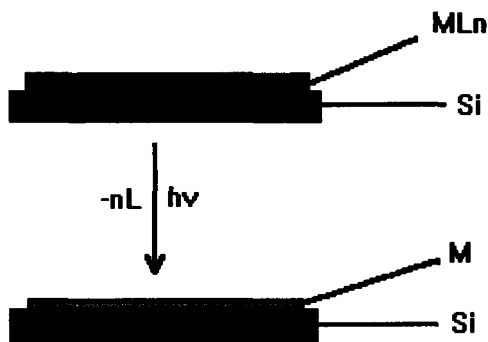

Figure 1-1 An illustration of PDSF

A solution of a photosensitive molecular precursor (MLn) containing desired material (M) is first prepared. The thin amorphous film of MLn is then obtained by dropping the solution on to a spinning Si chip. The photolysis of this thin film leads to the loss of the organic ligands resulting in desired material thin film (Figure 1-1). The photolysis can be done under vacuum, in the air or in other atmospheres such as H_2, H_2S, N_2, O_2 in order to obtain different materials or to study different photochemistry.

1.3 A Comparison of CVD with PDSF

Chemical vapour deposition, as its name suggests, means the formation of a stable film on a substrate, produced by the reaction of chemicals from the vapour phase.[4] According to the source of the activating energy, thermally activated CVD, plasma-enhanced CVD, photo-enhanced CVD, laser-induced CVD and electron-beam and ion-

beam assisted CVDs are all different CVD processes. They have been summarized in Table 1-4. Figure 1-2 shows one of the simplest thermal activated CVD processes.

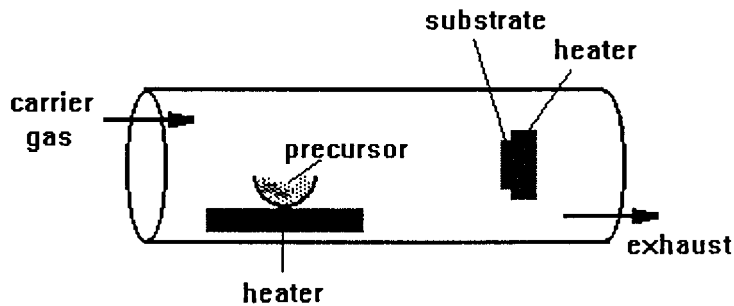

Figure 1-2 One of the simplest thermal activated CVD processes

In order to compare CVD and PDSF, we must know the requirements for both processes. Table 1-5 lists the basic requirements for CVD and PDSF.

Table 1-5 Requirements of CVD and PDSF

requirement	CVD	PDSF
precursor	volatile thermally sensitive	non-volatile photosensitive spin-coatable
substrate	any	any
temperature	high	ambient
pressure	must be controlled	ambient

CVD can produce uniform, reproducible, pure and stable films with high rates.[4] PDSF can also produce and reproduce uniform, pure and stable films. Because of the comparatively high processing temperature and controllable pressure (in some cases high

pressure), there are some disadvantages in CVD processes, such as, toxic exhaust, high equipment cost and relatively complicated operation procedures. In comparison to CVD processes, the above disadvantages are greatly reduced due to the use of ambient temperature and pressure in PDSF. The equipment cost is almost nothing for PDSF. The PDSF process is simple as shown in Figure 1-1. The photoejected ligands or fragments in PDSF can be easily designed as non-toxic hydrocarbon compounds. Furthermore, the requirement of volatile precursors, limits the selection of precursors for CVD processes. A larger selection of precursors is available for PDSF since volatile precursors are not required. In addition, PDSF is a lithographic process hence no photoresists are required. This eliminates etching and stripping steps.

1.4 The Laws of Photochemistry and Quantum Yields

1.4.1 First law of photochemistry

The first law of photochemistry states "Only radiations which are absorbed by the reacting system can be effective in producing photochemical changes." [32]

1.4.2 Quantum yields

The quantum yield is defined as the number of molecules that have undergone a photoprocess divided by the number of photons absorbed. In order to determine a quantum yield, two quantities are needed. First we need to know the change in the number of molecules of the reactant (or products). We also must know the number of photons absorbed by the reactant.

For the basic photoreaction outlined below (Equation 1-1),

$$A \xrightarrow{h\nu} B \qquad 1\text{-}1$$

the simplest mechanism is shown in Equation 1-2, 1-3, 1-4.

$$A \xrightarrow{h\nu} A^* \qquad 1\text{-}2$$

$$A^* \xrightarrow{k_d} A \qquad 1\text{-}3$$

$$A^* \xrightarrow{k_r} B \qquad 1\text{-}4$$

where, A is the reactant;

A* is the exited state of A;

B is the product.

We can express the change in the number of molecules of A, da/dt, using Equation 1-5. The change in the number of molecules of A*, da*/dt is shown in Equation 1-6.

$$da/dt = d(h\nu)/dt + k_d\, a^* \qquad 1\text{-}5$$

$$da^*/dt = -d(h\nu)/dt - k_d\, a^* - k_r\, a^* \qquad 1\text{-}6$$

With the steady-state approximation, da*/dt = 0, the steady molecular number a* is given by Equation 1-7.

$$a^* = -(d(h\nu)/dt)/(k_d + k_r) \qquad 1\text{-}7$$

Substituting a* into equation 1-5, we obtain Equation 1-8.

$$da/d(h\nu) = k_r/(k_d + k_r)$$

$$= \Phi \qquad 1\text{-}8$$

Equation 1-8 is the expression for the quantum yield of the decomposition of A or the formation of B. From equation 1-8, we know that the quantum yield is not a function of a single rate constant, even for the simplest reaction A $\rightarrow$ B. It depends on the ratio of $k_d/(k_d + k_r)$. Because of this, the interpretation of quantum yields becomes difficult.

1.4.3 Second law of photochemistry

The second law of photochemistry states "The absorption of light by a molecule is a one-quantum process, so that the sum of the primary process quantum yields must be unity." [33]

1.5 Auger Electron Spectroscopy—A Sensitive Surface Analysis Technique

As one of most widely used surface analysis techniques, Auger electron spectroscopy (AES) is a sensitive method to obtain the chemical composition of a surface.[34] An Auger process (KL1L2 Auger transition) is described below.

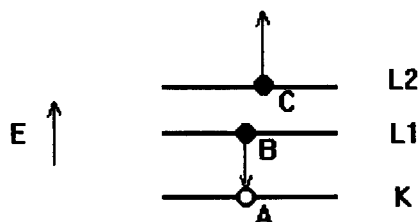

Figure 1-3 An Auger process

(K, L——principal quantum numbers)

The vacancy A in the core level of the atom (K) is generated by the ionization from electron bombardment. The vacancy A is filled immediately by an electron, B, from the higher energy level L1 (Figure 1-3). The energy (E_K-E_{L1}) resulting from this transition can

be transferred to another electron (C) in L2 level. The energized C electron is called an Auger electron, which is then ejected from the atom with an energy E_A shown in equation 1-9. The final state of the atom is a doubly ionized state.

$$E_A = E_K - E_{L1} - E_{L2} - \phi_D \qquad 1\text{-}9$$

where ϕ_D is the work function of the detector.

There are other Auger processes occurring. Most common ones are KLL, LMM and MNN (K, L, M and N are the principal quantum numbers) families that involve electrons of neighboring orbitals. A general equation (1-10) is given for estimating the kinetic energy of Auger electrons from WXY transition.

$$E_{WXY} = E_W - E_X - E_Y(\Delta) - \phi_D \qquad 1\text{-}10$$

Because of the small difference in energy between doubly ionized state and the sum of two individual ionization of the same level, Δ is introduced. The Auger electron energies are characteristic of the target material, which provides the information for the identification of elements.

Quantitative analysis to determine the elemental composition is more complicated than qualitative analysis described above. Here, I introduce the method that we used to determine the composition of photochemical deposited thin films. The method uses the relative sensitivity of elements.[35] For the element *i*, the atomic fraction C_i is given by Equation 1-11.

$$C_i = (I_i/S_i)/\Sigma(I_i/S_i) \qquad 1\text{-}11$$

where, I_i is the current of emitted Auger electrons, S_i is the relative sensitivity factor of element i, and $\Sigma(I_i/S_i)$ is the summation of (I_i/S_i) ratio of all elements detected in the Auger spectrum.

1.6 Reasons of Studying Uranium

Understanding the thin film solid state photochemistry of inorganic, metal organic and organometallic compounds has been a goal of our research group for some time.[36-40] The solid state photochemistry of copper, platinum, nickel, iron, titanium, chromium, molybdenum, and tungsten compounds has been studied recently. The deposition of metals (Cu, Pt, Ni);[36, 37, 39] metal oxides (CuO, Cu_2O, Fe_2O_3, TiO, Cr_2O_3);[37, 38, 40] metal sulfide (MoS_4)[40] as well as mixed metal oxides[40] has been successfully achieved. Some of these materials are useful in the electronics industry as conductors, resistors, solar cell and semitransparent materials.[41]

Uranium is of particular interest due to its potential application as a mask material for X-ray lithography. A lithographic mask usually consists of two parts, a substrate that is transparent to the irradiation light, and an absorber that stops the irradiation light. the most common photolithography mask is made of Cr patterns on a glass substrate.[42] X-ray lithography has been found to have advantages over optical lithography. One of the advantages is that X-ray reduces diffraction limits far below deep-ultraviolet. Lowered defect level due to the relative insensitivity of organic contamination to X-rays is the other one.[43] In theory, X-ray lithography is able to print features with sub-0.1 μm resolution, however, the mask fabrication has been a concern.[44] Commonly, X-ray lithography masks consist of a low X-ray-absorbing substrate supporting a high X-ray-absorbing pattern.[43] Although gold has been used as a mask absorber material, the use of uranium patterns is preferable since in general, uranium possesses a higher X-ray absorption cross-section than gold.[45] The use of thinner films on the mask substrate should be possible with uranium, thereby reducing Fresnel or near-field diffraction.[46]

1.7 Research Objectives

The goal of this study was to investigate the deposition of uranium oxide patterns for the application of making a high resolution X-ray lithographic mask material. In order to reach this goal, my first approach was to photochemically deposit uranium oxide films as well as uranium oxide patterns. This would show the possibility of obtaining the right materials by means of photochemical deposition. Electron-beam lithography is the approach to obtain high resolution features. The study of photochemistry of uranium compounds helped us to understand the mechanism of the photoreactions. Based on the understanding of the mechanism of the photoreactions, we could then effectively reach the goal.

The choice of suitable uranium compounds as precursors for the deposition of uranium oxides is discussed in Chapter 2. The preparation and characterization of these precursors, quality of precursor films and the formation of uranium oxide films by means of PDSF are also presented in Chapter 2.

Following the synthesis of suitable uranium compounds, we were able to study the mechanism of photoreactions of uranium compounds as thin amorphous films on Si substrates. Monitoring the photolysis of uranium compounds by Fourier Transform Infrared (FTIR) spectroscopy provided us with the information about the ejection of ligands and the formation of intermediates as well as the information about final photoproducts left on the substrates. Quantum yield measurements allowed us to compare the photoefficiency of uranyl complexes with different ligands and to further study the mechanism. Using mass spectrometry to identify volatile products of the photoreaction in order to gather information for the mechanistic study will also be discussed. All these subjects will be presented in Chapter 3.

To reach the research goal, optical lithography was used to show the possibility of patterning uranium oxide lines by a photochemical means. Electron-beam lithography was the approach to improve the resolution of features. The detailed results are reported in

Chapter 4.

Chapter 2. Synthesis of Uranium Trioxide Film

2.1 Introduction

An ideal X-ray lithography mask material has a high X-ray absorption cross section. Both uranium and uranium oxide have high X-ray absorption cross sections and may be suitable for X-ray lithography mask materials. The deposition of metal,[47-49] metal oxide,[50-52] metal nitride[53, 54] and metal carbide[53] films has been studied extensively, however, little has been done on uranium material.[55, 56] Uranium metal films are not stable as they oxidize in the presence of air.[57] This results in the formation of discontinuous uranium oxide films because the volume expands upon oxidation. In contrast, uranium oxide films are stable.[58] A uniform uranium oxide film can be obtained by the photoejection of the organic ligands from an uranyl organic complex film. The presence of the oxygen in the uranium oxide films does not preclude the application as a potential material for making an X-ray lithography mask since uranium is such a heavy atom. Uranium oxide can stop X-rays more effectively than uranium when the wavelength of X-rays used is 12.4 nm due to the high photon attenuation coefficient[59] of oxygen at this wavelength. Equation 2-1 below can be used in conjunction with mass density and μ to calculate the thickness of uranium and uranium oxide needed to attenuate 99.99% of X-rays. Table 2-1 lists the thickness, x, required for the attenuation of 99.99% of the X-rays with the wavelengths of 12.4, 1.24 and 0.124 nm.

$$I/Io = e^{-\rho\mu x} \qquad 2\text{-}1$$

where, Io is the initial light intensity,

I is the light intensity after path length x,

ρ is the mass density of the material,

μ is the photon attenuation coefficient that is additive for the elements present.

Table 2-1 Thickness of U and UO_3 needed to attenuate 99.99% of X-rays

X-ray wavelength	thickness (μm)	
	U	UO_3
12.4 nm	0.25	0.16
1.24 nm	0.73	1.74
0.124 nm	27.1	73.5

In this chapter, I describe the photochemical synthesis of uranium oxide films. The logic surrounding the choice of precursor molecules is discussed. The qualities of precursor films are compared. The characterizations of the uranium oxide films are also described.

2.2 Results and Discussion

2.2.1 The choice of precursor molecules

Molecules must be photosensitive and thermally stable to serve as precursors for the formation of uranium oxide films. The photosensitivity of the precursors would allow us to achieve the photochemical deposition. The thermal stability allows us to study the photochemistry in the absence of thermal side reactions. The ability to form amorphous films by spin-coating is another requirement for precursor molecules. Ionic inorganic compounds (no organic components), such as $CuCl_2$, are not ideal. These types of complexes tend to form crystalline films because of the strong intermolecular forces. This affects the photoreactivity of the films, due to the recombination of photochemical fragments under the lattice force. In amorphous films, there are no such lattice forces. Therefore, the photochemical fragments diffuse and are ejected from the films. Low volatility and air stability are also requirements for precursor molecules. These quantities result in stable precursor films both in the air and under vacuum.

Previously in our laboratory,[60] four uranyl complexes, $UO_2(NCS)_2(OP(C_6H_5)_3)_2$, $UO_2(NO_2)_2(OP(C_6H_5)_3)_2$, $UO_2(NO_3)_2(OP(C_6H_5)_3)_2$, and $UO_2(OH_2)(O_2C_5H_7)$ ($O_2C_5H_7$= $CH_3C(O)CHC(O)CH_3$ = acac) have been studied. The investigation indicated that $UO_2(NO_2)_2(OP(C_6H_5)_3)_2$ and $UO_2(NO_3)_2(OP(C_6H_5)_3)_2$ did not spin coat as amorphous films. The other two uranyl complexes, $UO_2(NCS)_2(OP(C_6H_5)_3)_2$ and $UO_2(OH_2)(acac)_2$ had a low photosensitivity. The investigation also showed that $UO_2(OH_2)(acac)_2$ formed a thinner film (approximately 50 monolayers) than satisfactory but it produced UO_3 on photolysis. The photolysis of $UO_2(NCS)_2(OP(C_6H_5)_3)_2$ resulted in the loss of only the NCS ligands (Scheme 2-1). This reaction does not result in a uranium oxide film.

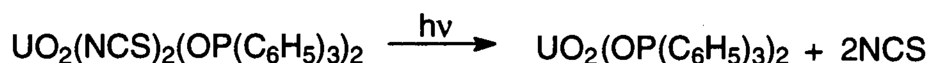

Scheme 2-1

Considering the above requirements and the results obtained previously in our laboratory, the uranyl 1,3-diketonate complex $UO_2(OH_2)(O_2C_{11}H_{19})_2$ ($O_2C_{11}H_{19}$ = $(CH_3)_3CC(O)CHC(O)C(CH_3)_3$ = t-butylacac) shown in Figure 2-1, was chosen as a potential precursor. This complex has larger organic components than $UO_2(OH_2)(acac)_2$. We choose $UO_2(OH_2)$(t-butylacac)$_2$ in the expectation that spin coating will result in a thicker amorphous precursor film. We also expected it would undergo similar photochemistry to $UO_2(OH_2)(acac)_2$ producing uranium oxide upon photolysis. With the highly amorphous film, the photoefficiency of $UO_2(OH_2)$(t-butylacac)$_2$ is also expected to be higher than $UO_2(OH_2)(acac)_2$.

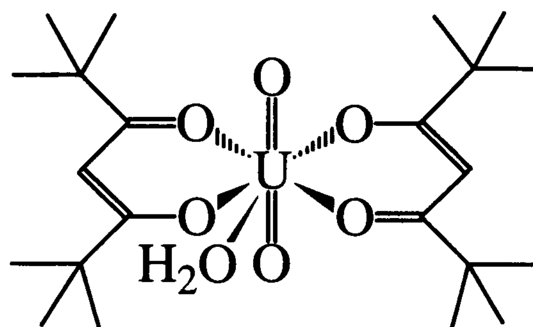

Figure 2-1 Structure of $UO_2(OH_2)$(t-butylacac)$_2$

Uranyl carboxylate complexes with the structure shown in Figure 2-2 were also chosen as precursors. We expect these metal organic complexes to have weak intermolecular forces; therefore they should be able to form amorphous films. Carboxylate

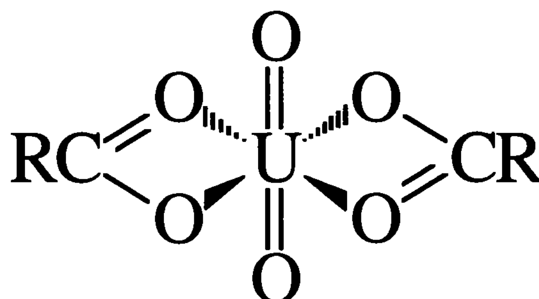

Figure 2-2 General structure of uranyl carboxylate complexes

complexes are expected to be photosensitive. In solution they have been found to decarboxylate forming CO_2 and alkyl radicals. The reaction is thought to occur via a ligand to metal charge transfer excitation.[61] We can vary the alkyl group R to control both film quality and photosensitivity. The uranyl group oxygen, contained in both classes of molecules, contributes to the air stability of the precursors.

2.2.2 Synthesis of uranyl 1,3-diketonate complexes and uranyl carboxylate complexes

A single step synthesis combining metathesis and neutralization was used for the preparation of $UO_2(OH_2)(t\text{-butylacac})_2$.[62] The reaction equation is shown in Scheme 2-2.

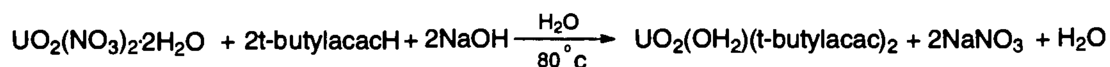

Scheme 2-2

The preparation of the uranyl carboxylate complexes followed Yokoyama's synthesis of $UO_2(OOCC_2H_4OC_2H_5)_2$ and $UO_2(OOCCH_2OC_2H_5)_2$.[63] The reactions are shown in Scheme 2-3. The first step is a metathesis step between KOH and $UO_2(NO_3)_2$ to precipitate uranium hydroxide. Uranium hydroxide is then neutralized by an organic acid in the second step.

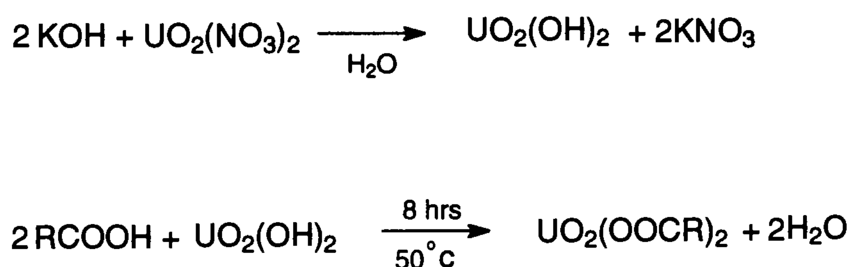

Scheme 2-3

2.2.3 Characterization of uranyl 1,3-diketonate complexes

FTIR spectroscopy was used to characterize $UO_2(OH_2)$(t-butylacac)$_2$ and $UO_2(OH_2)(acac)_2$. The FTIR spectrum of a film of $UO_2(OH_2)(acac)_2$ on a silicon surface was similar to the literature[62] spectrum for crystalline IR samples. The FTIR absorption bands of a film of $UO_2(OH_2)$(t-butylacac)$_2$ were identical to those reported by Belyaeva[64] within experimental error. Belyaeva's spectrum was obtained for crystalline sample. The FTIR spectroscopic data for these two complexes is summarized in Table 2-2.

Table 2-2 A comparison of IR absorption data of uranyl diketonate complexes in crystalline states and as films on Si surface

Complex	crystalline state (cm^{-1})[62, 64]	film(cm^{-1}) (log ε)	assignments[64-67]
$UO_2(OH_2)(acac)_2$	1570	1574(2.24)	ν_s(C=O)
	1529	1524(2.30)	ν_{as}(C=C)
	1437	1429(1.73)	(C-H)
	1351	1362(2.18)	ν_{as}(C=O)
	1227	1271(1.80)	ν_s(C=C)
	1024, 1014	1015(1.63)	(CH_3)
	925	920(2.11)	ν_{as}(U-O)
$UO_2(OH_2)$(t-butylacac)$_2$	1565, 1545	1564, 1547 (2.46, 2.53)	ν_s(C=O)
	1535	1537(2.08)	ν_{as}(C-C-C)
	1500	1503(2.46)	ν_{as}(C=O)
	1372,1350	1374, 1351 (2.37, 2.42)	$\delta(CH_3)$
	1246	1247(1.78)	ν_s(C-C-C))
	1224	1226(1.94)	$\rho(CH_3)$
	1145	1146(2.08)	δ(CH)
	892	887(2.28)	ν_{as}(U=O)

The absorbance of a precursor film is a function of the amount of the precursor molecule deposited on a silicon surface as a film. The modified Beer's Law* was used to calibrate the absorbance. A standard calibration experiment was done by dropping a small amount of a stock solution of a uranyl complex onto a silicon chip and allowing the solvent to evaporate. The FTIR spectrum was recorded after each drop was deposited on to the surface. Since the concentration of the stock solution and the volume of the drop are known, we can calculate the surface coverage (molecules/$\mathring{A}^2$) by measuring the area of the drop. Figure 2-3(a) shows overlaid FTIR spectra from the calibration experiment for $UO_2(OH_2)$(t-butylacac)$_2$. Figure 2-3(b) shows the linear relationship between FTIR absorbance (at 1337 cm^{-1}) and the surface coverage.

The calibration of FTIR absorbances of $UO_2(OH_2)(acac)_2$ was also conducted. The calibration curve is shown in Figure 2-5. The extinction coefficient (ε) of all of the FTIR bands of these two complexes are listed in Table 2-2.

---

* Beer's Law[68]: $A=\varepsilon bc$, where A is the absorbance of the chosen absorption band;
ε is the extinction coefficient of this absorption;
b is the path length (cm);
c is the concentration of the solution (mole/l).
We used $A=\varepsilon a$ for the calibration. Where a is the surface coverage (mole/cm^2).

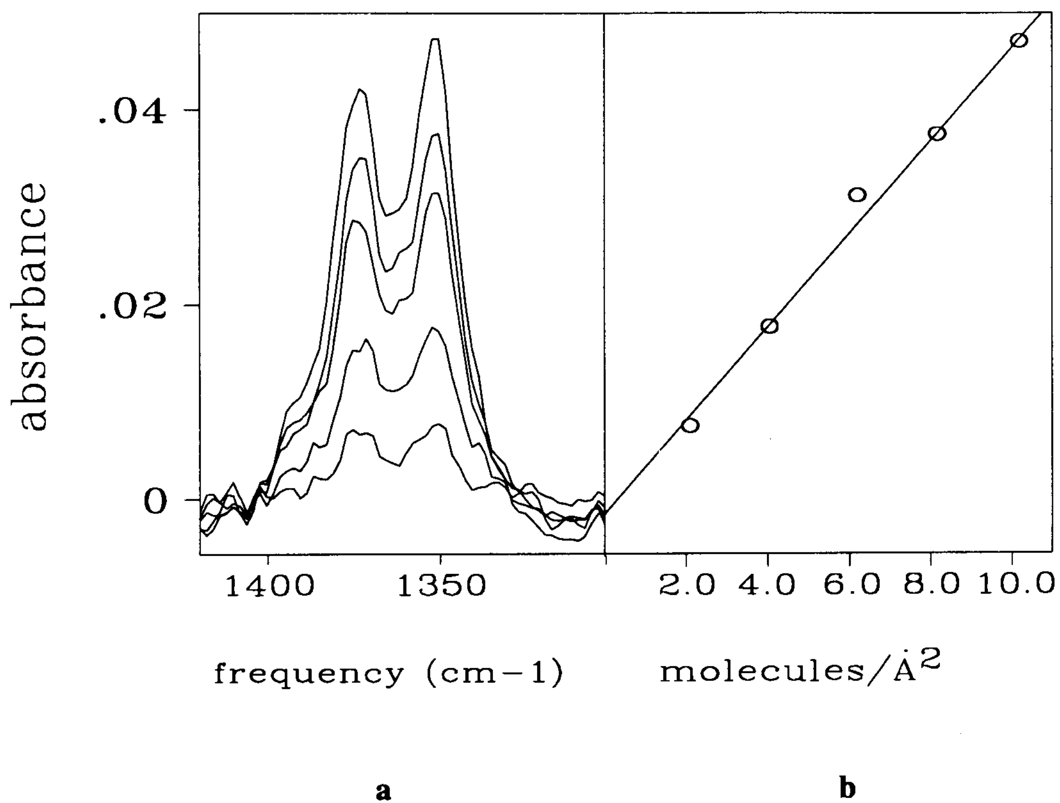

Figure 2-3 a) FTIR spectra of $UO_2(OH_2)$(t-butylacac)$_2$ for 2.0, 4.0, 6.0 8.0, and 10.0 molecules per Å^2 on a Si surface.

b) Plot of the absorbance of 1351 cm^{-1} band of $UO_2(OH_2)$(t-butylacac)$_2$ versus coverage

UV-Vis spectroscopy was also used to characterize $UO_2(OH_2)(t\text{-butylacac})_2$ and $UO_2(OH_2)(acac)_2$. The UV-Vis spectra of $UO_2(OH_2)(acac)_2$ had absorption bands in the region of 290 and 370 nm (Table 2-3). The absorption band at 290 nm is assigned to intraligand π-π^* transition.[69] Since the shape of this band is asymmetric, there might be a ligand to metal charge transfer band obscured on the higher energy side. This ligand to metal charge transfer band is not resolvable as a shoulder. A band in the region of 370 nm is associated with the uranyl group.[70]

Table 2-3 UV-Vis data of uranyl 1,3-diketonate complexes as films on Si surfaces

complex	λmax, (nm) film	log ε[a]	λmax, (nm) soln.[54]
$UO_2(OH_2)(acac)_2$	290	3.34	273
	365	2.59	347
$UO_2(OH_2)(t\text{-butylacac})_2$	290	3.48	
	370	2.85	

a) Calculated based on IR absorption calibration data.

The energy of the transitions observed in thin films are shifted 18 nm to lower energy compared to the result in ethanol solution reported by Comyns.[62] This presumably results from the interaction between polar solvent and sample molecules. It is known that a polar solvent usually increases the energies of π-π^* transitions.[71] In films, there is no solvent-sample interaction, so the absorption energies we obtained from films appeared to lower energies.

The UV-Vis spectrum of $UO_2(OH_2)(t\text{-butylacac})_2$ thin film was very similar to the spectrum of $UO_2(OH_2)(acac)_2$. The absorption bands and the extinction coefficients are listed in Table 2-3.

The elemental analysis gave the result of C% (25.02), H% (3.32) for $UO_2(OH_2)(acac)_2$, which is close to the calculated value: C% (24.69), H% (3.29). The elemental analysis of $UO_2(OH_2)$(t-butylacac)$_2$ was also done. The result was: found: C% (40.37), H% (6.16); calculated: C% (40.32), H% (6.22).

2.2.4 Characterization of uranyl carboxylate complexes

The FTIR spectroscopic data of uranyl carboxylate complex films on Si(111) are presented in Table 2-4. The carboxylate groups were identified by two strong absorptions, ν_{as}(COO) and ν_s(COO). The asymmetric stretching vibration ν_{as}(COO) in all seven uranyl complexes appeared in a lower energy region than that in the free carboxylic acids due to the coordination to uranium. The coordination also causes the Δ values (ν_{as}(COO)-ν_s(COO)) of these uranyl complexes to become significantly smaller than that of the free ligands. (In free ligands, the Δ is typically about 500 cm^{-1}). The simplified explanation for the change in Δ is that the coordination averages the bond order (length and strength as well) of C=O and C-O bonds leading to a weakened C=O bond and a strengthened C-O bond. Therefore, in the FTIR spectrum, we see a lower energy ν_{as}(COO) and a higher energy ν_s(COO). This FTIR result confirms that the complexes have the chelating (bidentate) structure[72] shown in Figure 2-2.

The calibration of the FTIR absorption of $UO_2(OOCC_5H_{11})_2$ was done in the same manner as described for $UO_2(OH_2)$(t-butylacac)$_2$. Figure 2-4(a) shows the overlaid FTIR spectra from the calibration experiment of $UO_2(OOCC_5H_{11})_2$. Figure 2-4(b) shows a linear relationship between FTIR absorbance and the surface coverage. The calibration of FTIR absorption of all of other uranyl carboxylate complexes were done in the same way. The calibration curves are shown in Figure 2-5 and Figure 2-6.

UV-Vis spectroscopic data of uranyl carboxylate complexes in methanol solution and as films on silicon surfaces were obtained. The results are listed in Table 2-5.

Table 2-4. FTIR spectroscopic data of $UO_2(OOCR)_2$ and RCOOH on Si(111)

R	*$UO_2(OOCR)_2$*				*RCOOH*		
	$\nu_{as}(COO)$ $(cm^{-1})(\log \varepsilon)$	$\nu_s(COO)$ $(cm^{-1})(\log \varepsilon)$	$\Delta\nu^a$ (cm^{-1})	$\nu_{as}(O=U=O)$ $(cm^{-1})(\log \varepsilon)$	$\nu_{as}(COO)$ (cm^{-1})	$\nu_s(COO)$ (cm^{-1})	$\Delta\nu^a$ (cm^{-1})
$C_2H_5OCH_2$	1560(2.48)	1465(1.90)	95	938(2.28)	1736	1232	504
$C_2H_5OC_2H_4$	1539(2.42)	1465(2.29)	74	927(2.36)	1720	1198	522
$C_2H_5OC_6H_4$	1525(2.85)	1455(2.71)	70	928(2.72)	1736	1236	500
CH_3	1529(2.46)	1450(2.30)	99	938(2.30)	1700	1250	450
i-C_3H_7	1529(2.49)	1441(2.21)	88	932(2.30)	1710	1230	480
C_5H_{11}	1539(2.80)	1467(2.71)	72	933(2.63)	1722	1250	470
$CH_2C_6H_5$	1541(2.56)	1448(2.48)	93	926(2.43)	1699	1229	470

a) $\Delta\nu = \nu_{as}(COO) - \nu_s(COO)$

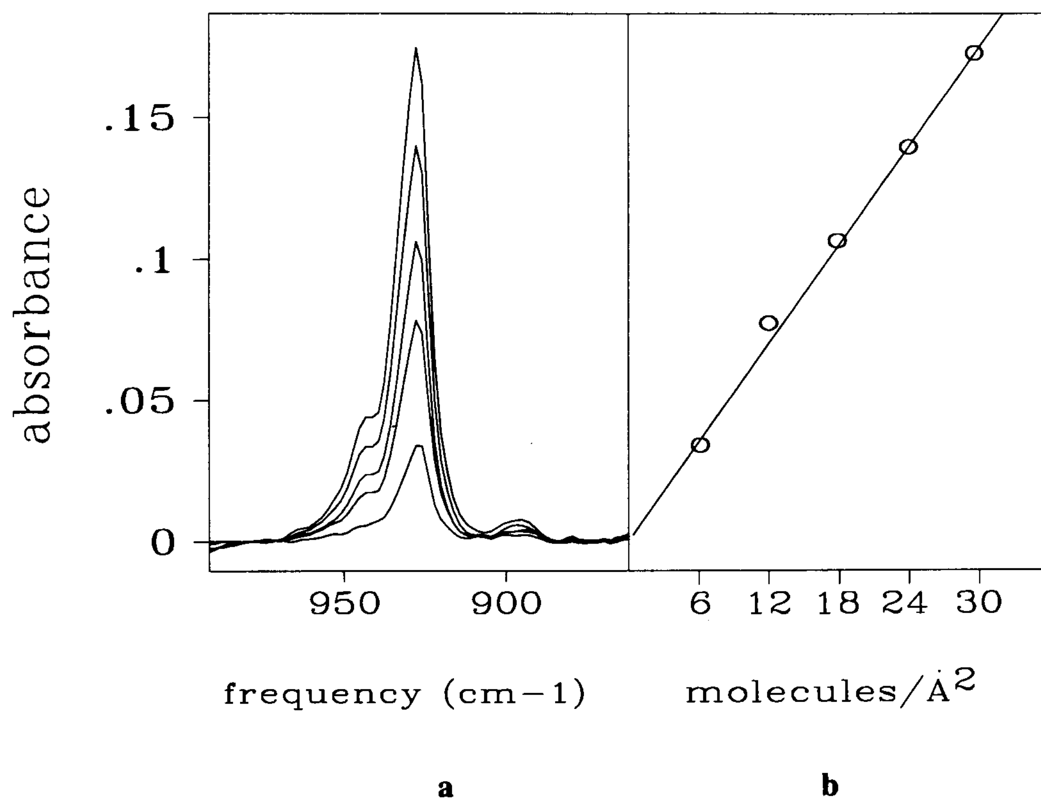

Figure 2-4 a) FTIR spectra of $UO_2(OOCC_5H_{11})_2$ for 5.9, 11.8, 17.7, 23.6, and 29.5 molecules per $Å^2$ on a Si surface.
b) Plot of the absorbance of $\nu_{as}(O{=}U{=}O)$ of $UO_2(OOCC_5H_{11})_2$ versus coverage

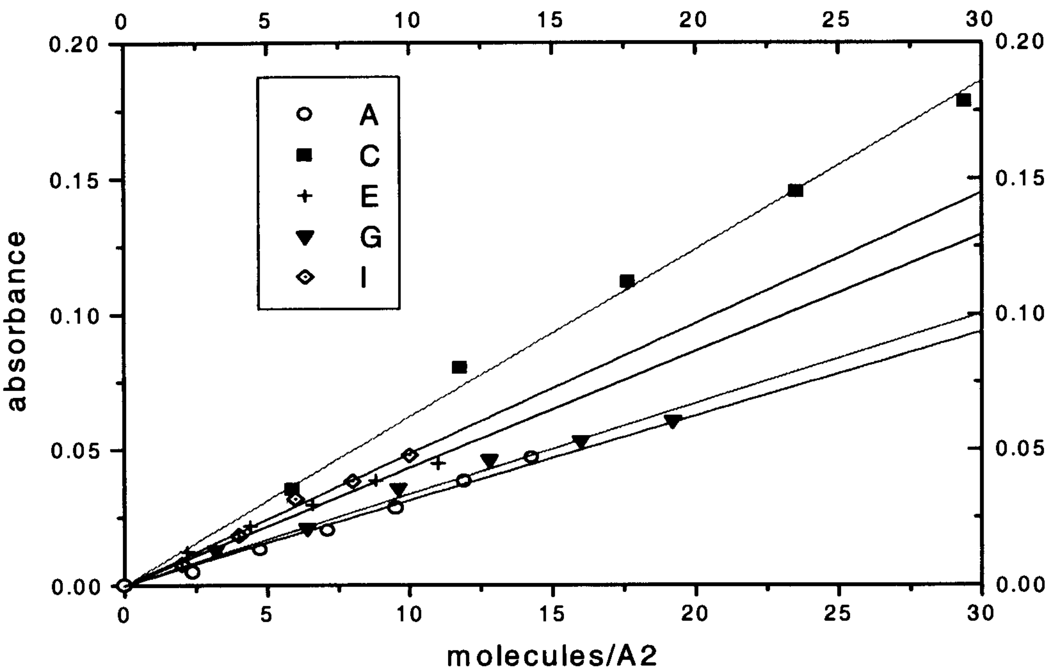

Figure 2-5 Plots of the absorbances of $\nu_{as(O=U=O)}$ versus coverage for uranyl complexes on Si surfaces

A) $UO_2(OOCCH_2OC_2H_5)_2$ C) $UO_2(OOCC_5H_{11})_2$ E) $UO_2(OOCCH_2C_6H_5)_2$

G) $UO_2(OH_2)(acac)_2$ I) $UO_2(OH_2)$(T-butylacac)$_2$

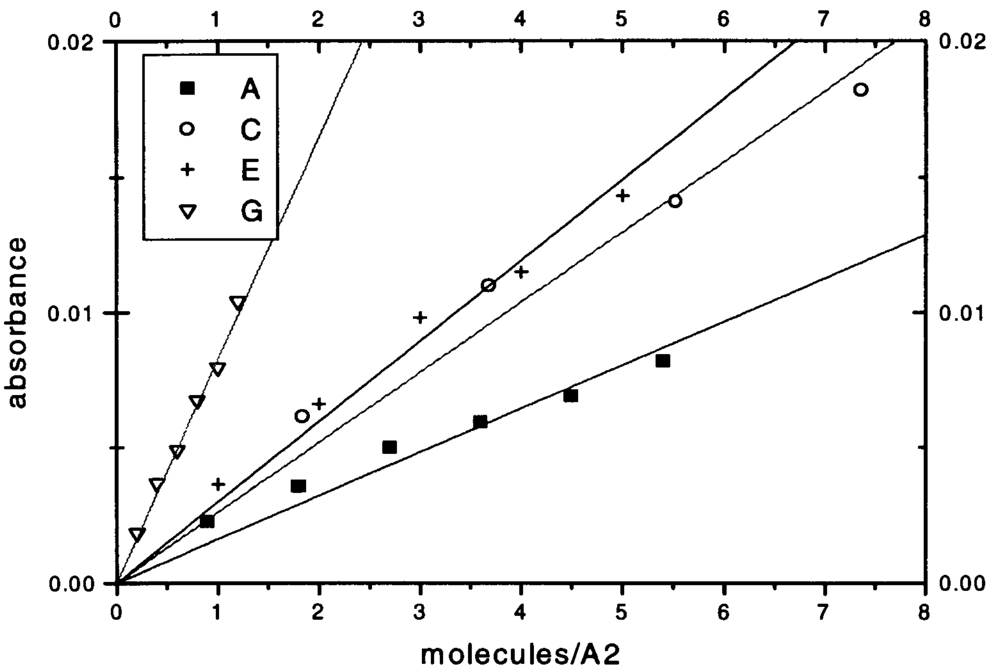

Figure 2-6 Plots of the absorbances of $\nu_{as(O=U=O)}$ versus coverage for uranyl complexes on Si surfaces

A) $UO_2(OOCC_2H_4OC_2H_5)_2$ C) $UO_2(OOC(i)\text{-}C_3H_7)_2$

E) $UO_2(OOCCH_3)_2$ G) $UO_2(OOCC_2H_4OC_6H_4)_2$

Table 2-5 UV-Vis data of uranyl carboxylate complexes

complex	λmax(nm)(film) [log ε[a]]	λmax(nm) (soln.[b])[log ε]	assignment[c]
$UO_2(OOCCH_2OC_2H_5)_2$	214(sh)[3.13]	210[3.55]	unassigned
		242[3.57]	LMCT
	302(sh)[2.29]	304(sh)[3.08]	UO_2^{2+}
	420[1.41]	430[2.11]	UO_2^{2+}
$UO_2(OOCC_2H_4OC_2H_5)_2$	231(sh)[3.00]	210[3.54]	unassigned
		240[3.48]	LMCT
	301(sh)[2.00]	302(sh)[2.90]	UO_2^{2+}
	432[1.51]	430[1.68]	UO_2^{2+}
$UO_2(OOCC_6H_4OC_2H_5)_2$	204[4.55]	212[4.36]	unassigned
	238[4.18]	234[4.18]	LMCT
	298[3.89]	292[3.79]	π-π* from benzene ring
		430[1.78]	UO_2^{2+}
$UO_2(OOCCH_3)_2$	206(sh)[3.16]	210[3.61]	unassigned
		264[3.52]	LMCT
	238(sh)[2.36]	314(sh)[3.04]	UO_2^{2+}
	402[2.06]	432[1.93]	UO_2^{2+}
$UO_2(OOC(i)\text{-}C_3H_7)_2$		210[3.64]	unassigned
	232(sh)[3.71]	240[3.55]	LMCT
		316(sh)[2.92]	UO_2^{2+}
		432[1.60]	UO_2^{2+}
$UO_2(OOCC_5H_{11})_2$	230[3.06]	206[3.66]	unassigned
		240[3.51]	LMCT
	302(sh)[1.82]	310(sh)[2.92]	UO_2^{2+}
	418[1.38]	432[1.88]	UO_2^{2+}
$UO_2(OOCCH_2C_6H_5)_2$	196[4.33],212[4.03]	214[4.09]	unassigned
	250(sh)[3.41]	244(sh)[3.68]	LMCT
		302(sh)[3.19]	UO_2^{2+}
		412(sh)[2.45]	UO_2^{2+}

a) Calculated from calibration data.

b) The solution absorption data was obtained from CH_3OH solution.

c) Assignments are tentative. See references 70, 71, 73-75, and in particular, the discussion in reference 73.

The elemental analysis (C, H) results for the carboxylate uranyl complexes are presented in Table 2-6. The analysis results of $UO_2(OOCCH_2OC_2H_5)_2$, $UO_2(C_2H_5OC_6H_4COO)_2$ and $UO_2(OOC(i)\text{-}C_3H_7)_2$ fit the simple formulation. Some other complexes, ($UO_2(OOCC_2H_4OC_2H_5)_2$, $UO_2(OOCC_5H_{11})_2$ and $UO_2(OOCCH_2C_6H_5)_2$), apparently crystallized with a half molecule of solvent (acetone). The elemental analysis result seemed to be consistent with the formula of $UO_2(OOCR)_2 \cdot 1/2(CH_3COCH_3)$ (R= $C_2H_4OC_2H_5$, C_5H_{11}, $CH_2C_6H_5$).

Table 2-6 Elemental analysis result of uranyl complexes

complex	Experimental		Calculated	
	C%	H%	C%	H%
$UO_2(OOCCH_2OC_2H_5)_2$	20.25	2.95	20.17	2.94
$UO_2(C_2H_5OC_6H_4COO)_2$	36.85	3.10	36.60	3.00
$UO_2(OOC(i)\text{-}C_3H_7)_2$	22.17	3.31	21.62	3.15
$UO_2(OOCC_2H_4OC_2H_5)_2 \cdot 1/2(CH_3COCH_3)$	25.53	3.86	25.89	3.94
$UO_2(OOCC_5H_{11})_2 \cdot 1/2(CH_3COCH_3)$	30.69	4.90	30.63	4.76
$UO_2(OOCCH_2C_6H_5)_2 \cdot 1/2(CH_3COCH_3)$	37.09	2.70	36.91	2.99

2.2.5 The quality of thin precursor films

The series of uranyl carboxylate complexes with the general formula $UO_2(OOCR)_2$ (R= CH_3, $i\text{-}C_3H_7$, C_5H_{11}, $CH_2C_6H_5$, $C_2H_5OCH_2$, $C_2H_5OC_2H_4$ and $C_2H_5OC_2H_4$) were examined to determine if they formed amorphous films by spin

coating from organic solvents. All of these complexes formed amorphous films. Five of them, $UO_2(OOCCH_2OC_2H_5)_2$, $UO_2(OOCC_2H_4OC_2H_5)_2$, $UO_2(OOCC_5H_{11})_2$, $UO_2(OOCCH_3)_2$ and $UO_2(OOCCH_2C_6H_5)_2$, formed uniform films. The other two complexes, $UO_2(OOC(i)\text{-}C_3H_7)_2$ and $UO_2(OOCC_6H_4OC_2H_5)_2$, formed discontinuous films. The complex, $UO_2(OH_2)$(t-butylacac)$_2$ formed films up to approximately 600 monolayers thick. This is thicker than films of $UO_2(OH_2)(acac)_2$ which were only up to 100 monolayers.

In choosing suitable organic solvents for spin coating a precursor film, the first property to be considered is the solubility. Obviously, a solvent which does not dissolve the precursor complex should not be chosen. Studies[76, 77] have shown that the film thickness is dependent on the concentration of the solution at a constant spin speed. The higher concentration gives a thicker film. Usually, the solvent in which the precursor is reasonably soluble should be chosen. However, solvents which contain hydrogen bonds (such as methanol) resulted in discontinuous films. The quality of films apparently depends not only on the intermolecular forces between the precursor molecules but also on the interaction of the solvent with the substrate surface. The two diketonate complexes were spin coated from CH_2Cl_2. A mixed solvent of acetone and methanol (4:1) was used for both $UO_2(OOCCH_3)_2$ and $UO_2(OOCC_6H_4OC_2H_5)_2$. These two complexes are very soluble in methanol and only slightly soluble in acetone. This mixed solvent solved the solubility problem and weakened the hydrogen-bonding. The other carboxylate complexes were spin coated from acetone solutions.

The film thickness (l) depends on the spin speed. It has the relationship with spin speed, ω, shown in equation 2-2.[76] The lower the spin speed used, the thicker the film formed. A high solution concentration combined with a low spin speed sometimes resulted in a crystalline film.

$$l = KC^{2.1}/\omega^{0.5} \qquad \text{2-2}$$

where, K is a constant.

C is the concentration (volume fraction) of the precursor solution.

ω is the spin speed.

Silicon, glass, calcium fluoride and quartz were used as substrates for the film preparation to compare the quality of films. The result indicated that the quality of a film depends very little on substrates, as long as the surfaces of the substrates are clean and smooth. Due to the light interference, the colors of the films on different substrates sometimes looked different. The films of $UO_2(OOCC_5H_{11})_2$, used for comparing the film quality on different substrates were prepared from acetone solution. Hydrogen-bonding solvents were not involved in these experiments. Thus, hydrogen-bonding interactions between the precursor solution and the substrate surface were small.

2.2.6 Photochemical deposition and characterization of uranium oxide films

A room temperature, photochemical method was used for the deposition of uranium oxide films via uranyl complex thin film precursors. A thin amorphous film of $UO_2(OH_2)(acac)_2$ was prepared by spin-coating. This thin film was photolyzed in the air or under low vacuum (1 torr). The photolysis led the loss of the organic ligands to form UO_3 film. Transmission FTIR was used to monitor the photoreactions. The photolysis of amorphous thin films of $UO_2(OH_2)(acac)_2$ resulted in the loss of all IR absorption bands associated with the acetylacetonate ligand. These bands were at 1574 cm^{-1}, 1524 cm^{-1}, 1429 cm^{-1}, 1362 cm^{-1}, 1271 cm^{-1} and 1015 cm^{-1}. The loss of the asymmetric stretching of uranyl group at 916 cm^{-1} was also observed. A band at 908 cm^{-1} appeared during the photolysis. The FTIR spectrum of the resultant film from photolysis was similar to the IR spectrum of UO_3 powder as well as that reported for δ-UO_3 by Hoekstra and Siegal.[78] Based on the similarity, the uranium containing product is assigned as UO_3.

Similar results were obtained for the photolysis of $UO_2(OH_2)$(t-butylacac)$_2$ thin films. The photolysis of $UO_2(OH_2)$(t-butylacac)$_2$ led to the loss of diketonate ligands. The FTIR results indicated the formation of UO_3 film.

The photolysis of thin films of $UO_2(OOCC_5H_{11})_2$ resulted in a reduction of the IR bands due to the carboxylate groups (1539 cm^{-1} and 1467 cm^{-1}). The intensity of the IR band of the U-O asymmetric stretch at 933 cm^{-1} was also reduced. These bands decreased to the baseline after prolonged photolysis. During the photolysis, a broad band at 890 cm^{-1} grew in (Figure 2-7). The appearance of the broad band at 890 cm^{-1} is presumably due to the formation of an intermediate. This band decreased and a band at 873 cm^{-1} appeared after prolonged photolysis. Based on the IR information and the literature data[78], we can conclude that the carboxylate ligands had been lost and uranium oxide (UO_3) had formed after prolonged photolysis.

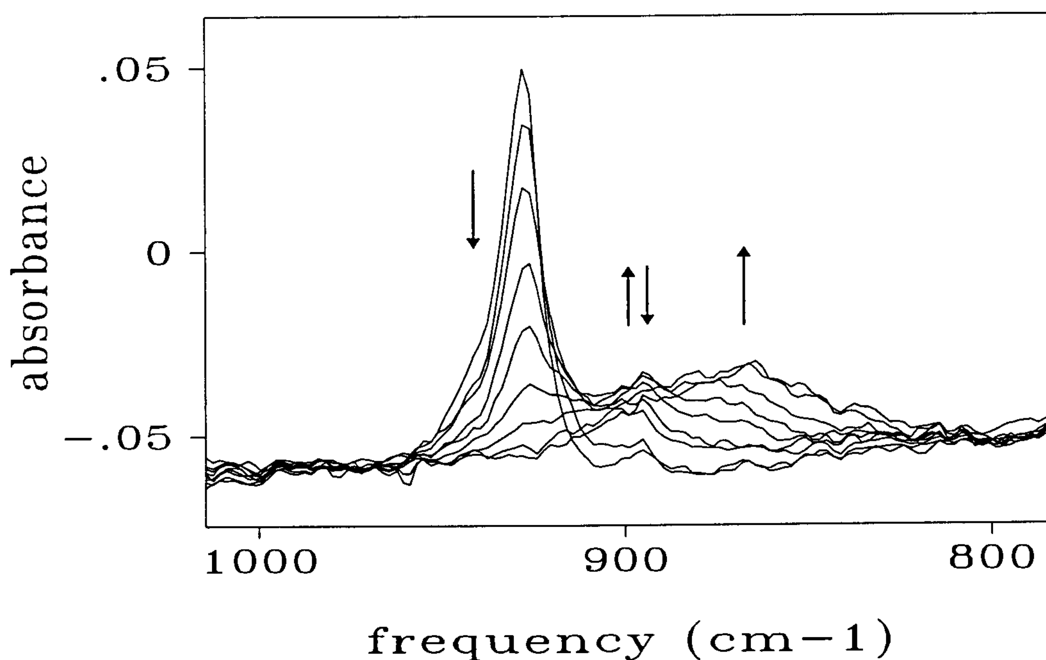

Figure 2-7 FTIR spectra of $UO_2(C_5H_{11}COO)_2$ upon photolysis with 334 nm light for 0, 20, 40, 60, 80, 100, 120, 168 and 1300 minutes

Similar experiments were conducted for all uranyl carboxylate complexes. Two of them showed similarly stable intermediates as described above during photolysis. The other four did not exhibit observable intermediates. A detailed description of the intermediates will be given in Chapter 3. The final FTIR spectra indicated the loss of all the carboxylate ligands and the formation of UO_3 except for complex $UO_2(OOCC_6H_4OC_2H_5)_2$. In this case the prolonged photolysis did not result in the disappearance of IR absorption bands associated with organic ligands. The film resultant from the photolysis of $UO_2(OOCC_6H_4OC_2H_5)_2$ still contains the carboxylate group.

Auger electron spectroscopy was also used to examine the films resulting from photolysis. The quantitative analysis of uranium by AES has been difficult due to the lack of a uranium sensitivity factor. The composition analysis of the resultant uranium oxide films was accomplished by comparing the Auger electron spectra of the resultant films with a standard UO_3 sample. The relative uranium and oxygen peak ratio obtained from the standard UO_3 sample was compared with the uranium and oxygen peak ratio found in the spectra of resultant films.

An Auger spectrum of a UO_3 pellet made of UO_3 powder was first obtained. Peaks at 72, 87, 280 eV corresponding to uranium and a peak at 500 eV associated with oxygen appeared clearly on the spectrum. The ratio of the intensity of the 500 eV and the 72 eV peaks (I_O/I_U) was found to be about 3.9. According to the Equation 1-8, the atomic fraction for the standard UO_3 is shown in Equation 2-3.

$$[C_O/C_U]_{standard} = (I_O/S_O)/(I_U/S_U) = (I_O/I_U)(S_U/S_O) = 3 \qquad 2\text{-}3$$

where, C_O is the atomic fraction of O in the sample;

C_U is the atomic fraction of U in the sample;

I_O is the intensity of the 500 eV peak in the UO_3 Auger spectrum.

I_U is the intensity of the 72 eV peak in the UO_3 Auger spectrum.

S_O and S_U are the sensitivity factors of O and U.

By knowing the I_O/I_U ratio, which was measured to be 3.9, S_U/S_O is calculated to be 3/3.9. Equation 2-4 is then used to calculate the O, U atomic ratio of the resultant photolyzed films.

$$[C_O/C_U]_{film} = (I'_O/S_O)/(I'_U/S_U) = (I'_O/I'_U)(S_U/S_O)$$
$$= (3/3.9)(I'_O/I'_U) \qquad 2\text{-}4$$

where, I'_O is the intensity of the 500 eV peak in the Auger spectrum of the film.

I'_U is the intensity of the 78 eV peak in the Auger spectrum of the film.

The Auger spectrum of a film resulting from the photolysis of $UO_2(OOCC_5H_{11})_2$ was compared with the Auger spectrum of the UO_3 pellet. The spectra were found to be similar as shown in Figure 2-8(a) and (b). The I'_O/I'_U in the spectrum of the resultant film was 1:3.9, which is the same as that found in the UO_3 pellet spectrum. Therefore, the AES is consistent with the FTIR result, both indicating the production of a UO_3 film from the photolysis of a $UO_2(OOCC_5H_{11})_2$ film.

All of the films produced by photolysis of the uranyl complex thin films were examined by AES. The results are listed in Table 2-7. The results showed that all of the uranyl complexes except $UO_2(OOCCH_2OC_2H_5)_2$ had the same approximate composition, which was $UO_{3\pm1}$ for final photolysis films. The result for $UO_2(OOCCH_2OC_2H_5)_2$ was $UO_{7\pm1}$. The film produced by the photolysis of $UO_2(OOCCH_2OC_2H_5)_2$ was very thin. This may affect the O:U ratio due to the contribution of oxygen from the substrate (SiO_2).

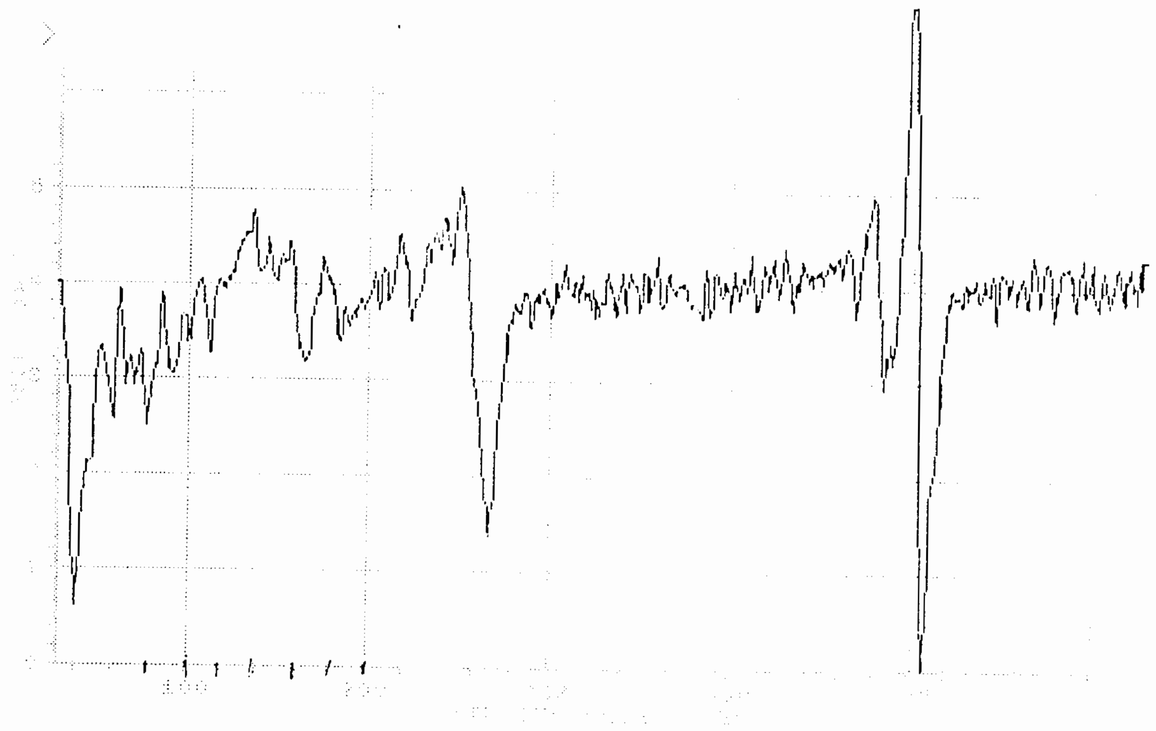

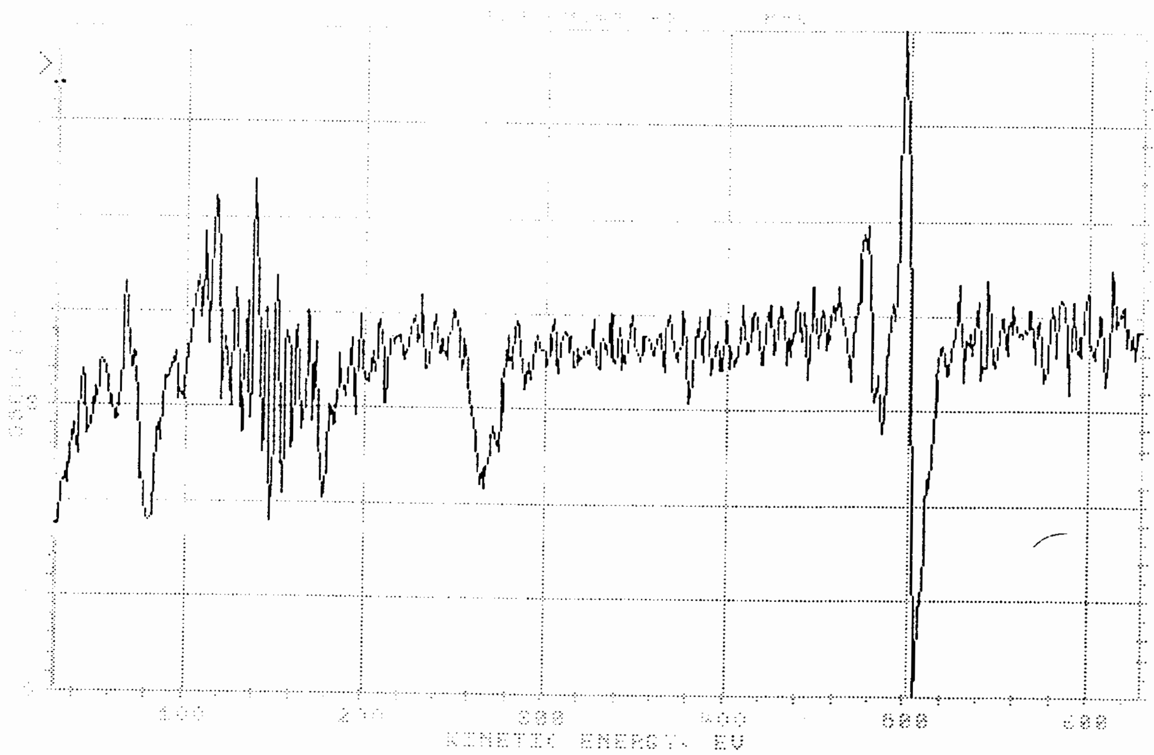

Figure 2-8 a) Auger electron spectrum of UO_3 pellet

b) Auger electron spectrum of a film resulting from the photolysis of $UO_2(OOCC_5H_{11})_2$

Table 2-7 Auger electron spectroscopic analysis data[a]

precursor	I_O/I_U [b]	composition (O/U)
UO_3 pellet	3.9	3
$UO_2(OOCCH_2OC_2H_5)_2$	9	7
$UO_2(OOCC_2H_4OC_2H_5)_2$	4.5	3.5
$UO_2(OOCCH_3)_2$	4.5	3.5
$UO_2(OOC(i)\text{-}C_3H_7)_2$	4.5	3.5
$UO_2(OOCC_5H_{11})_2$	3.9	3
$UO_2(OOCC_7H_7)_2$	3.9	3
$UO_2(OH_2)(acac)_2$	3.9	3
$UO_2(OH_2)(t\text{-}butylacac)_2$	4.5	3.5

a) Approximate 30% error in the measurements due to the noisy spectra obtained.

b) Use of 10 sec. sputtered spectra for the measurements.

The adhesions of resultant uranium oxide films on silicon substrates were examined by the Scotch Tape method.[79] Uranium oxide films resulting from all of the precursors showed good adhesion.

2.3 Conclusion

The photochemical deposition of uranium trioxide films though thin films of metal organic complex precursors has been demonstrated. Uranyl carboxylate and uranyl 1,3-diketonate complexes were found to be suitable precursor molecules. It has been shown that the uniformity of precursor films depends very little on the substrates. This makes the deposition of uranium oxide on X-ray transparent substrates for the purpose of making X-ray lithography mask possible.

2.4 Experimental Section

FTIR spectra were obtained with a Bomen MB-120 spectrophotometer at 4 cm-1 resolution. UV spectra were obtained using a HP 8452A diode array spectrophotometer. Elemental analyses were performed by M. K. Yang of the Micro analytical Laboratory at Simon Fraser University. Auger spectra were obtained using a PHI double pass CMA at 0.85 eV resolution with 3 kV ionization electron beams. Sample sputtering was done using 3 kV electron beam ionized Ar. They were done at the Surface Physics Laboratory, Department of Physics, Simon Fraser University. Film quality examination and film thickness measurements were conducted using a Leitz optical microscope equipped with an interferometer.

P-type Si(111) and p-type Si(100) wafers were purchased from Pacific Microelectronics Center and cut into 1x1.2 cm chips in house. The CaF_2 crystals were obtained from Wilmad Glass Co. Inc. $UO_2(OOCCH_3)_2 \cdot 2H_2O$ was purchased from Fluka Chemika. Uranium oxides were purchased from Strem Chemicals, Inc.

2.4.1 Synthesis of uranyl carboxylate complexes

All the complexes were characterized by Fourier transform infrared (FTIR) spectroscopy, UV -Vis spectroscopy and elemental analysis. The results were shown in Tables 2-3, 2-4, 2-5 and Table 2-6.

1) Preparation of uranium hydroxide:

$UO_2(OH)_2$ was prepared by the literature procedure.[80] A solution of uranium nitrite was prepared by dissolving 1.25 g of $UO_2(NO_3)_2 \cdot 6H_2O$ in 2 ml distilled water. A solution of KOH was prepared with 0.28 g KOH in 1 ml distilled water.

The KOH solution was gradually added to the stirred $UO_2(NO_3)_2$ solution. A yellow suspension was formed during the addition. The solution was filtered under water

filtration pump. The yellow filter residue, $UO_2(OH)_2$, was washed with water then methanol and dried under vacuum to give the desired compound $UO_2(OH)_2$.

2) Preparation of bis-(ethoxyacetato)dioxouranium (vi) $UO_2(OOCCH_2OC_2H_5)_2$ and bis-(β-ethoxypropionato)dioxouranium (vi) $UO_2(OOCC_2H_4OC_2H_5)_2$

The preparation of $UO_2(OOCCH_2OC_2H_5)_2$ and $UO_2(OOCC_2H_4OC_2H_5)_2$ were carried out by literature procedures.[63]

The $UO_2(OH)_2$ used in this preparation was obtained by the above procedures.

3) Preparation of $UO_2(OOC(i)\text{-}C_3H_7)_2$, $UO_2(OOCC_5H_{11})_2$, $UO_2(OOCC_6H_4OC_2H_5)_2$ and $UO_2(OOCCH_2C_6H_5)_2$

0.5 g ground $UO_2(OH)_2$ powder was reacted with 3 ml of iso-butanioc acid, (i-C_3H_7COOH), in a flask at 50°C while stirring overnight. A yellow liquid was obtained after reaction. Approximately 5 ml of anhydrous diethyl ether was added into the yellow liquid; the product was precipitated out. The flask was then put into a refrigerator for approximately 4 hours. The solution was carefully removed by pipette and the precipitate (product) was washed with anhydrous diethyl ether 6 times. The residue was redissolved in acetone. The acetone solution was filtered through a medium fine porosity fritted glass funnel to remove the unreacted $UO_2(OH)_2$. The pure product was obtained by removing the solvent under vacuum.

A similar procedure was used for the preparation of $UO_2(OOCC_5H_{11})_2$, $UO_2(OOCC_6H_4OC_2H_5)_2$ and $UO_2(OOCCH_2C_6H_5)_2$. For the preparation of $UO_2(OOCCH_2C_6H_5)_2$, phenyl acetic acid (1g) ligand, was dissolved in 5 ml benzene prior to the reaction with $UO_2(OH)_2$.

4) Preparation of uranyl 1,3-diketonate complexes: $UO_2(OH_2)(acac)_2$ and UO_2(t- butylacac)$_2$

The preparation of $UO_2(OH_2)(acac)_2$ and $UO_2(OH_2)(t\text{-butylacac})_2$ was carried out by literature methods.[62]

Yellow needle-like crystals of $UO_2(OH_2)(acac)_2$ were obtained by dissolving the raw product in hot CH_2Cl_2 and slowly adding a small amount of hexane. Cooling the solution in the refrigerator resulted in the crystallization of $UO_2(OH_2)(acac)_2$.

The purification of $UO_2(OH_2)(t\text{-butylacac})_2$ was done by washing the orange colored crystals resulting from the reaction with anhydrous diethyl ether.

2.4.2 Calibration of FTIR absorption on Si surfaces:

The calibration of absorption intensities for a uranyl complex, $UO_2(OOCCH_2OC_2H_5)_2$, was conducted. The procedure is described below.

A solution of $UO_2(OOCCH_2OC_2H_5)_2$ (0.0032g) was prepared in acetone (2 ml). A reference IR spectrum of Si substrate (a Si chip) was obtained. A drop of this solution (3.3 μl) was then placed on the Si chip. The solvent evaporated to leave a $UO_2(OOCCH_2OC_2H_5)_2$ film on the Si surface. The FTIR spectrum was then recorded. The area of the film was measured to be 0.28 cm^2 corresponding to a coverage of 2.4 molecules per $Å^2$. The same process was repeated several times giving the FTIR spectra shown in Figure 2-9(a). The corresponding calibration curve of absorbance at 931 cm^{-1} vs. molecules per $Å^2$ is shown in Figure 2-9(b). The slope of this calibration line (3.2×10^{-3} $Å^2$/molecule) was used to calculate the extinction coefficient, i.e., the absorbance cm^2/mol. The calculation, therefore, gave a value of 1.9×10^5 cm^2/mol that can be converted to 1.6×10^{-4}/monolayer by assuming that the volume of a $UO_2(OOCCH_2OC_2H_5)_2$ molecule[81] is 326 $Å^3$. Based on the calibration data, we can estimate the thickness of precursor films.

Similar experiments were conducted for all of the studied uranyl complexes. The linear calibration curves are shown in Figure 2-5 and 2-6. Table 2-8 is a summary of the calibration data of all precursor complexes.

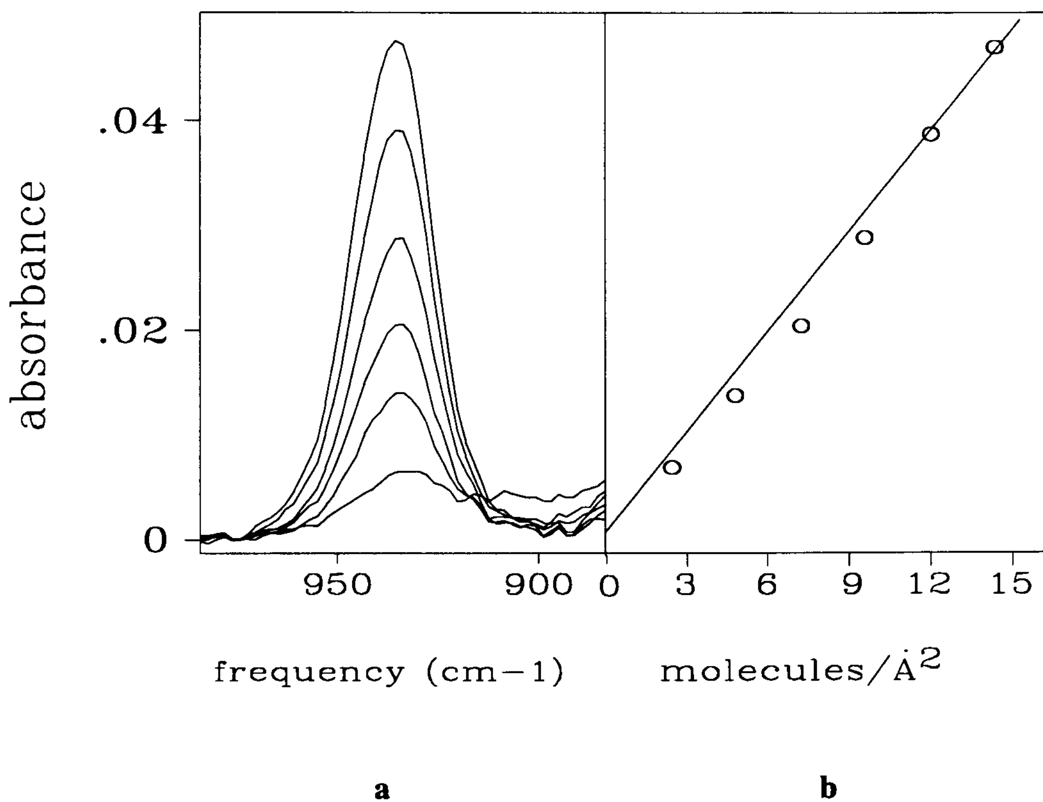

Figure 2-9 a) FTIR spectra of $UO_2(OOCCH_2OC_2H_5)_2$ for 2.4, 4.8, 7.2, 9.6, 12.0 and 14.4 molecules per $Å^2$ on a Si surface.

b) Plot of the absorbance of $\nu_{as}(O{=}U{=}O)$ of $UO_2(OOCCH_2OC_2H_5)_2$ versus coverage.

Table 2-8 Calibration of IR absorption on Si surface

complex	concentration of stock soln. ($10^{-3}M$)	calibration band	coverage of the complex (molecules./Å^2)	slope of the calibration curve (Å^2/10^3molecules)	estimated molecular V (Å^3)	ε^d ($cm^2/10^{-5}mol$) (abs./10^4mono-layer)
$UO_2(OOCCH_2OC_2H_5)_2$	3.36	938	2.38	3.2	326[a]	1.9(1.6)
$UO_2(OOCC_2H_4OC_2H_5)_2$	5.0	927	1.2	3.8	361[a]	2.3(2.3)
$UO_2(OOC(i)\text{-}C_3H_7)_2$	3.8	932	1.84	3.3	285[b]	2.0(1.4)
$UO_2(OOCC_5H_{11})_2$	9.2	933	5.88	7.1	361[b]	4.3(8.2)
$UO_2(OOCC_2H_4OC_6H_4)_2$	.50	928	0.2	8.6	513[c]	5.2(.27)
$UO_2(OOCCH_3)_2$	4.2	938	1.0	3.3	209[b]	2.0(.94)
$UO_2(OOCCH_2C_6H_5)_2$	4.1	926	2.2	4.4	437[b]	2.7(2.2)
$UO_2(OH_2)(acac)_2$	3.7	1524	3.2	3.3	323[c]	2.0(1.3)
$UO_2(OH_2)$(T-butylacac)$_2$	3.0	1351	2.0	4.4	551[c]	2.6(1.3)

a) Calculated from crystal structure data.[63]

b) Used the average atomic size of 19 Å^3/atom (not counting H atoms) from a) to calculate.

c) No. of atoms (excluding H atom) times 19 Å^3. The data is approximate due to structural difference.

d) Approximately 10% error due to the multiple measurements.

2.4.3 Preparation of thin films of uranyl complexes

Thin amorphous uranyl complex films on different substrates were prepared by the spin coating technique shown in Figure 2-10. A typical film preparation is described below:

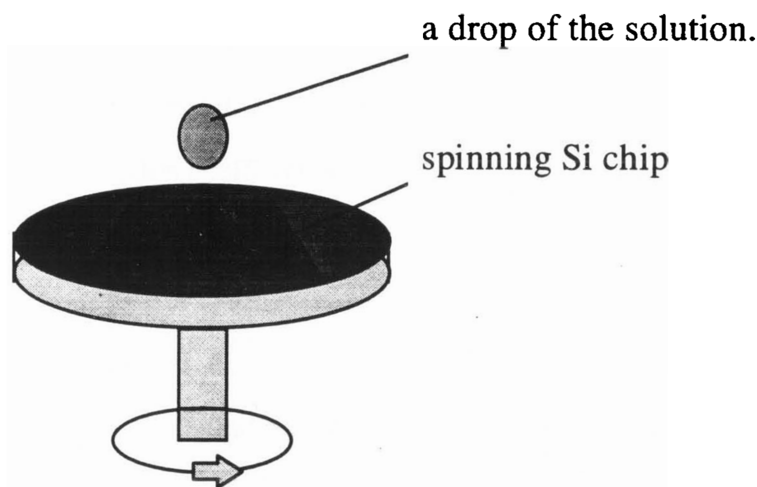

Figure 2-10 An illustration of the spin coating process

A p-type Si (111) chip was placed on the platform of a spinner. A fresh solution of $UO_2(OOCCH_2OC_2H_5)_2$ was prepared in acetone. A drop of this solution was then placed on the spinning Si chip. The solution spread due to the spinning and the volatile solvent, acetone, evaporated to leave a thin amorphous film on the Si surface.

The quality of films was checked by a Leitz optical microscope and the film thickness was measured by optical interferometry.[82]

The Scotch Tape method[79] was used to test the adhesion of the photodeposited uranium oxide films on silicon substrates. The test was done by pressing a piece of Scotch Tape onto the film and determining if the film is removed, partially removed or stayed on the substrate after the tape is pulled off.

2.4.4 Extinction coefficient of UV bands

A reference UV absorption spectrum and a FTIR spectrum of CaF_2 crystal were obtained prior to the film deposition. A film of uranyl complex was deposited on the CaF_2 surface by the spin coating technique described above. The UV-Vis absorption spectrum of this film was then recorded with a HP 8452A diode array spectrophotometer over a wavelength range of 190-800 nm. Subsequently, a FTIR spectrum of the same film was obtained at 4 cm^{-1} resolution with a Bomem MB-120 spectrophotometer.

The molar extinction coefficients of the UV bands are given by equation 2-3.

$$\varepsilon = A_{UV}\, \varepsilon_{IR} / A_{IR} \qquad 2\text{-}3$$

Where, ε_{IR} is the IR extinction coefficient calculated from the calibration experiment described in 2.4.2 and listed in Table 2-8.

A_{UV} is the UV absorbance at λmax.

A_{IR} is the absorbance of the IR band chosen in calibration curve.

2.4.5 Photolysis experiments

The photolysis of all of the uranyl complexes was done using the same procedure and is illustrated in Figure 2-11. The vacuum chamber that has a sample holder is made of aluminum. Two NaCl crystal windows are on the sides of the chamber to allow the irradiating UV light and monitoring IR beam to go through. A typical experiment was performed as follows: A p-type Si(111) chip was first placed on the sample holder to obtain a reference IR spectrum under vacuum prior to the film deposition. A thin amorphous film of complex $UO_2(OOCC_2H_4OC_2H_5)_2$ was deposited on the Si surface by spin coating from an acetone solution. The coated Si chip was then transferred to the vacuum chamber. The system was evacuated and the FTIR spectrum obtained. The

sample of $UO_2(OOCC_2H_4OC_2H_5)_2$ was then irradiated by the UV light (75 W high pressure Xe lamp) through a 10 cm water filter for 5 minutes. The FTIR spectrum obtained again. This procedure was repeated for the following accumulated photolysis times, 15, 40, 80, 140, 200 and 320 minutes, until all the IR bands due to the starting material decreased to the baseline.

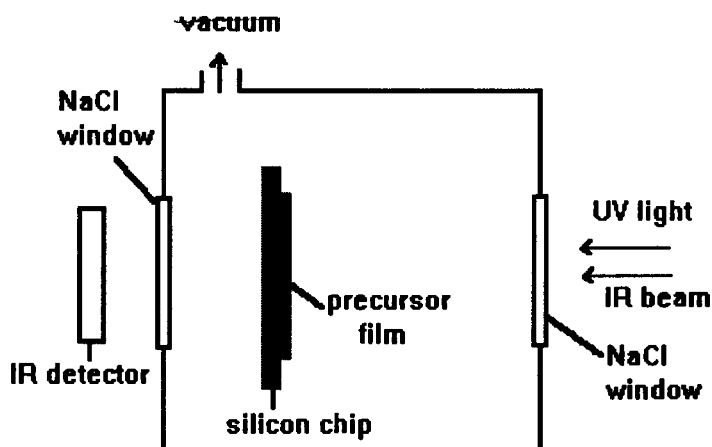

Figure 2-11 Photolysis experiment

Thin amorphous films of $UO_2(OOCC_2H_4OC_2H_5)_2$ were also photolyzed with a 254 nm output Hg arc lamp in air atmosphere. The procedure was as described above, but it was not necessary to put the film into the vacuum chamber.

2.4.6 Auger electron spectroscopy

A UO_3 pellet (about 0.1 cm thick) was made by mechanically conpressing the UO_3 powder. The UO_3 pellet was adhered on a silicon chip by silver paste and then placed on the sample holder used in the Auger spectrometer. Several Auger electron spectra were obtained for this UO_3 pellet sample. The average intensity ratio of the uranium and

uranium and oxygen peaks in the Auger electron spectra of the UO_3 pellet was used as a relative standard.

The initial Auger electron spectrum of the thin film resulting from photolysis of $UO_2(OOCC_5H_{11})_2$ was obtained. The film sample was then sputtered by Ar ions for 10 seconds. After sputtering, another Auger electron spectrum was obtained.

Auger electron spectra for all of the thin films resulting from the photolysis of other uranyl complexes were obtained in the same way. The intensity ratio of the uranium and oxygen peaks in the Auger electron spectrum of each resultant film were measured and compared to the ratio obtained for the UO_3 pellet. The stoichiometry was then determined.

Chapter 3. Mechanistic Study of The Photochemistry of Uranyl 1,3-diketonate Complexes and Uranyl Carboxylate Complexes as Thin Films on Silicon Surfaces

3.1 Introduction

A large amount of research has been done on the photochemistry of transition metal compounds. However, most photochemical studies have been conducted on species in solution, in the gas phase, or in a low temperature glass.[83] Due to the difficulties of separation and analysis of reactants and products, less work has been done in the solid state. [84] The photochemistry of compounds, in thin amorphous film state, remains relatively unexplored at the moment. As a reaction medium, amorphous thin films offer different properties from crystalline, solution and gaseous states. As described in chapter 2, we can make thin films of useful materials through this medium by using the technique, PDSF, developed in our laboratory. The deposition of thin films is an active area due in part to the applications in the electronics industry.[47-54, 85-88]

The study of the chemistry occurring in the amorphous thin film medium is to understand the mechanism of making useful materials. An understanding of the mechanism should allow us to design better precursors and processing conditions.. In this chapter, the mechanisms of photoreactions of uranyl carboxylate and uranyl 1,3-diketonate complexes as thin amorphous films on silicon surfaces are discussed.

3.2 Results

3.2.1 Photolysis of uranyl 1,3-diketonate complexes as thin films on silicon surfaces: quantum yields

The photolysis of $UO_2(OH_2)$(t-butylacac)$_2$ was conducted using 254 nm monochromatic light with an intensity of 9.3 x 10^{-10} Einsteins per second.* The FTIR spectroscopic changes of an approximately 580 monolayer $UO_2(OH_2)$(t-butylacac)$_2$ film upon photolysis were obtained. The photolysis of $UO_2(OH_2)$(t-butylacac)$_2$ led to the loss of all of the FTIR bands associated with diketonate ligand at 1564 cm^{-1}, 1547 cm^{-1}, 1503 cm^{-1}, 1374 cm^{-1}, 1351 cm^{-1}, 1226 cm^{-1} and 1146 cm^{-1} (Figure 3-1). The asymmetric stretching band of O=U=O at 887 cm^{-1} (not shown) decreased to leave a broad band with the frequency of 904 cm^{-1} after prolonged photolysis. The band of 904 cm^{-1} is consistent with the formation of UO_3.[71] There was no detectable intermediate observed during the photolysis.

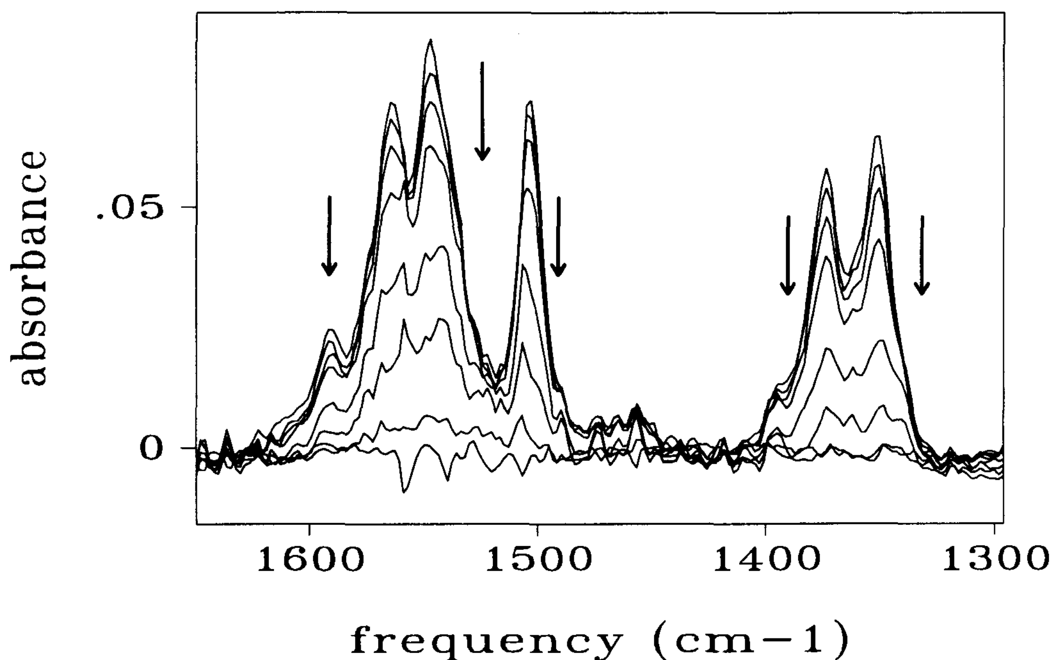

Figure 3-1 Changes in FTIR spectra of $UO_2(OH_2)$(t-butylacac)$_2$ thin film upon photolysis at 254 nm for 0, 35, 70, 130, 255, 420, 740 and 1360 minutes

---

*Light intensity was measured in mW/cm^2 using a radiometer. See the experimental section for the conversion of mW/cm^2 to einsteins/second.

The decomposition quantum yield of $UO_2(OH_2)$(t-butylacac)$_2$ was determined based on the FTIR spectroscopic data of the photolysis experiment. The IR absorbance of the starting material at 1351 cm^{-1} (Ao) and the absorbance of this band as a function of photolysis time (At) were measured. A plot of ln(Ao/At) versus photolysis time (Figure 3-2) was then made. This linear plot is consistent with a single photon process. The quantum yield was determined by the slope of the plot, the intensity of the irradiation light and the extinction coefficient of absorption at the irradiation wavelength according to Equation 3-24. The quantum yield was found to be 0.02.

A similar photolysis experiment was conducted with $UO_2(OH_2)(acac)_2$. The photolysis of thin films of $UO_2(OH_2)(acac)_2$ resulted in the loss of all IR absorption bands associated with the acetylacetonate ligand at 1574 cm^{-1}, 1524 cm^{-1}, 1429 cm^{-1}, 1362 cm^{-1}, 1271 cm^{-1} and 1015 cm^{-1}. The loss of the asymmetric stretching band of O=U=O at 916 cm^{-1} was accompanied by the appearance of a band at 908 cm^{-1} associated with the asymmetric stretching of UO_3.[53] The plot of ln(Ao/At) for the absorption at 1524 cm^{-1} versus photolysis time is a straight line (Figure 3-3) indicating a single photon process. The disappearance quantum yield of $UO_2(OH_2)(acac)_2$ was found to be 0.01.

$UO_2(OH_2)$(t-butylacac)$_2$ reacted with a higher quantum yield than $UO_2(OH_2)(acac)_2$. This is attributed to the bulky ligand in $UO_2(OH_2)$(t-butylacac)$_2$ molecule. The bulky ligand, t-butylacac, creates spaces between molecules in the film to allow the photochemically produced fragments to eject from the surface.

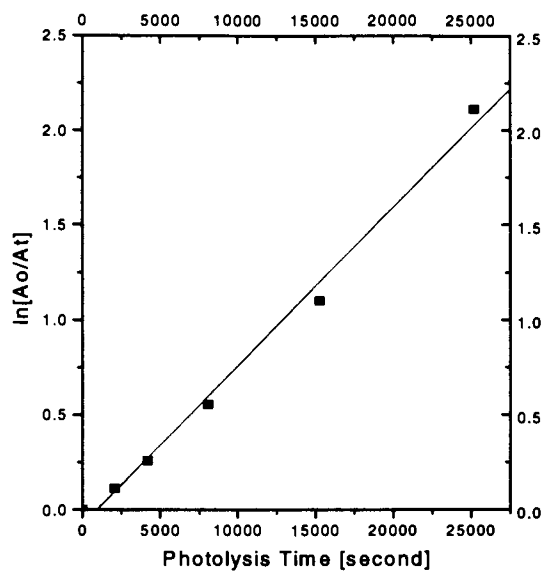

Figure 3-2 Logarithmic plot of absorbances versus photolysis time in the photolysis of $UO_2(OH_2)$(t-butylacac)$_2$ at 254 nm

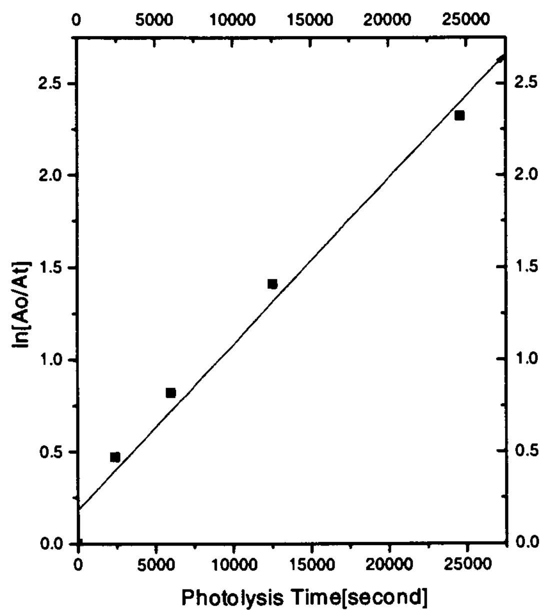

Figure 3-3 Logarithmic plot of absorbances versus photolysis time in the photolysis of $UO_2(OH_2)(acac)_2$ at 254 nm

Both the photolysis of $UO_2(OH_2)(acac)_2$ and $UO_2(OH_2)$(t-butylacac)$_2$ are single photon processes. The photoreaction of $UO_2(OH_2)(acac)_2$ and $UO_2(OH_2)$(t-butylacac)$_2$ can be outlined by Equation 3-1 and 3-2.

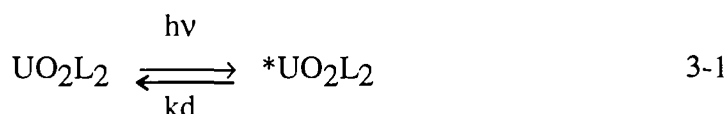

$$UO_2L_2 \underset{kd}{\overset{h\nu}{\rightleftarrows}} {}^*UO_2L_2 \qquad 3\text{-}1$$

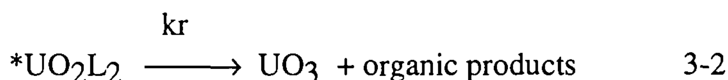

$$^*UO_2L_2 \xrightarrow{kr} UO_3 + \text{organic products} \qquad 3\text{-}2$$

L= acac or t-butylacac

3.2.2 Photolysis of $UO_2(OOCC_5H_{11})_2$, $UO_2(OOCC_2H_4OC_2H_5)_2$ and $UO_2(OOCCH_2OC_2H_5)_2$ as thin films on silicon surfaces: quantum yields

The photolysis of an amorphous film of $UO_2(OOCC_5H_{11})_2$ was conducted using 254 nm light with an intensity of 4.3 x 10^{-9} Einsteins per second. This resulted in a reduction in the intensity of the FTIR bands due to $\nu_{as}(COO)$, $\nu_s(COO)$ at 1538 and 1467 cm^{-1} as well as the FTIR band at 933 cm^{-1} due to $\nu_{as}(O=U=O)$. This indicated the loss of the $C_5H_{11}COO$ ligand from the precursor. A band at 890 cm^{-1} grew in (Figure 3-4). The appearance of this band at 890 cm^{-1} is presumably due to the formation of an intermediate. Upon further photolysis, this band decreased and was accompanied by the appearance of a broad band at 873 cm^{-1}. After prolonged photolysis, the 1538, 1467, and 933 cm^{-1} bands were no longer apparent indicating the loss of all of the carboxylate ligands. The broad band at 873 cm^{-1} remained after prolonged photolysis. The 873 cm^{-1} band is associated with the product, UO_3.

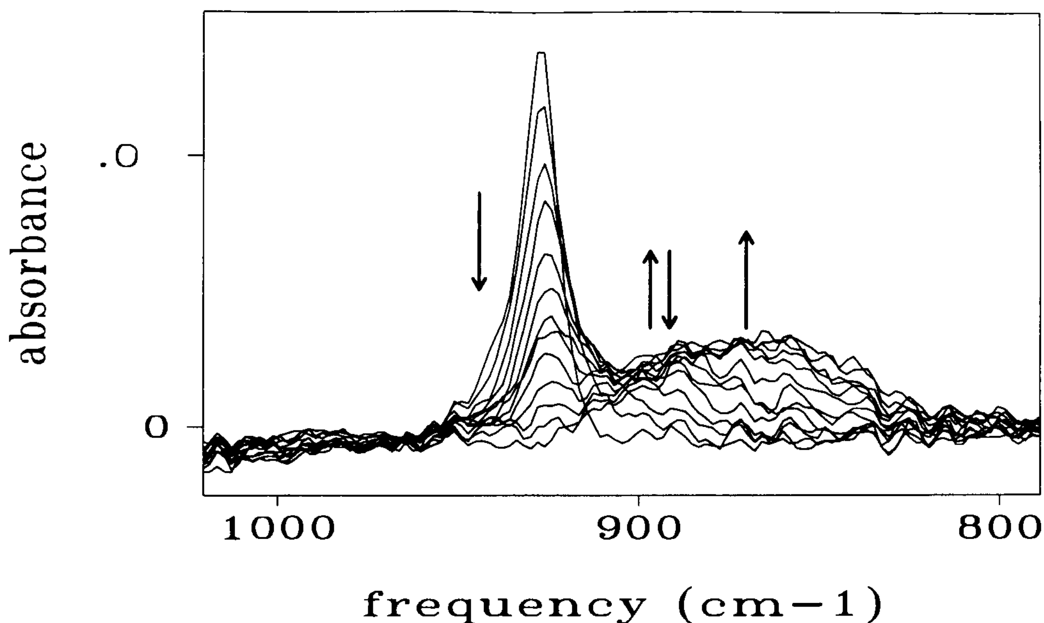

Figure 3-4 FTIR spectroscopic changes in ν_{as}(U-O) of a thin film of $UO_2(OOCC_5H_{11})_2$ on a Si surface upon photolysis for 0, 1, 2.5, 4, 6, 8, 10, 12, 15, 18, 22, 40 and 345 minutes

The decomposition quantum yield of $UO_2(OOCC_5H_{11})_2$ was determined. The ν_{as}(U-O) absorption band exhibited a single exponential decay as shown by a linear relationship between ln(Ao/At) and photolysis time. A plot of ln(Ao/At) versus photolysis time is shown in Figure 3-5. The quantum yield was determined using the slope of the line, the intensity of the irradiation light and the extinction coefficient (Equation 3-26). The quantum yield was found to be 0.36. However, the disappearance of the ν_{as}(COO) absorption band did not give a linear plot of ln(Ao/At) versus photolysis time. This is presumably due to the formation of a thermally stable intermediate having the same ν_{as}(COO) absorption band as the starting material. By plotting $\ln[(A_o-A_\infty)/(A_t-A_\infty)]$ (where A_∞ is the absorbance of the intermediate at maximum concentration) versus photolysis time; a straight line is obtained (Figure 3-6). Taking the slope of this line in conjunction with the light intensity as well as extinction coefficient, the same quantum yield (0.36) was obtained.

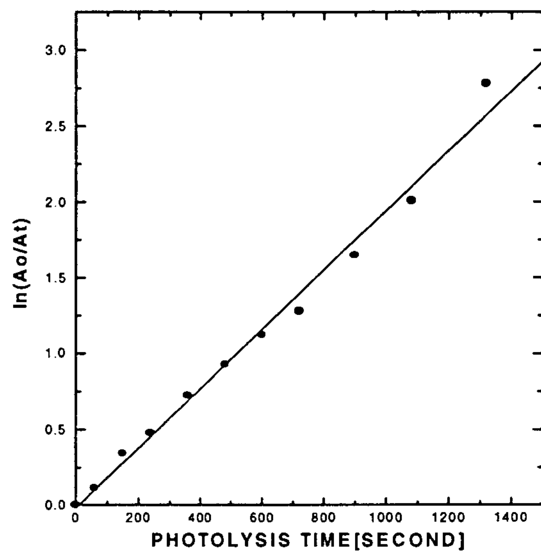

Figure 3-5 Logarithmic plot of Ao/At at ν_{as}(O=U=O) in $UO_2(OOCC_5H_{11})_2$ versus photolysis time

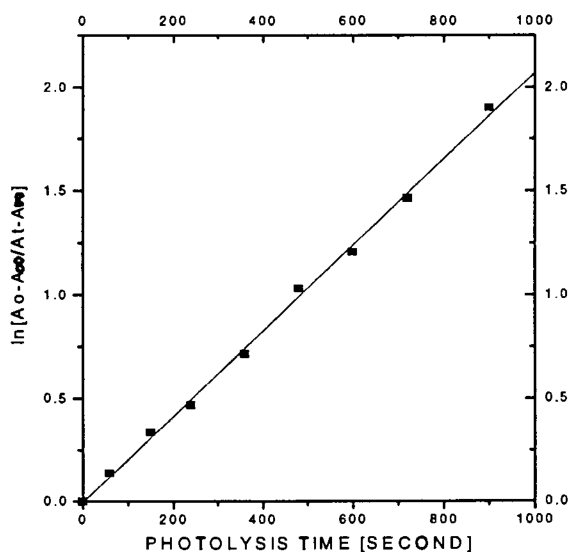

Figure 3-6 Logarithmic plot of (Ao-A∞)/(At-A∞) at ν_{as}(COO) in $UO_2(OOCC_5H_{11})_2$ versus photolysis time

The photolysis of an amorphous film of $UO_2(OOCC_5H_{11})_2$ was also conducted using 334 nm light with an intensity of 2.8×10^{-8} Einsteins per second. Similar results were obtained. To determine the disappearance quantum yield of the photolysis of $UO_2(OOCC_5H_{11})_2$ at 334 nm, the absorbances of $\nu_{as}(COO)$ absorption band were used to plot $\ln[(Ao-A\infty)/(At-A\infty)]$ versus photolysis time. The calculation gave the quantum yield of 0.04.

A 1000 monolayer amorphous film of $UO_2(OOCC_2H_4OC_2H_5)_2$ on a Si(100) surface was photolyzed at room temperature under vacuum (1 torr). The loss of absorptions at 1539 cm^{-1} and 1465 cm^{-1}, associated with $\nu_{as}(COO)$ and $\nu_s(COO)$ from the carboxylate group was evident. The photolysis also resulted in a reduction of absorption due to $\nu_{as}(O=U=O)$ at 927 cm^{-1} accompaning by the appearance of a band at 890 cm^{-1} (Figure 3-7). The intensity of this band increased upon photolysis, reached a maximum, and subsequently decreased upon further photolysis.

The reduction ratio* of bands assigned as due to $\nu_{as}(COO)$ and $\nu_s(COO)$ was found to be different from the reduction ratio of the band associated with $\nu_{as}(O=U=O)$. The $\nu_{as}(O=U=O)$ band decreased at a greater rate than the $\nu_{as}(COO)$ and $\nu_s(COO)$ bands. This indicates that an intermediate is formed during the photolysis and the intermediate has the FTIR bands consistent with those assigned to $\nu_{as}(COO)$ and $\nu_s(COO)$. After prolonged photolysis, the absorption bands assigned as $\nu_{as}(COO)$, $\nu_s(COO)$ and $\nu_{as}(O=U=O)$ decreased to the baseline indicating the loss of all of the organic ligands. The 890 cm^{-1} absorption band associated with the intermediate, decreased in intensity and was accompanied by the appearance of a broad band at 880 cm^{-1}. This broad absorption band remained after prolonged photolysis.

* reduction ratio is defined as :(Ao-At)/Ao, where Ao and At are the IR band absorbances at the photolysis time of 0 and t.

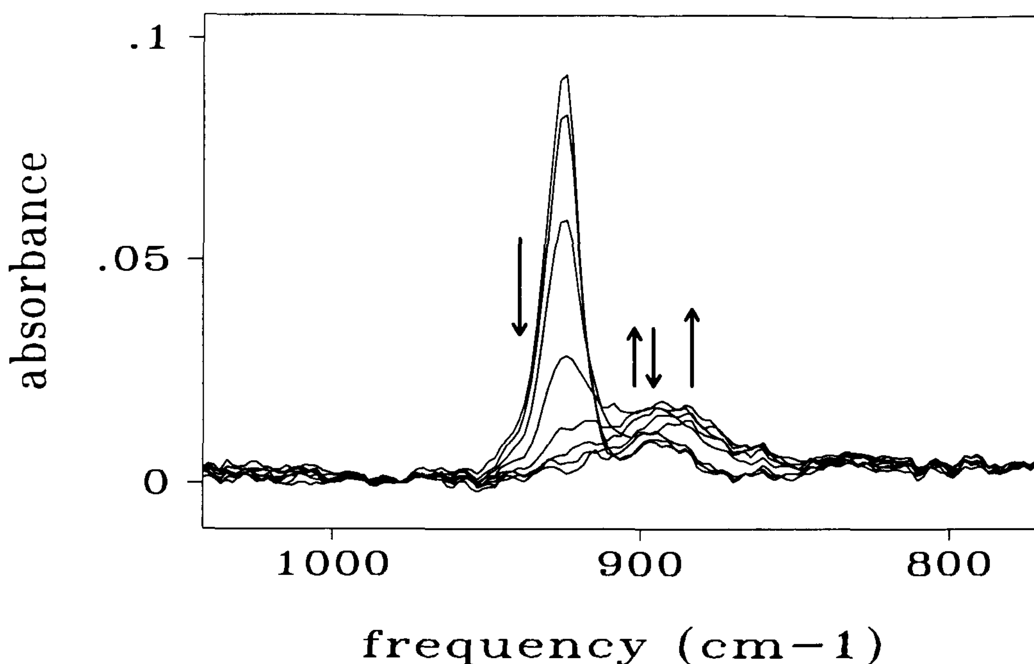

Figure 3-7 FTIR spectroscopic changes in ν_{as} (U-O) of a thin film of $UO_2(OOCC_2H_4OC_2H_5)_2$ on a Si surface upon photolysis for 0, 5, 15, 40, 80, 140, 200 and 320 minutes

The photolysis of a $UO_2(OOCC_2H_4OC_2H_5)_2$ film on a silicon surface was also conducted in the air using 254 nm light. The results obtained were as described above. The quantum yield for the decomposition of $UO_2(OOCC_2H_4OC_2H_5)_2$ upon irradiation at 254 nm was determined using the absorbances of ν_{as}(COO) absorption band. From the slope of the plot of $\ln[(A_o-A_\infty)/(A_t-A_\infty)]$ versus photolysis time, the quantum yield was determined to be 0.30.

A similar photolysis experiment was conducted on $UO_2(OOCC_2H_4OC_2H_5)_2$ films with 334 nm light. The disappearance quantum yield of $UO_2(OOCC_2H_4OC_2H_5)_2$ at 334 nm was found to be 0.10.

The photolysis of $UO_2(OOCCH_2OC_2H_5)_2$ also resulted in an observable intermediate. The FTIR bands associated with ν_{as}(COO), ν_s(COO) decreased at a lower

rate than the FTIR band of $\nu_{as}(O=U=O)$. This indicates that the intermediate contains a carboxylate group. This intermediate is itself photosensitive. Both the absorption bands of the carboxylate group (1560 cm^{-1} and 1448 cm^{-1}) and uranyl group (938 cm^{-1}) decreased to the baseline upon prolonged photolysis.

Quantum yields for the decomposition of $UO_2(OOCCH_2OC_2H_5)_2$ upon irradiation at 254 nm and at 334 nm were measured as described for $UO_2(OOCC_2H_4OC_2H_5)_2$. The quantum yields were found to be 1.44 and 1.19 for 254 nm and 334 nm irradiation respectively.

The photoreactions of $UO_2(OOCC_5H_{11})_2$, $UO_2(OOCC_2H_4OC_2H_5)_2$ and $UO_2(OOCCH_2OC_2H_5)_2$ as thin films are summarized in Equations 3-3, 3-4 and 3-5. An intermediate with the carboxylate ligand portion was generated during the photolysis. The organic photofragments were ejected from the films as gaseous products. UO_3 was formed as final photolysis product.

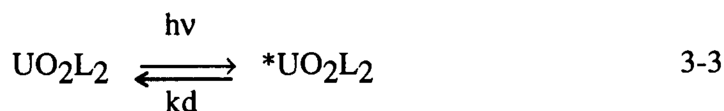

$$UO_2L_2 \underset{kd}{\overset{hv}{\rightleftarrows}} {}^*UO_2L_2 \qquad 3\text{-}3$$

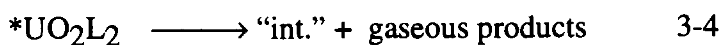

$$^*UO_2L_2 \longrightarrow \text{“int.”} + \text{gaseous products} \qquad 3\text{-}4$$

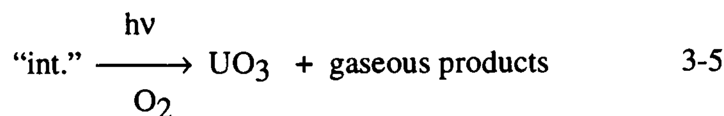

$$\text{“int.”} \xrightarrow[O_2]{hv} UO_3 + \text{gaseous products} \qquad 3\text{-}5$$

L= $OOCC_5H_{11}$, $OOCC_2H_4OC_2H_5$ or $OOCCH_2OC_2H_5$

“int.” = intermediate containing the carboxylate ligand

3.2.3 Photolysis of $UO_2(OOCCH_3)_2$, $UO_2(OOC(i)\text{-}C_3H_7)_2$ and $UO_2(OOCCH_2C_6H_5)_2$ as thin films on silicon surfaces: quantum yields

The photolysis experiment for thin films of $UO_2(OOCCH_3)_2$, was conducted at 254 nm using the same procedure. There was no intermediate observed. The intensity of the absorption bands of the carboxylate group (1529 cm^{-1} and 1450 cm^{-1}) and uranyl group (938 cm^{-1}) decreased at the same rate during photolysis. All of these absorption bands decayed to the baseline. A band at 873 cm^{-1}, which appeared during photolysis, is attributed to the formation of UO_3 as in the examples above.

Similar results were obtained for the photolysis of thin films of $UO_2(OOC(i)\text{-}C_3H_7)_2$ and $UO_2(OOCCH_2C_6H_5)_2$. The decomposition quantum yields of $UO_2(OOCCH_3)_2$, $UO_2(OOC(i)\text{-}C_3H_7)_2$ and $UO_2(OOCCH_2C_6H_5)_2$ films upon irradiation at 254 nm were measured to be 0.03, 0.10 and 0.52 respectively. The quantum yield of $UO_2(OOCCH_3)_2$ upon 334 nm irradiation was also measured and it was found to be 0.01.

Equation 3-6 and 3-7 summarize the photoreactions of thin films of $UO_2(OOCCH_3)_2$, $UO_2(OOC(i)\text{-}C_3H_7)_2$ and $UO_2(OOCCH_2C_6H_5)_2$.

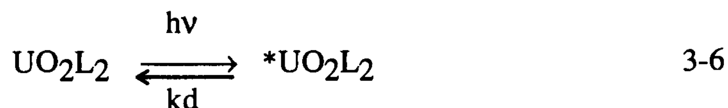

$$UO_2L_2 \underset{kd}{\overset{hv}{\rightleftharpoons}} {}^*UO_2L_2 \qquad 3\text{-}6$$

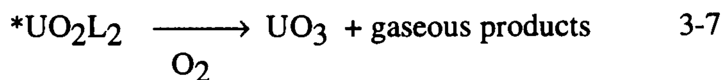

$$ {}^*UO_2L_2 \underset{O_2}{\longrightarrow} UO_3 + \text{gaseous products} \qquad 3\text{-}7$$

L= $OOCCH_3$, $OOC(i)\text{-}C_3H_7$ or $OOCCH_2C_6H_5$

3.2.4 Photolysis of $UO_2(OOCC_6H_4OC_2H_5)_2$ as thin films on silicon surfaces: quantum yields

The photolysis of thin films of $UO_2(OOCC_6H_4OC_2H_5)_2$ resulted in a reduction of the absorption bands corresponding to the carboxylate ligands. These bands did not completely disappear. Approximately 10% (intensity) of these bands remained after prolonged photolysis. This is attributed to the formation of a photo and thermally stable product. This stable product is proposed to be an U(IV) species having the formula of $UO(OC_6H_4OC_2H_5)(OOCC_6H_4OC_2H_5)$. This is consistent with the FTIR spectroscopic data. In section 3.3.2, the discussion of some intermediates having the similar formula as this product is given. Further study of this complex was not carried out since the complex is not suitable for making the material we need.

The quantum yield was measured for the reaction of $UO_2(OOCC_6H_4OC_2H_5)_2$ film with 254 nm light. The plot of $\ln[(A_o-A_\infty)/(A_t-A_\infty)]$ versus photolysis time was obtained. The quantum yield is determined to be 0.002. The photoreaction is outlined in Equation 3-8 and 3-9.

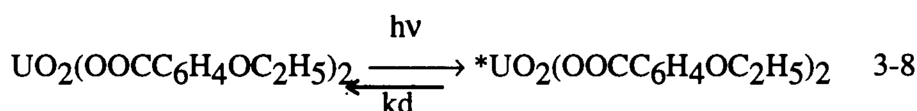

$$UO_2(OOCC_6H_4OC_2H_5)_2 \underset{kd}{\overset{h\nu}{\rightleftarrows}} {}^*UO_2(OOCC_6H_4OC_2H_5)_2 \qquad 3\text{-}8$$

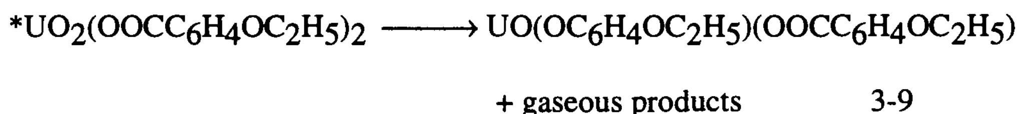

$$ {}^*UO_2(OOCC_6H_4OC_2H_5)_2 \longrightarrow UO(OC_6H_4OC_2H_5)(OOCC_6H_4OC_2H_5) + \text{gaseous products} \qquad 3\text{-}9$$

3.2.5 Summary of quantum yields

The quantum yields of all studied uranyl complexes are summarized in Table 3-1.

Table 3-1 Decomposition quantum yields for the photoreactions of uranyl complexes

complexes	Φ^{a}_{254}	Φ^{b}_{334}
$UO_2(OOCCH_2OC_2H_5)_2$	1.44	1.19
$UO_2(OOCCH_2C_6H_5)_2{}^{c}$	0.52	
$UO_2(OOCC_5H_{11})_2$	0.36	0.04
$UO_2(OOCC_2H_4OC_2H_5)_2$	0.30	0.10
$UO_2(OOC(i)\text{-}C_3H_7)_2$	0.10	
$UO_2(OH_2)(t\text{-butylacac})_2{}^{c}$	0.02	
$UO_2(OOCCH_3)_2$	0.03	0.01
$UO_2(OH_2)(acac)_2{}^{c}$	0.01	
$UO_2(OOCC_6H_4OC_2H_5)_2$	0.002	

a. λ=254 nm, I≈4.3 x 10^{-9} einsteins/sec.
b. λ=334 nm, I≈2.8 x 10^{-8} einsteins/sec.
c. λ=254 nm, I≈9.3 x 10^{-10} einsteins/sec.

3.2.6 Radical initiation experiments

A radical initiator, azo-isobutronitrile (AIBN), was added to solutions of uranyl carboxylate complexes to make precursor films composed of a uranyl complex and AIBN. FTIR spectroscopic changes in the dark were monitored in order to determine if the starting material will react with organic radical, R (R=$\cdot NCC(CH_3)_3$), produced from AIBN shown in Equation 3-10.

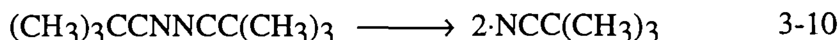

$$(CH_3)_3CCNNCC(CH_3)_3 \longrightarrow 2\cdot NCC(CH_3)_3 \qquad 3\text{-}10$$

A film prepared with AIBN and $UO_2(OOCC_5H_{11})_2$ was monitored by FTIR. In Figure 3-8, the overlaid FTIR spectra of a film of $UO_2(OOCC_5H_{11})_2$ co-deposited with AIBN in the region of the $\nu_{as}(COO)$ and the $\nu_s(COO)$ absorption bands are shown. The

presence of the radical initiator in the film resulted in a reduction of the intensities of FTIR bands associated with $\nu_{as}(COO)$, $\nu_s(COO)$ and $\nu_{as}(O{=}U{=}O)$ absorption. A band at 894 cm^{-1} (not shown) increased in intensity accompanying by the reduction of the bands associated with the starting material. The further reduction of the intensities of $\nu_{as}(COO)$, $\nu_s(COO)$ and $\nu_{as}(O{=}U{=}O)$ absorption bands did not happen after 4 days of prolonged reaction. This is presumably due to the generation of a stable species. This stable species is proposed to be UOORL since the intensities of $\nu_{as}(COO)$ and $\nu_s(COO)$ bands were 50% of that in the initial FTIR spectrum.

Similar results were obtained for the films composed of AIBN and either $UO_2(OOCCH_2OC_2H_5)_2$ or $UO_2(OOCC_2H_4OC_2H_5)_2$. The intensities of $\nu_{as}(COO)$ and $\nu_s(COO)$ bands reduced and remained at certain points. The results indicated a thermally stable species formed in the reaction of each case. The reduction ratios are shown in Table 3-2.

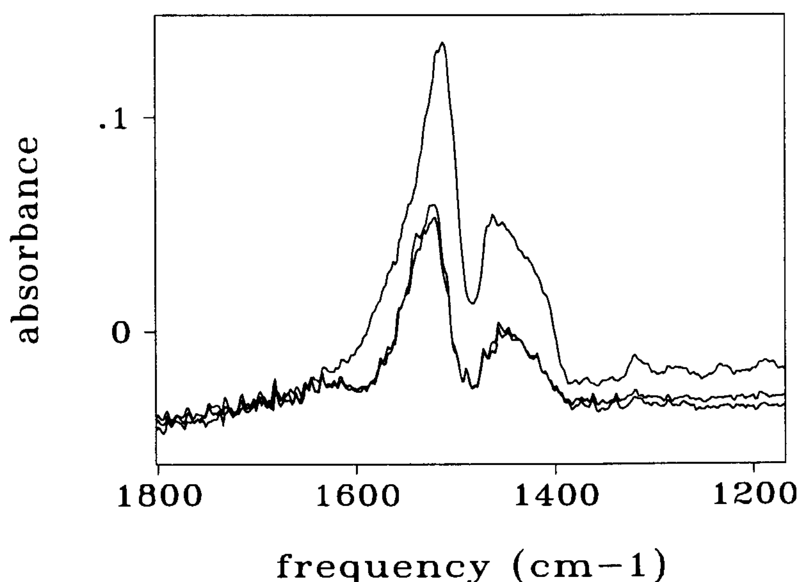

Figure 3-8 FTIR spectroscopic changes in the dark of a film with $UO_2(OOCC_5H_{11})_2$ and radical initiator AIBN

top: initial; middle: 18 hrs. bottom: 30 hrs.

Equation 3-11 describes the reactions of the radical initiator with $UO_2(OOCCH_2OC_2H_5)_2$, $UO_2(OOCC_2H_4OC_2H_5)_2$ and $UO_2(OOCC_5H_{11})_2$.

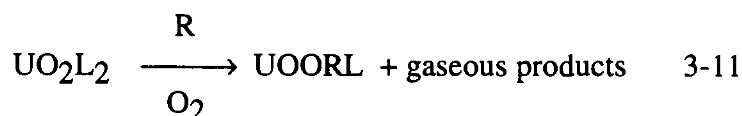

$$UO_2L_2 \xrightarrow[O_2]{R} UOORL + \text{gaseous products} \qquad 3\text{-}11$$

$R = \cdot NCC(CH_3)_3$

$L = OOCC_5H_{11}$, $OOCC_2H_4OC_2H_5$ or $OOCCH_2OC_2H_5$

The radical initiator AIBN co-deposited with $UO_2(OOCCH_3)_2$, $UO_2(OOC(i)\text{-}C_3H_7)_2$ or $UO_2(OOCCH_2C_6H_5)_2$ resulted in the loss of the intensity of the FTIR absorption bands associated with the $\nu_{as}(COO)$, $\nu_s(COO)$ and $\nu_{as}(U\text{-}O)$. No thermally stable intermediate was observed during the reaction. The reactions resulted in the formation of UO_3. Equation 3-12 summarizes the reaction.

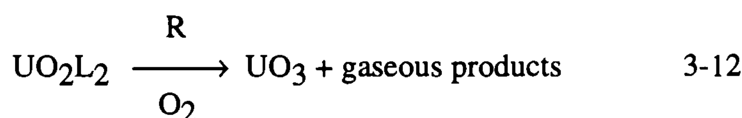

$$UO_2L_2 \xrightarrow[O_2]{R} UO_3 + \text{gaseous products} \qquad 3\text{-}12$$

$R = \cdot NCC(CH_3)_3$

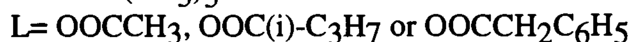

$L = OOCCH_3$, $OOC(i)\text{-}C_3H_7$ or $OOCCH_2C_6H_5$

The absorption bands for the co-deposited thin film of AIBN with $UO_2(OOCC_6H_4OC_2H_5)_2$ did not change. This indicates no reaction between AIBN and $UO_2(OOCC_6H_4OC_2H_5)_2$.

Table 3-2 summarizes the results of radical initiation experiments for all of uranyl carboxylate complexes. The absorption bands of $\nu_{as}(COO)$ and $\nu_s(COO)$ in $UO_2(OOCCH_3)_2$, $UO_2(OOC(i)\text{-}C_3H_7)_2$ and $UO_2(OOCCH_2C_6H_5)_2$ disappeared upon reacting with AIBN. For $UO_2(OOCCH_2OC_2H_5)_2$, $UO_2(OOCC_2H_4OC_2H_5)_2$ and $UO_2(OOCC_5H_{11})_2$, the intensities of $\nu_{as}(COO)$ and $\nu_s(COO)$ bands reduced to a certain

degree. The intensities of $\nu_{as}(COO)$ and $\nu_s(COO)$ bands in $UO_2(OOCC_6H_4OC_2H_5)_2$ did not change.

Table 3-2 Reduction ratio of the intensities of $\nu_{as}(COO)$ and $\nu_s(COO)$ bands upon radical initiation for 24 hrs

complexes	reduction ratio[a] (%)
$UO_2(OOCCH_2OC_2H_5)_2$	80
$UO_2(OOCC_2H_4OC_2H_5)_2$	40
$UO_2(OOCC_6H_4OC_2H_5)_2$	0
$UO_2(OOCCH_3)_2$	100
$UO_2(OOC(i)\text{-}C_3H_7)_2$	100
$UO_2(OOCC_5H_{11})_2$	50
$UO_2(OOCCH_2C_6H_5)_2$	100

a) (Ai-Af)/Ai, where Ai is the initial absorbance of $\nu_{as}(COO)$ or $\nu_s(COO)$ band of the co-deposited film. Af is absorbance of $\nu_{as}(COO)$ or $\nu_s(COO)$ band upon initiation for 24 hr.

3.2.7 Mass spectrometric analyses of organic photoproducts

Electron impact mass spectrometry (EIMS) was used for the identification of the volatile organic photoproducts. MS analysis of the volatile organic products formed from photolysis of a $UO_2(OH_2)(acac)_2$ film on silicon substrate was conducted. An $UO_2(OH_2)(acac)_2$ film on a silicon chip was prepared by spin-coating from an acetone solution. The film was irradiated in a sealed vessel under a static vacuum (10^{-3} torr). The mass spectra of the background (due to the air and the pumping system) were recorded. The valve of the vessel was then opened. About 200 mass spectra were recorded. A mass spectrum of the volatile photolysis products was obtained by subtracting the mass spectrum of the background from sample spectra. The spectrum had signals associated

with the molecular ion and fragments due to acetylacetone (acacH). Another organic photoproduct observed in the spectrum was an isomer of acacH, 3-hydroxyl, 3-methyl cyclobutanone. The MS result is listed in Table 3-3.

Table 3-3 MS analysis results of volatile products resulting from the photolysis of uranyl 1,3-diketonates

complex	M/Z	assignment[88, 90]
$UO_2(OH_2)(acac)_2$	100, 85, 43.	acacH
	100, 71, 57, 43.	$CH_2C(O)C(OH)(CH_3)CH_2$ (cyclic)
$UO_2(OH_2)$(t-butylacac)$_2$	184, 127, 109, 85, 81, 69, 57, 43, 41.	t-butylacacH
	114, 109, 57.	$(CH_3)_3CC(CH_3)_3$
	100, 85, 57, 43.	$CH_3COC(CH_3)_3$
	86, 85, 71, 57, 43.	$(CH_3)_3CCHO$
	84, 69, 43, 41.	$CH_2C(CH_3)COCH_3$

A similar experiment was conducted with $UO_2(OH_2)$(t-butylacac)$_2$. The result showed that the photolysis of a $UO_2(OH_2)$(t-butylacac)$_2$ film produced the free ligand, t-butylacacH. Other organic products observed in MS were $(CH_3)_3CC(CH_3)_3$, $CH_3COC(CH_3)_3$, $(CH_3)_3CCHO$ and $CH_2C(CH_3)COCH_3$. The detailed MS analysis result is listed in Table 3-3.

Combining the results obtained from the photolysis experiment and MS analysis, the photoreaction for $UO_2(OH_2)(acac)_2$ can be described in Equation 3-13. Equation 3-14 presents the photoreaction of $UO_2(OH_2)$(t-butylacac)$_2$.

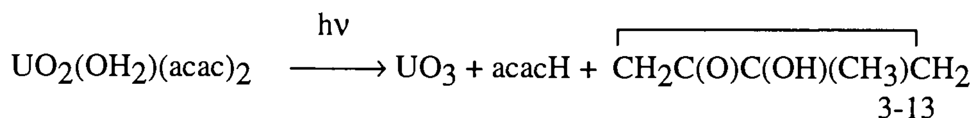

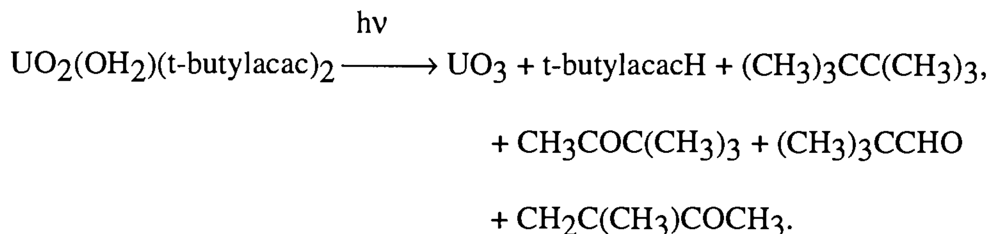

MS analysis of volatile organic products formed from photolysis of $UO_2(OOC(i)\text{-}C_3H_7)_2$ clearly showed the peaks for CO_2, C_6H_{14}, C_3H_8 and C_3H_6. CO_2 is the product of decarboxylation of the carboxyl radical $\cdot OOC(i)\text{-}C_3H_7$. The alkyl radical, $\cdot i\text{-}C_3H_7$ is the other half of the decarboxylation product. This alkyl radical leads to the radical coupling product, C_6H_{14} and radical disproportionation products, C_3H_8 and C_3H_6.

Similar MS analysis results have been obtained for the photolysis of thin films of $UO_2(OOCC_5H_{11})_2$. CO_2, $C_{10}H_{22}$, C_5H_{10} and C_5H_8 were observed in MS. CO_2 is the decarboxylation product. $C_{10}H_{22}$ is the coupling product of the alkyl radical $\cdot C_5H_{11}$. C_5H_{10} and C_5H_8 are the radical disproportionation products of $\cdot C_5H_{11}$.

Combining the results obtained from the photolysis experiment, radical initiation and MS analysis, the overall photoreaction of thin films of $UO_2(OOC(i)\text{-}C_3H_7)_2$ and $UO_2(OOCC_5H_{11})_2$ is given in Equation 3-15.

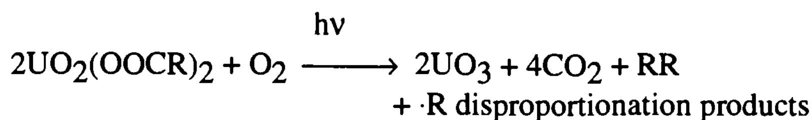

$$2UO_2(OOCR)_2 + O_2 \xrightarrow{h\nu} 2UO_3 + 4CO_2 + RR + \cdot R \text{ disproportionation products}$$

3-15

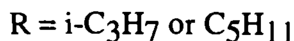

$R = i\text{-}C_3H_7$ or C_5H_{11}

The volatile products of the photolysis of a $UO_2(OOCCH_2OC_2H_5)_2$ film observed in MS were CO_2, $CH_3OC_2H_5$ and $CHOC_2H_5$. Again, CO_2 is the decarboxylation product. $CH_3OC_2H_5$ and $CHOC_2H_5$ are the radical disproportionation products of $\cdot CH_2OC_2H_5$. The radical coupling product, $C_2H_5OCH_2CH_2OC_2H_5$, was not observed in MS. Equation 3-16 presents the overall reaction for the photolysis of $UO_2(OOCCH_2OC_2H_5)_2$ films on silicon surfaces.

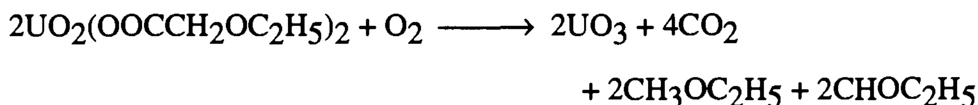

$$2UO_2(OOCCH_2OC_2H_5)_2 + O_2 \longrightarrow 2UO_3 + 4CO_2 + 2CH_3OC_2H_5 + 2CHOC_2H_5$$

3-16

MS analysis of the atmosphere over a photolyzed $UO_2(OOCCH_2C_6H_5)_2$ film indicated CO_2 and toluene. CO_2 is the decarboxylation product. Toluene is one part of the disproportionation products of the radical $\cdot CH_2C_6H_5$, which was formed from the decarboxylation of the carboxyl radical. The other half of the disproportionation products, C_6H_5CH, (benzoyl carbene) was not shown since this species is highly reactive.[91] The radical coupling product of $\cdot CH_2C_6H_5$, $C_{14}H_{14}$, showed only its fragments (M/Z91, 77, 65, 64, 63, 51, 50, 39, 38) in the spectrum due to its high tendency of fragmentation.[92]

The MS analysis results showed that the photolysis of a film of $UO_2(OOCCH_3)_2$ produced CO_2, methane and ethane as organic products.

Equation 3-17 presents the overall photoreaction of thin films of $UO_2(OOCCH_2C_6H_5)_2$ and $UO_2(OOCCH_3)_2$.

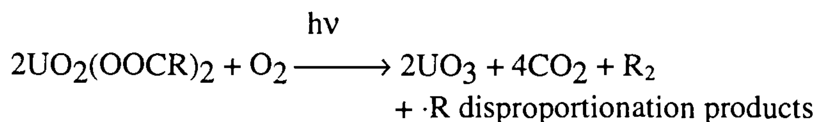

$$2UO_2(OOCR)_2 + O_2 \xrightarrow{h\nu} 2UO_3 + 4CO_2 + R_2 + \cdot R \text{ disproportionation products}$$

3-17

$$R = CH_2C_6H_5 \text{ or } CH_3$$

MS analysis of the atmosphere over a photolyzed $UO_2(OOCC_2H_4OC_2H_5)_2$ film indicated CO_2, $C_2H_5OCH{=}CH_2$, $C_2H_5OC_2H_5$, C_2H_5OH, CH_3CHO and ethylene. The MS result showed the radical disproportionation products resulted from the initial alkyl radical $\cdot C_2H_4OC_2H_5$. They were $C_2H_5OCH{=}CH_2$ and $C_2H_5OC_2H_5$. The radical disproportionation products resulting from the OC_2H_5 radical, C_2H_5OH and CH_3CHO, were also observed in MS. Presumably the radical $\cdot OC_2H_5$ and ethylene are formed from $\cdot C_2H_4OC_2H_5$ by β-scission.[93] The overall photoreaction of the thin film of $UO_2(OOCC_2H_4OC_2H_5)_2$ is outlined in Equation 3-18

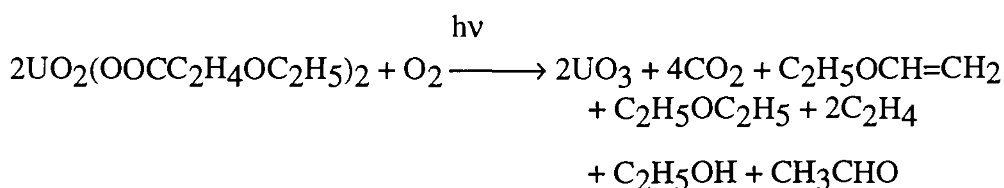

$$2UO_2(OOCC_2H_4OC_2H_5)_2 + O_2 \xrightarrow{h\nu} 2UO_3 + 4CO_2 + C_2H_5OCH{=}CH_2 + C_2H_5OC_2H_5 + 2C_2H_4 + C_2H_5OH + CH_3CHO$$

3-18

Mass spectrometry indicates that the major volatile products resulting from photolysis of uranyl carboxylate complexes are decarboxylation product, CO_2 and alkyl radical coupling product as well as radical disproportionation products. The results are summarized in Table 3-4.

Table 3-4. Results of MS analysis of volatile products from photolysis

complex	R	M/Z[a]	assignment[90, 92]
$UO_2(OOC(i)\text{-}C_3H_7)_2$	$i\text{-}C_3H_7$	86	C_6H_{14}
		44[b]	C_3H_8
		42	C_3H_6 ($CH_3CH{=}CH_2$)
		44[b]	CO_2
$UO_2(OOCC_5H_{11})_2$	C_5H_{11}	142	$C_{10}H_{22}$
		72	C_5H_{12}
		70	C_5H_{10} ($C_3H_7CH{=}CH_2$)
		44	CO_2
$UO_2(OOCCH_2OC_2H_5)_2$	$CH_2OC_2H_5$	60	$C_2H_5OCH_3$
		58	C_2H_5CHO
		44	CO_2
$UO_2(OOCCH_3)_2$	CH_3	44	CO_2
		30	C_2H_6
		16	CH_4
$UO_2(OOCCH_2C_6H_5)_2$	$CH_2C_6H_5$	92	C_7H_8
		44	CO_2
$UO_2(OOCC_2H_4OC_2H_5)_2$	$C_2H_4OC_2H_5$ (C_2H_4 R')	74	$C_2H_5OC_2H_5$ (RH)
		72	$C_2H_5OCH{=}CH_2$
		46	C_2H_5OH (R'H)
		44	CH_3CHO
		44	CO_2

a. molecular ions only
b. M+1 was used to distinguish these two products.

3.3 Discussion

3.3.1 Mechanism of the photolysis of uranyl 1,3-diketonate complexes

FTIR spectroscopy indicated that the photolysis of $UO_2(OH_2)(acac)_2$ film did not result in a thermally stable intermediate. The linear plot of ln[Ao/At] versus photolysis time for the 254 nm photolysis of $UO_2(OH_2)(acac)_2$ was consistent with a single photon process. Both FTIR and Auger electron spectroscopy indicated that the photolysis of $UO_2(OH_2)(acac)_2$ generated UO_3 as the surface product. MS indicated that the organic photoproducts were Hacac and 3-hydroxy, 3-methyl cyclobutanone. The mechanism of the photoreaction of $UO_2(OH_2)(acac)_2$ film, shown in Scheme 3-1, is consistent with all these results.

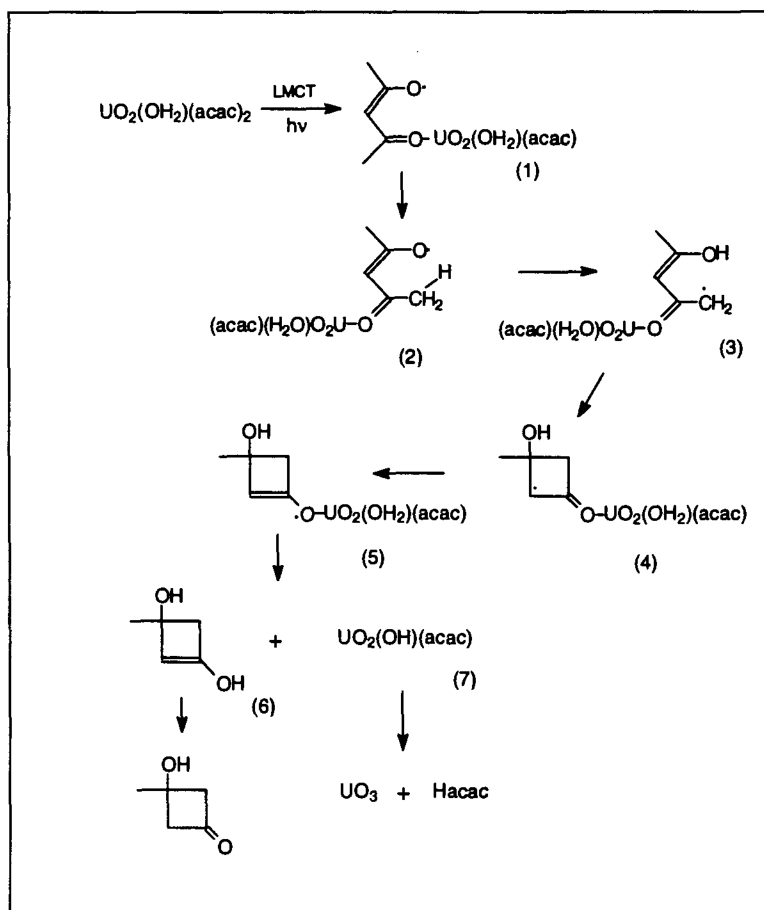

Scheme 3-1 Mechanism of the photoreaction of uranyl 1,3-diketonate complexes

The starting material, $UO_2(OH_2)(acac)_2$, absorbs a photon undergoing a ligand to metal charge transfer (LMCT) to generate radical species (1). (1) isomerizes to form species (2) via bond rotation. A γ-hydrogen transfer, though a five-member ring,[94] leads to radical species (3). The radical (3) cyclizes to form radical (4). (4) becomes (5) via a radical rearrangement. (5) undergoes a hydrogen abstraction to give a four-member ring (6) and $UO_2(OH)(acac)$ (7). (6) is unstable. It isomerizes to give the product, 3-hydroxy, 3-methyl cyclobutanone.[95] (7) is also unstable. It decomposes to produce UO_3 and acacH.

For the photolysis of $UO_2(OH_2)(t\text{-butylacac})_2$ film, the FTIR spectroscopy indicated that the reaction was a single photon process. As the result of the single photon process, the plot of ln[Ao/At] versus photolysis time was linear. Both FTIR and Auger electron spectroscopy indicated that UO_3 was the final surface product. The organic products generated from the photolysis were t-butylacacH, $(CH_3)_3CC(CH_3)_3$, $CH_3COC(CH_3)_3$, $CH_2C(CH_3)COCH_3$ and $(CH_3)_2CHCOCH_3$. These products were observed in mass spectrometry. Scheme 3-2 is the proposed mechanism that accounts for all of the observations.

Absorption of a photon by the starting material results in a MLCT transition. This leads to the production of species (1). The unstable species (1) fragments[96] to form (2) and (3). (2) undergoes a disproportionation process to give product (4) and (5). The carbonyl radical (2) also undergoes fragmentation[97] to form carbon monoxide and a t-butyl radical. This t-butyl radical formed radical coupling product, 2,2,3,3-tetramethyl butane. (3) becomes a neutral molecule (6) by hydrogen abstraction from a coordinated water molecule. UO_3 and t-butylacac radical are also produced in this step. Molecule (6) is an unstable enol form. It rearranges to the stable ketone form (7) as the product. The radical generated from the fragmentation of (3), t-butylacac radical, reacts with (2) to produce t-butylacacH and (5).

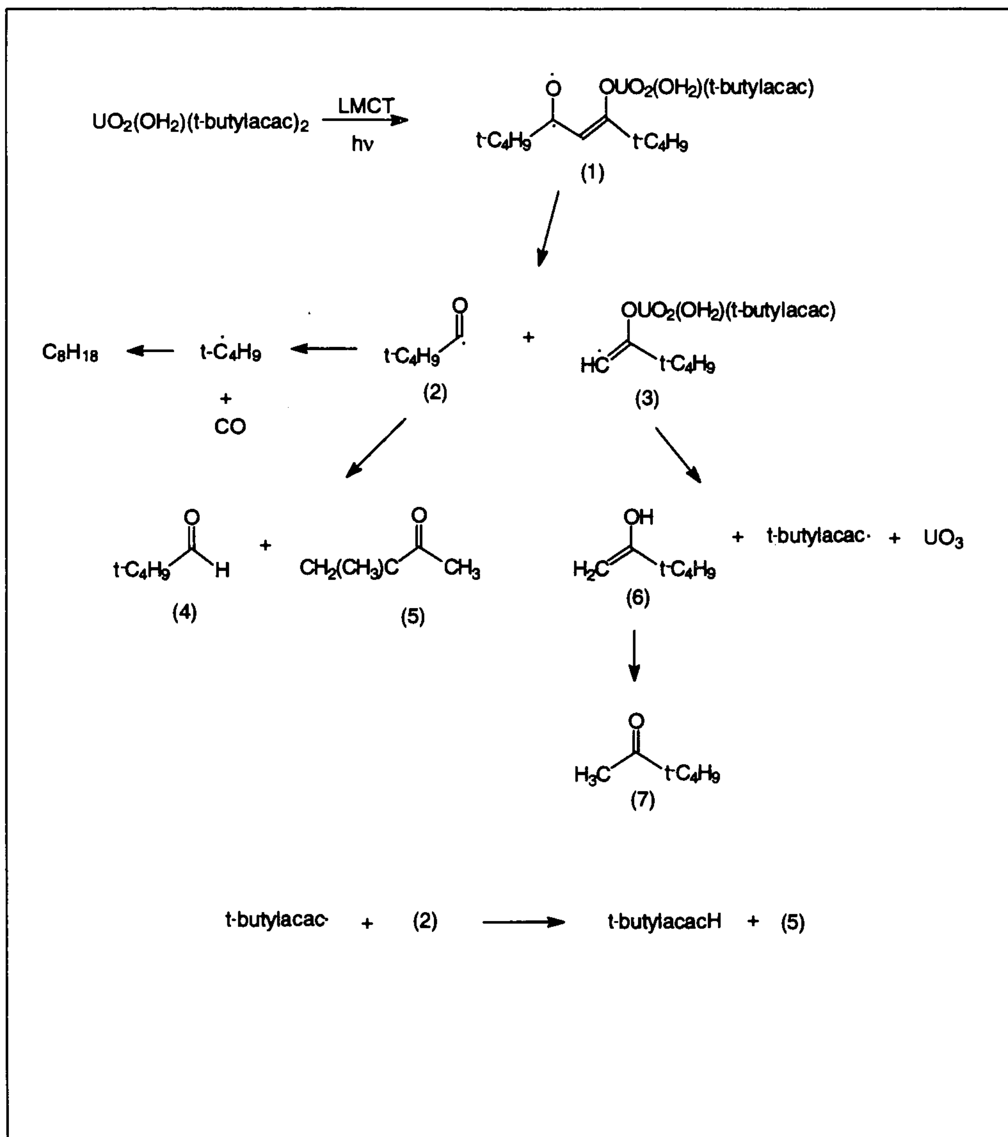

Scheme 3-2 Mechanism of photoreactions of $UO_2(OH_2)$(t-butylacac)$_2$

3.3.2 Photochemistry of uranyl carboxylate complexes as thin films on silicon surfaces

The quantum yields (254 nm) for uranyl carboxylate complexes were high. Both $UO_2(OOCCH_2OC_2H_5)_2$ and $UO_2(OOCCH_2C_6H_5)_2$ reacted with the quantum yields greater than 1. This may indicate a chain process exists according to the second law[98] of photochemistry. Most likely the chain process is a radical chain process since our experiments showed products consistent with radical reactivity. A reaction product or an intermediate must react with the starting material to result in a chain reaction. The results of radical initiation experiments demonstrated that the uranyl carboxylate complexes can react with a radical. This supports the radical chain process hypothesis. The radical produced in the first photochemical step of the photolysis further reacts with the starting material resulting in a high quantum yield or a quantum yield greater than 1. The photolysis products also supported the radical chain process hypothesis. This was demonstrated by seeing the products of radical reactions in MS.

Two types of photoreaction processes can be written for the uranyl carboxylate complexes. Process type 1 is for the complexes, $UO_2(OOCCH_2OC_2H_5)_2$, $UO_2(OOCC_2H_4OC_2H_5)_2$ and $UO_2(OOCC_5H_{11})_2$. Intermediates were observed in the FTIR during the photoreaction of these complexes. Process type 2 is for the reactions of $UO_2(OOCCH_3)_2$, $UO_2(OOC(i)\text{-}C_3H_7)_2$, and $UO_2(OOCCH_2C_6H_5)_2$. No intermediates were observed during the photoreaction of these complexes.

Here, $UO_2(OOCC_5H_{11})_2$ is used as an example to describe type 1 photoreactions. In the first step, the starting material $UO_2(OOCC_5H_{11})_2$ decarboxylated[99] upon absorbing a photon to give CO_2, UO_2 and radical $\cdot C_5H_{11}$. This was indicated by the observation of the reduction of the intensity of $\nu_{as}(COO)$, $\nu_s(COO)$ and $\nu_{as}(O{=}U{=}O)$ absorption bands upon photolysis. It was also evidenced by the radical coupling and disproportionation products of $\cdot C_5H_{11}$ in MS. The observation of CO_2 in

MS demonstrated this decarboxylation step. The radical $\cdot C_5H_{11}$ could then react with the starting material forming a stable intermediate, $UOO(C_5H_{11})(OOCC_5H_{11})$. This intermediate was consistent with the FTIR spectra obtained for the photolysis experiment. By showing 50% reduction of the intensities of $\nu_{as}(COO)$ and $\nu_s(COO)$ bands, the radical initiation experiment was also consistent with the formation of a stable intermediate. The final step was that the thermally stable intermediate, $UOO(C_5H_{11})(OOCC_5H_{11})$, absorbed a photon to generate CO_2, UO_2 and $\cdot C_5H_{11}$. This is also demonstrated by the disappearance of $\nu_{as}(COO)$, $\nu_s(COO)$ and $\nu_{as}(U\text{-}O)$ absorption bands on photolysis.

The decomposition of $UO_2(OOCCH_3)_2$, $UO_2(OOC(i)\text{-}C_3H_7)_2$, and $UO_2(OOCCH_2C_6H_5)_2$ belongs to the type 2 photoreactions. As an example, $UO_2(OOC(i)\text{-}C_3H_7)_2$ decarboxylated by the activation of a photon. This resulted in the production of CO_2, UO_2 and radical, $\cdot i\text{-}C_3H_7$. The radical $\cdot i\text{-}C_3H_7$ underwent radical coupling and disproportionation producing C_6H_{14}, C_3H_8 and C_3H_6. The radical $\cdot i\text{-}C_3H_7$ also reacted with the starting material $UO_2(OOC(i)\text{-}C_3H_7)_2$ to form a thermally unstable intermediate, $UOO(i\text{-}C_3H_7)(OOC(i)\text{-}C_3H_7)$. This unstable intermediate decomposed to give CO_2, UO_2 and radical coupling and disproportionation products. All these organic products had been evidenced by MS. The non-stable intermediate hypothesis is consistent with the FTIR spectra obtained from photolysis and radical initiation experiments.

We propose the following mechanism for the photo-decomposition of uranyl carboxylate complexes to uranium trioxide shown in Scheme 3-3. This mechanism can explain two types of reactions for uranyl carboxylate complexes.

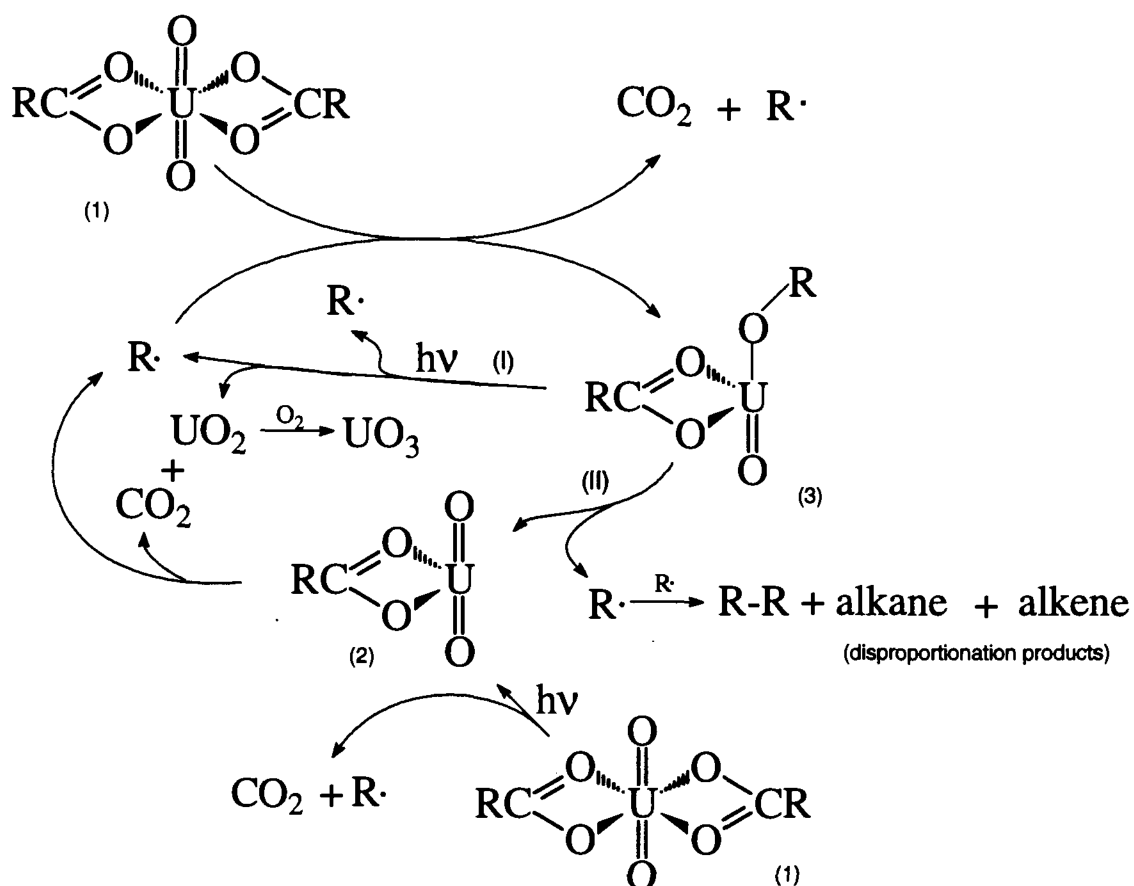

Scheme 3-3 Proposed mechanism of uranyl carboxylate photoreactions

The starting material $UO_2(OOCR)_2$ (1) upon absorption of a photon undergoes a LMCT to produce an unstable U(V) species $UO_2(OOCR)$ (2) and a radical ·OOCR. The unstable U(V) species (2) is then decomposes to form UO_2, CO_2 and alkyl radical R·. Radical ·OOCR decarboxylates forming CO_2 and the alkyl radical R·. The alkyl radical R· can further react with the starting material (1) to form an intermediate $(R)UO_2(OOCR)$ (3). The stability of this intermediate (3) depends on the alkyl radical R· . The intermediate (3) is stable in the cases of $UO_2(OOCCH_2OC_2H_5)_2$, $UO_2(OOCC_2H_4OC_2H_5)_2$ and $UO_2(OOCC_5H_{11})_2$. A second photon is required for these complexes to keep the reaction going (pathway I). In the cases of

$UO_2(OOCCH_3)_2$, $UO_2(OOC(i)\text{-}C_3H_7)_2$, and $UO_2(OOCCH_2C_6H_5)_2$, the intermediate is unstable due to the presence of the radicals $\cdot CH_3$, $\cdot i\text{-}C_3H_7$ and $\cdot CH_2C_6H_5$. In these cases, the reaction carries on by taking pathway (II). The UO_2 formed during the photoreactions is oxidized by oxygen in the atmosphere to give UO_3.

3.4 Conclusion

The photochemistry of two uranyl 1,3-diketonate complexes and seven uranyl carboxylate complexes has been studied in the solid state by means of FTIR, MS and Auger electron spectroscopy.

Uranyl diketonates undergo a single photon process in the photolysis to generate UO_3 and free ligands. An isomer of acacH was also produced upon photolysis of a $UO_2(OH_2)(acac)_2$ film. In addition to the free ligand t-butylacacH, other organic photofragments were also generated in the photolysis of thin films of $UO_2(OH_2)$(t-butylacac)$_2$.

A radical chain process in the photolysis of uranyl carboxylate complexes ($UO_2(OOCR)_2$) is demonstrated in the solid state for the first time. This has provided a practically efficient photochemical process for the deposition of uranium oxide film. As a precursor, $UO_2(OH_2)$(t-butylacac)$_2$ is more efficient than $UO_2(OH_2)(acac)_2$ for the deposition of uranium oxides. In the group of carboxylate complexes, $UO_2(OOCCH_2OC_2H_5)_2$ is the most efficient precursor complex.

3.5 Experimental Section

Photolysis experiments have been described in Chapter 2.

3.5.1 Quantum yield measurements and calculations

1. Quantum yield experiment

Quantum yield experiments of uranyl complexes were conducted both in the air and under vacuum. The procedures for those carried out under vacuum are very similar to that of the photolysis experiments described in Chapter 2, except monochromatic light was used instead of the broad band UV light. The wavelengths of 334 nm and 254 nm were chosen as the irradiating sources.

A typical quantum yield experiment performed in the air is described below. A Si chip with a $UO_2(OOCCH_2OC_2H_5)_2$ film was placed on a brass sample holder. An Oriel 254 nm monochromatic pencil-type low pressure Hg lamp equipped with a 6047 AC power supply was then placed 1.5 cm from the film. The FTIR spectrum of the starting film was first obtained. The film was then irradiated for 1 minute and the FTIR spectrum obtained again. The same procedure was followed and FTIR spectra were recorded for each subsequent irradiation period of 3, 7, 15, 31, 60, 120, 240,520 and 1480 minutes. The absorbances of the band at $\nu_{as}(COO)$ region of the FTIR spectra were recorded for the plot of At (t=0-1480 minutes, when t=0, the absorbance is Ao.) versus photolysis time. By fitting the plot with a single exponential decay function, a A'o is obtained. The difference of Ao and A'o is $A\infty$. At this point, $A\infty$ is considered to be the absorbance of the intermediate at $\nu_{as}(COO)$. $\ln[(Ao-A\infty)/(At-A\infty)]$ versus photolysis time is then plotted in order to get the slope for the quantum yield calculation.

2. Quantum yield calculation

The quantum yield of a photoreaction is defined as: the number of molecules undergoing process divided by the number of photons absorbed.

For the photoreaction:

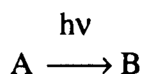

we have,

$$\Phi = -da/d(h\nu) \qquad 3\text{-}19$$

where, a is the number of molecules of the reactant A.

With a constant intensity irradiation source, the light absorbed by the reaction mixture, I_a, is given by Equation 3-20:

$$I_a = I(1-10^{-At}) \qquad 3\text{-}20$$

where, I is the incident light intensity;

At is the absorbance of the reaction mixture at time t.

The light absorbed by the starting material, A, $d(h\nu)/dt$ is then given by Equation 3-21:

$$d(h\nu)/dt = I(1-10^{-At})(A_A/(A_A+A_B))$$
$$= I(1-10^{-At})(A_A/At) \qquad 3\text{-}21$$

where, A_A is the absorbance of the reactant A at time t;

A_B is the absorbance of the product B at time t.

$(At = (A_A+A_B))$.

Since the starting material is a thin film with low overall absorbance, the approximation of $1-10^{-At} \approx 2.303At$ can be made. As a result of this assumption, Equation 3-21 simplifies as 3-22:

$$d(h\nu)/dt = 2.303IA_A$$

$$= 2.303Ia\varepsilon_A \qquad 3\text{-}22$$

where, ε_A is the extinction coefficient of A.

Solving 3-22 and 3-19 for $d(h\nu)$ and setting them equal gives Equation 3-23:

$$da/a = -(2.303I\Phi\varepsilon_A)dt \qquad 3\text{-}23$$

Integration of 3-23 leads to Equation 3-24.

$$\ln(a_t/a_o) = -(2.303I\Phi\varepsilon_A)t \qquad 3\text{-}24$$

where, a_o is the number of molecules of the starting material at photolysis time $t = 0$;

a_t is the number of molecules of the starting material at photolysis time t.

Representing the number of molecules of the starting material, a, in terms of absorbances leads to Equation 3-25.

$$\ln[(Ao-A\infty)/(At-A\infty)] = -(2.303I\Phi\varepsilon_A)t$$

$$= -\phi t \qquad 3\text{-}25$$

where, Ao is the IR absorbance at photolysis time $t = 0$;

$A\infty$ is the IR absorbance at photolysis time $t = \infty$;

$\phi = 2.303I\Phi\varepsilon_A$, which is the slope of $\ln[(Ao-A\infty)/(At-A\infty)]$ versus photolysis time.

Thus, the decomposition quantum yield of a starting material upon irradiation is given in Equation 3-26.

$$\Phi = -\phi/2.303I\varepsilon_A \qquad 3\text{-}26$$

The intensity of the light source Io (W/cm^2) was measured with an International Light IL 1350 Radiometer and converted to I (Einsteins per second) by the Equation 3-27.

$$I = Io\lambda/(Nhc) \qquad 3\text{-}27$$

where, Io is the intensity of the irradiation light, W/cm^2;

N is Avogadro's number, 6.022×10^{23} molecule/mole;

h is Planck's constant, 6.626×10^{-34} J·sec.;

c is the traveling speed of light, 3.0×10^{10} cm/sec.;

λ is the wavelength of the irradiation light, cm.

3.5.2 Mass spectrometric analyses of volatile products:

The system shown in Figure 3-9 was designed for collecting volatile products from a photolysis experiment. The bottom part of the system is a sample tube made of quartz in order to let the irradiating light pass through it.

A Si chip (1.0 x 2.5 cm) coated with a film of $UO_2(OOCC_5H_{11})_2$ was placed in the tube. The top and the bottom parts of the system were joined with a greased vacuum o-ring. The valve was closed after the system was evacuated to a vacuum of approximately 10^{-3} torr. The sample was then irradiated by 254 nm UV light for 10 hrs. The volatile products generated from the photolysis of $UO_2(OOCC_5H_{11})_2$ remained in the system ready for the MS analysis.

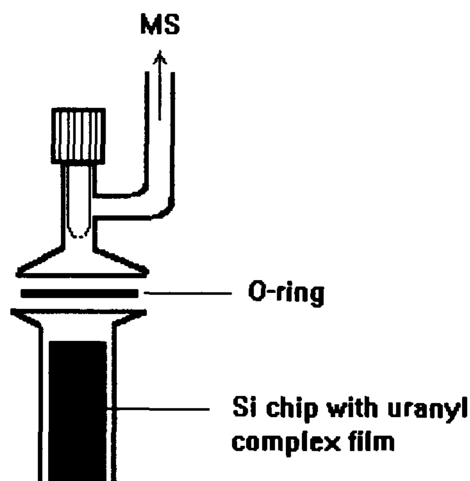

Figure 3-9 A designed system for MS sample collection

The MS sample preparation for all of the other uranyl complexes was done in the same way. The irradiation time varied for different complexes depending on the efficiency of the photoreactions.

The mass spectra were recorded with a HP 5958 GC/MS spectrometer. An electron-impact ion source was used and the ion source temperature was 200°C. The resolution was 1000 amu.$^{-1}$. Electron energy for ionization was 70 ev. About 200 MS spectra were recorded for rebuilding a total ion current (TIC) spectrum. The scanning mass range was 20-300 amu.

3.5.3 Radical initiation experiments

A radical initiation experiment for $UO_2(OOCC_5H_{11})_2$ was conducted as described below. An acetone solution of $UO_2(OOCC_5H_{11})_2$ and a radical initiator, azo-isobutyro nitrile (AIBN) (about 1:1) was prepared. A film composed of $UO_2(OOCC_5H_{11})_2$ and AIBN on a silicon chip was obtained by spin-coating the above solution. An FTIR spectrum of this film was obtained. The film was then transferred into a dark place for 30 minutes and the FTIR spectrum was obtained again. This step was

repeated to get the FTIR spectra for reaction times of 1 hrs., 3 hrs. and 24 hrs. A plot of overlaid FTIR spectrua was then obtained and is shown in Figure 3-8.

Similar radical initiation experiments were conducted for all of the other uranyl complexes. The results were summarized in Table 3-2.

Chapter 4 Optical and Electron Beam Lithography of Uranium Oxide Patterns on Silicon Substrates

4.1 Introduction

Lithography is the process of printing from a smooth surface (e.g. a metal plate) treated so that ink adheres only to the design to be printed.[100] Initially, it was a term used primarily in the printing industry. Lithographic techniques were introduced into microelectronics fabrication in the 1950's.

Lithographic techniques had been used over 100 years ago, in the graphic arts industry, as a process for making printing plates.[101] The monolithic integrated circuit designed by Jack Kilby and Robert Noyce in 1960[102] was a remarkable invention in the microelectronics industry. Since then, the microelectronics industry has made rapid progress. The resolution of lithography is getting better, hence smaller devices (high density circuits) can be made, therefore greatly increasing the number of devices on a single chip. Table 4-1 shows the progress in lithography for the production of dynamic random access memory (DRAM) in the past two decades.[102, 103]

Table 4-1 Progress in lithography and a rough relationship between minimum feature size and capacity of DRAM

Year	Minimum feature size[a] (μm)	Capacity of DRAM device (bit)
1975	6	4-K
1980	4	16-K
1982	2.5	64-K
1985	1.5	256-K
1990	0.6	4-M
1992	0.5	16-M
1995	0.35	64-M

a) Minimum feature size on a metal oxide semiconductor DRAM device.

There are four basic kinds of lithographic techniques, photo, X-ray, e-beam and ion-beam lithography. Photolithography was the first technique developed and is the most widely used. One current photolithography process includes coating, irradiating, developing, etching and stripping steps. The process is illustrated in Figure 4-1.

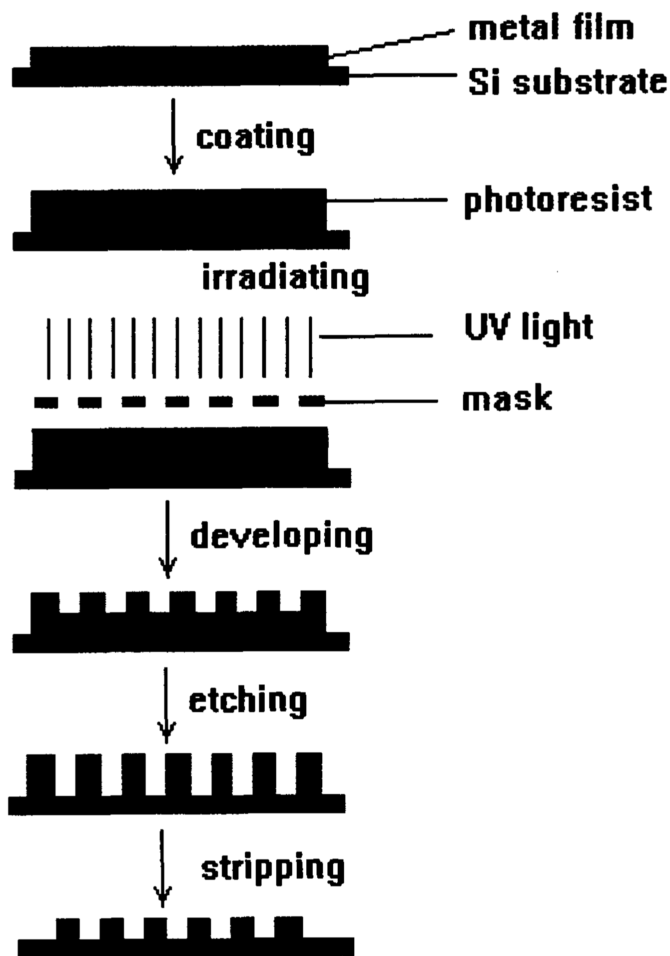

Figure 4-1. Major steps in a photolithography process

In this process, a film of metal is deposited on a substrate. A layer of photoresist is then deposited to cover the film. The film is then covered with a mask and irradiated. The exposed (or unexposed, depending on the character of the photoresist) portion of the photoresist is rinsed off with a solvent. The metal or metal oxide film is now only partially covered with photoresist. The parts of the film without protection by the photoresist are removed in the etching step. The remaining photoresist is stripped off to generate the final metal or metal oxide patterns.

A photoresist-free lithographic method for patterning materials has been developed in our laboratory[38, 39, 104] simplifying the overall lithographic procedure. In our technique, an amorphous precursor film is first deposited by spin-coating from an organic solvent. The film is then irradiated through a mask. The radiation converts the exposed material to an insoluble product. The unexposed portion of the film is rinsed off with a suitable solvent resulting in the patterns of the desired material. The technique is outlined in Figure 4-2.

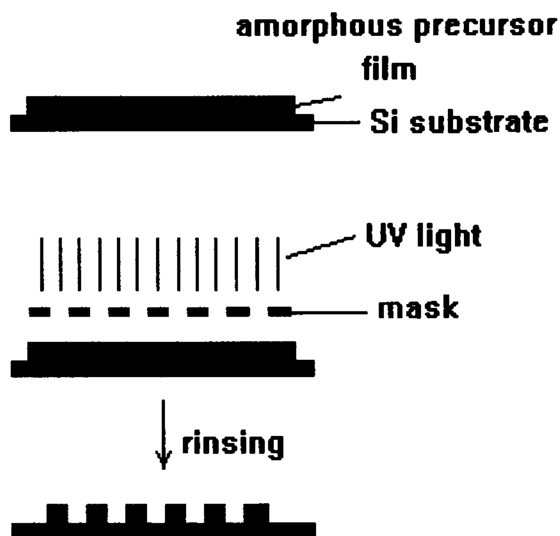

Figure 4-2 The lithographic technique used in our laboratory

The resolution of photolithography is limited by the wavelength of radiation due to diffraction.[105] In practice, one can only produce features of dimensions about 1.3 times[106] the exposure wavelength by photolithography. Shorter wavelength radiation could be used to improve resolution.

Electron-beams have much shorter wavelengths than the deep UV. Therefore, it has a higher resolution capability. The major advantages of electron-beam lithography are 1) the ability to register accurately over small areas of a wafer; 2) low defect levels; and 3) direct generation of patterns from circuit design data without masks.[107] Electron-beam lithography has been used to generate patterns for X-ray lithography masks.[108]

X-ray lithography, which has an exposure configuration similar to photolithography, offers a shorter wavelength than UV or Vis light. The wavelengths of X-rays range from 0.4 nm to 15 nm. The diffraction limit for X-rays is below that for deep UV light. Compared to photolithography, X-ray lithography has the advantage of lower defect levels[43] due to the X-ray's relative insensitivity to organic contamination. X-rays have been used to fabricate features as small as 0.02 μm.[109]

A potential application for uranium and uranium oxide is to be used as X-ray lithography mask materials. In order to accomplish this application, we need, first of all, to show the possibility of patterning uranium oxide. Our approach was to expose the uranyl complex thin films through a mask with UV light to photochemically produce uranium oxide, followed by rinsing off the unexposed areas.

The reason for the development of X-ray lithography was to reduce the high diffraction resulting from UV light in order to improve the resolution. For the purpose of making an X-ray lithography mask, we not only need to be able to pattern uranium oxide, we also need to obtain high resolution patterns. The approach we took was to use a focused electron-beam for the exposure of the uranyl complex precursor films.

In this chapter, the investigation of photopatterning uranium oxide lines through uranyl complex thin film precursors is presented. High resolution uranium oxide patterns by electron-beam direct writing of uranyl complex thin films are also discussed.

4.2 Results

4.2.1 Photolithography with uranyl 1,3-diketonate complexes

The photolysis of a $UO_2(OH_2)(acac)_2$ thin film on a Si(111) surface through a contact lithography mask resulted in the deposition of uranium trioxide patterns. This was done under a 1 torr vacuum. The irradiation source was a 75 W high pressure Xe lamp with a light intensity of 12.30 mW/cm^2. The solvent used to rinse off the unexposed parts of the film was hexane. The resolution was found to be sensitive to the photolysis time. The best patterns with 3 μm resolution were obtained after 4 days while no patterns were observed after two days. Overexposure resulted by irradiating the sample for 5 days.

Photolithography was also conducted with $UO_2(OH_2)$(t-butylacac)$_2$. The irradiation source was a 254 nm output low pressure Hg lamp with a light intensity of 6.9×10^{-9} Einstein/second. The spin coated thin film of $UO_2(OH_2)$(t-butylacac)$_2$ was irradiated through a lithography mask in air. After irradiation, the film was washed with acetone to remove the unexposed portion of the film. This resulted in 0.8 μm uranium oxide lines remaining on the Si surface. The image of one of the patterns obtained with an optical microscope is shown in Figure 4-3. A 0.8 μm pattern is the smallest pattern on the mask. It is possible that with finer detailed masks; smaller patterns could be lithographed. Unfortunately, the resolution is not going to be better than 0.33 μm due to the optical diffraction limitation.[106]

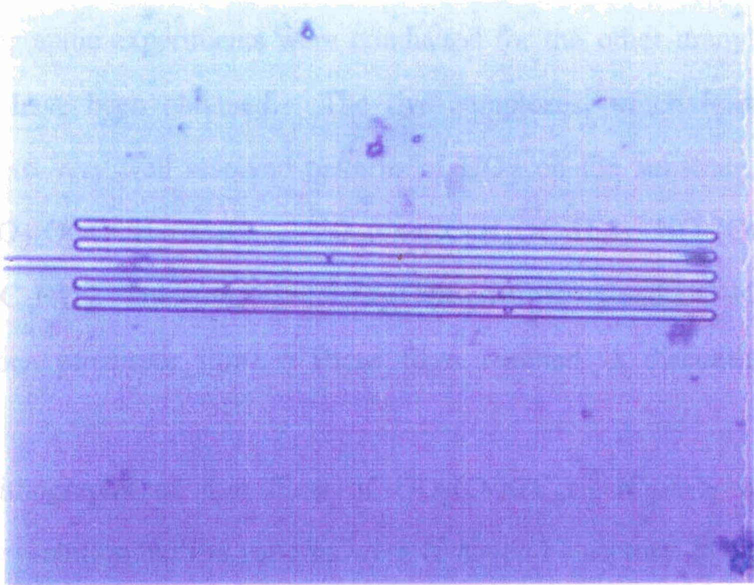

Figure 4-3 An uranium oxide pattern with 0.8 μm resolution on silicon surface resulting from the contact printing of a $UO_2(OH_2)$(t-butylacac)$_2$ film

4.2.2 Photolithography with uranyl carboxylate complexes

The photolithography using uranyl carboxylate complexes was done under low vacuum (1 torr). A thin film of $UO_2(OOCC_5H_{11})_2$ was irradiated through a standard lithography mask for 40 hours. Acetone was used to rinse off the unexposed portion of the film. This resulted in sub-1 μm uranium oxide lines remaining on the Si surface. A representative SEM image of one of the hundreds of patterns is shown in Figure 4-4.

Similar lithographic experiments were conducted for the other uranyl complexes and similar results have been obtained. The five complexes, which formed smooth precursor films led to very well resolved patterns of UO_3 on the substrate. The five complexes were $UO_2(OOCCH_2OC_2H_5)_2$, $UO_2(OOCC_2H_4OC_2H_5)_2$, $UO_2(OOCC_5H_{11})_2$ and $UO_2(OOCCH_2C_6H_5)_2$. The complexes, $UO_2(OOC(i)\text{-}C_3H_7)_2$ and $UO_2(OOCCH_3)_2$, formed discontinuous precursor films. These films resulted in discontinuous UO_3 patterns.

The photolithography of thin films of $UO_2(OOCC_6H_4OC_2H_5)_2$ also formed patterns with good resolution but the patterns were removed by acetone in the procedure of rinsing the film. As mentioned in chapter 3, the photoreaction of this complex led to the formation of a compound containing an organic group. Therefore, the patterns of this molecular compound dissolved in acetone.

Figure 4-4 SEM image of an uranium oxide pattern from the photolithography of $UO_2(OOCC_5H_{11})_2$

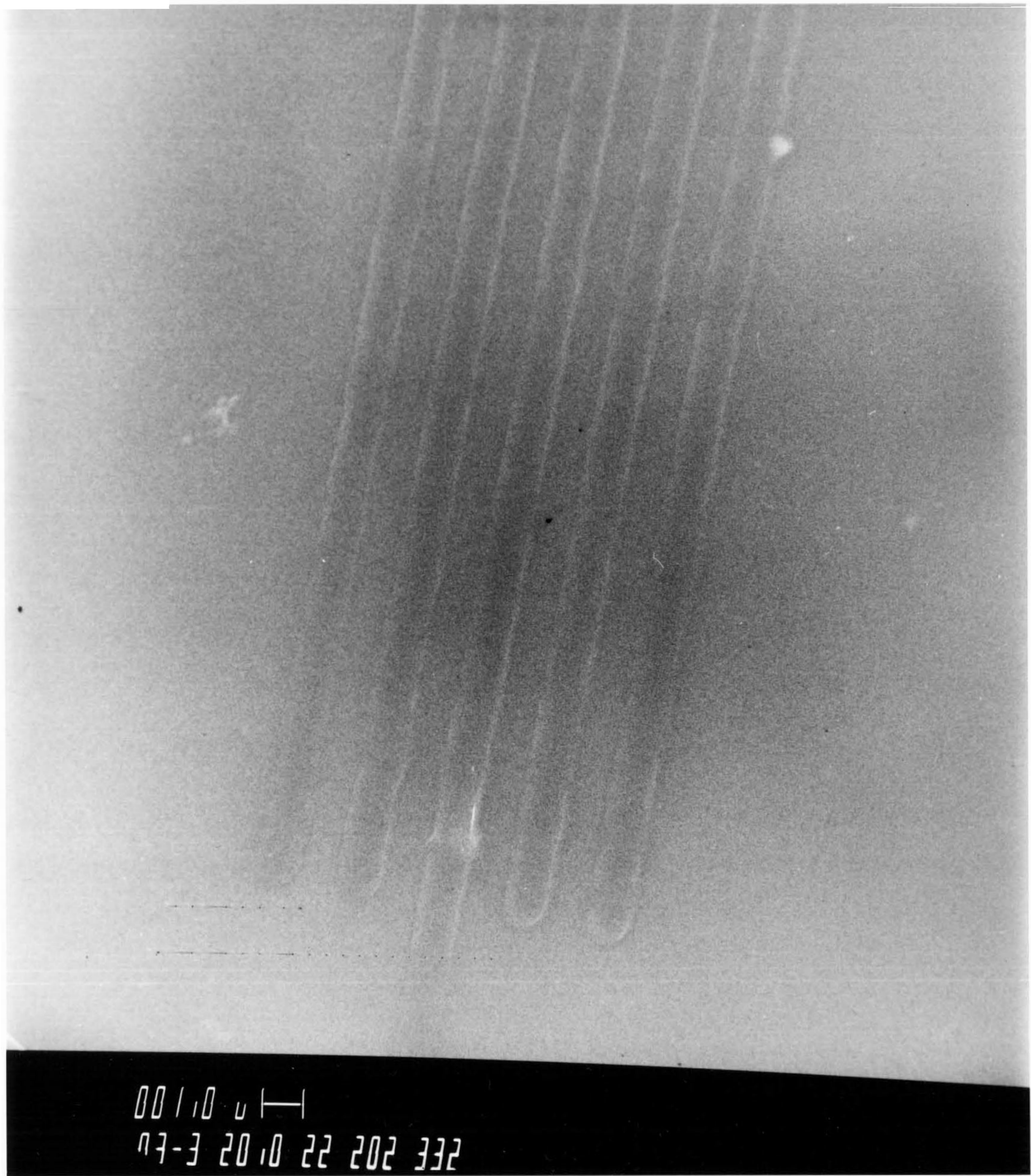

Figure 4-4

4.2.3 Comparison of the photolysis time needed for different uranyl complexes to form stable patterns by means of PDSF

A photolithographic experiment was done for all of the uranyl complexes (except $UO_2(OOCC_6H_4OC_2H_5)_2$) in order to determine the relative dose required for the formation of patterns. The irradiation source used for this experiment was a 254 nm output low pressure Hg lamp with a light intensity of 6.9 x 10^{-9} Einsteins/second. The experiment was done in the following way. Eight films of eight uranyl complexes were prepared by spin-coating. Half of each of these thin films was covered with aluminum foil. The other half of the films were irradiated in the air for 0.5 hr. The films were rinsed with acetone after irradiation. The same procedure was repeated with the photolysis times of 1 hour, 3 and 24 hours. Table 4-2 lists the results.

Table 4-2 A comparison of stability of photolithographic patterns[a]

	deposition observed			
photolysis time (hour)	**0.5**	**1**	**3**	**24**
complexes				
$UO_2(OOCCH_2OC_2H_5)_2$	yes	yes	yes	yes
$UO_2(OOCC_2H_4OC_2H_5)_2$	yes	yes	yes	yes
$UO_2(OOCCH_3)_2$	partially stayed	partially stayed	yes	yes
$UO_2(OOC(i)\text{-}C_3H_7)_2$	yes	yes	yes	yes
$UO_2(OOCC_5H_{11})_2$	yes	yes	yes	yes
$UO_2(OOCCH_2C_6H_5)_2$	yes	yes	yes	yes
$UO_2(OH_2)(acac)_2$	no	no	partially stayed	yes
$UO_2(OH_2)(t\text{-}butylacac)_2$	no	no	yes	yes

a. Whether the patterns stayed on the substrate after films rinsed with solvents.

The result showed that most uranyl complexes were efficient precursors, able to generate uranium oxide patterns, which stayed on the silicon surface. The complexes with lower quantum yields ($UO_2(OOCCH_3)_2$, $UO_2(OH_2)(acac)_2$, $UO_2(OH_2)$(t-butylacac)$_2$) required longer photolysis times to generate stable patterns. Not enough exposure resulted in incomplete photoreactions. Therefore the resultant patterns were rinsed off due to the presence of starting materials.

4.2.4 Electron beam lithography with uranyl complexes

The photolithographic results presented above indicated that the film quality is an important factor for the generation of high resolution patterns. Four complexes were chosen for the study of electron beam direct writing. They were $UO_2(OOCCH_2OC_2H_5)_2$, $UO_2(OOCC_2H_4OC_2H_5)_2$, $UO_2(OOCC_5H_{11})_2$ and $UO_2(OH_2)$(t-butylacac)$_2$. All of these complexes formed smooth amorphous films.

20 kv electron beam was used to write lines on the above selected uranyl complex films. The writing time by electron beams was examined to see what was a suitable time for producing resolvable images. Exposure times of 0.5, 1, 2, 3, 4, 8 and 40 minutes were all tried. A time of 0. 5 minute was not sufficient to produce an image a with good contrast. An exposure time longer than 4 minutes resulted in over exposed patterns. Considering the results of the four uranyl complexes studied here, the optimal exposure time did not depend on the complex. This insensitivity is probably due to the efficient electron induced reactions. An exposure time of 1 to 4 minutes could be used for all of these complexes in direct writing.

Patterns with a feature size of 0.2 μm have been produced. Figure 4-5 is the SEM image of the patterns produced from a film of $UO_2(OOCC_5H_{11})_2$. The sizes of the lines are 0.2 μm.

Figure 4-5 0.2 μm Electron-beam lithographic lines

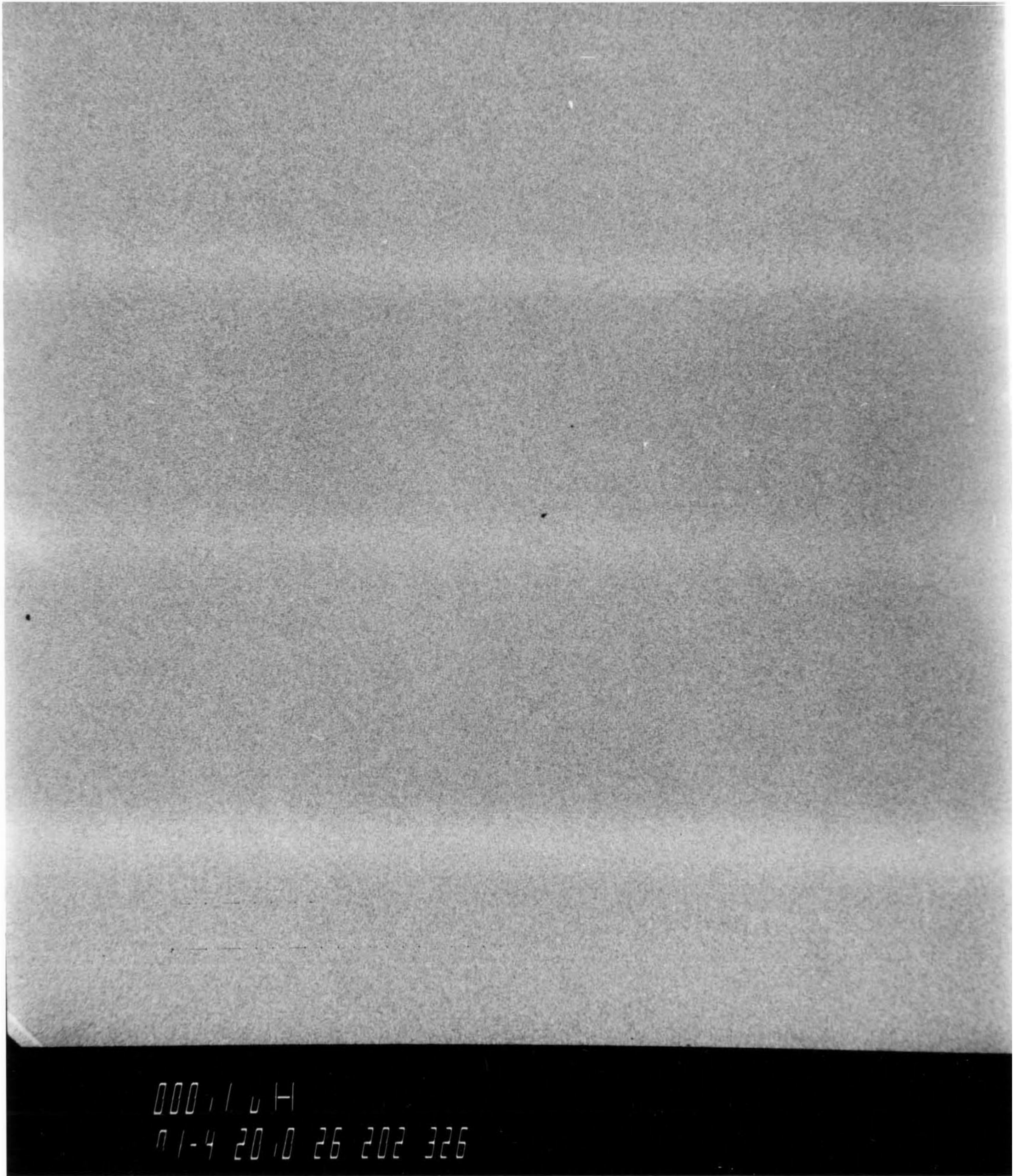

Figure 4-5

The electron-beam lithography experiments were conducted using an ETEC Autoscan SEM, which was not designed for e-beam lithography. We can not use this machine to write a long and thin line. The way to reduce the feature size by using this SEM is to increase the magnification. This is achieved by using a highly focused electron beam. Unfortunately, by increasing the magnification, the line is not only finer in width but it is also shorter in length. This results in a very small feature size that is very hard to relocate when the resolution is high. Therefore, we could not examine if the high resolution pattern stayed on the substrate after the film was rinsed. However, we were able to obtain a relatively low resolution (1 μm) electron-beam writing pattern, which stayed on the Si substrate after rinsing by a solvent. The 1 μm resolution electron-beam writing patterns were examined by an optical microscope.

4.3 Discussion

The quality of precursor films is an important factor in the lithography of uranyl complexes. An amorphous precursor film gives good resolution patterns efficiently. In contrast, a cloudy or discontinuous film results in discontinuous patterns with poor resolution. The complexes, $UO_2(OOCC_5H_{11})_2$ and $UO_2(OH_2)$(t-butylacac)$_2$, are the two complexes which produced the best photolithographic results based on the comparison of resolution and reproducibility. Both $UO_2(OOCC_5H_{11})_2$ and $UO_2(OH_2)$(t-butylacac)$_2$ form smooth, uniform, reproducible and thick films. These two complexes also offer reasonable efficiency for the photochemical deposition.

Photolithographic deposition of UO_3 lines on a silicon substrate has been demonstrated. The feature size obtained is limited by the photolithographic mask used. Higher resolution can be obtained although the resolution will reach a certain point due to the diffraction limit. The photolithography was done by a contact printing method. The gap between the mask and the film affects the printing resolution.[43] It was evident that poorer resolution was obtained by not contacting the mask to the film tightly. This is due

to Fresnel diffraction. The Fresnel diffraction is reduced by lowering the mask to film gap. Another factor affecting the resolution may be due to the environment. The lithographic experiments were not conducted in clean room conditions. Dust existed in the environment which could be responsible for making gaps between the mask and films. Therefore, the resolution of lithographic patterns is affected.

Considering the results obtained from both photolithography and e-beam lithography, the resolution was not limited by the chemistry we studied. Presumably the same chemistry ocurred in both lithographic processes. With better lithographic technique, the chemistry studied can be used to provide patterns with better resolution. Higher resolution patterns were obtained by the substitution of the UV light with electron beams.

The composition of the patterns from electron-beam lithography has not yet been confirmed because the patterns we generated were not big enough for Auger electron spectroscopic analysis. Due to the insolubility of the electron-beam generated patterns in an organic solvent, the composition of the patterns is probably purely inorganic. In the studied cases, the composition should be UO_2.

In electron-beam lithography, the electrons activate the reaction in the surface films. We have not obtained enough evidence to prove the mechanism of the reaction. A proposed mechanism for electron induced reaction of thin films of uranyl complexes is shown in Equation 4-1 and 4-2. The ionization of the starting material could be the first step for electron induced reactions. Further fragmentation of ionized starting material should occur.

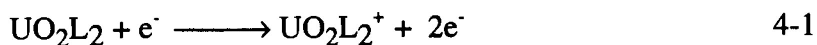

$$UO_2L_2 + e^- \longrightarrow UO_2L_2^+ + 2e^- \qquad 4\text{-}1$$

$$UO_2L_2^+ \longrightarrow UO_2 + \text{ organic fragments} \qquad 4\text{-}2$$

L = diketonate ligands and carboxylate ligands.

UO_2 is believed to be the final electron-beam lithographic product. The electron-beam lithography was conducted in a high vacuum SEM sample chamber (10^{-7} torr). Under these conditions, there was no oxygen for the oxidation of UO_2 to UO_3. Therefore, UO_2 is proposed as the final electron-beam lithography product.

4.4 Conclusion

An ambient temperature, efficient, photochemical method has been demonstrated for lithographic deposition of uranium oxide patterns from uranyl complex thin film precursors. Seven uranyl carboxylate complexes have been examined to compare the uranium oxide patterns formed from them. Sub-1 μm wide uranium oxide lines were generated from all seven carboxylate complexes. The resolution is the same as the mask used in the photolithographic experiments. The photolysis time needed to get stable uranium oxide patterns varies for different precursors. Except $UO_2(OOCC_6H_4OC_2H_5)_2$, six of the uranyl carboxylate complexes formed UO_3 patterns, which stayed on the substrates with good adhesion. The photoreaction of $UO_2(OOCC_6H_4OC_2H_5)_2$ did not result in uranium oxide.

Two 1,3-diketonate uranyl complexes were also studied for patterning uranium oxide lines by photochemical means. Photolithography using $UO_2(OH_2)$(t-butylacac)$_2$ was more successful than using $UO_2(OH_2)(acac)_2$. We can obtain stable sub-1 μm patterns from $UO_2(OH_2)$(t-butylacac)$_2$ easily.

Electron-beams were also used to write patterns on the uranyl complex thin films on Si substrates. The best resolution pattern achieved was 0.2 μm, and the precursor was $UO_2(OOCC_5H_{11})_2$.

4.5 Experimental Section

4.5.1 Photolithography

The photolithography mask was donated by IBM corporation.

The UV light used in these experiments was from a 75 W high pressure Xe lamp in an Oriel housing equipped with condenser lenses and filtered through a 10 cm water filter made of quartz.

A film of $UO_2(OOCC_5H_{11})_2$ was prepared on a 1.5x1.5 cm Si chip by the spin coating technique described in Chapter 2. The film was then transferred in to a vacuum chamber (1 torr) and clipped with a photolithography mask in contact. Irradiation of the film through the mask under low vacuum ocurred for 40 hours. After irradiation the mask was removed and the film was then rinsed with acetone. The unexposed portion of the film was rinsed off to leave uranium oxide patterns on the silicon chip. The patterns which remained on the silicon surface were examined by a Leitz optical microscope.

All of the lithography experiments were conducted using the same procedure except the experiment using $UO_2(OH_2)$(t-butylacac)$_2$. For this complex, a 254 nm output Hg arc lamp was used and the atmosphere was air.

The lithographic experiments for the comparison of photolysis time were conducted using the similar procedure as above. The irradiation source used for these experiments was a 254 nm output Hg arc lamp. Eight of the uranyl complex films were half covered with aluminum foil instead of covering with IBM masks (Figure 4-6).

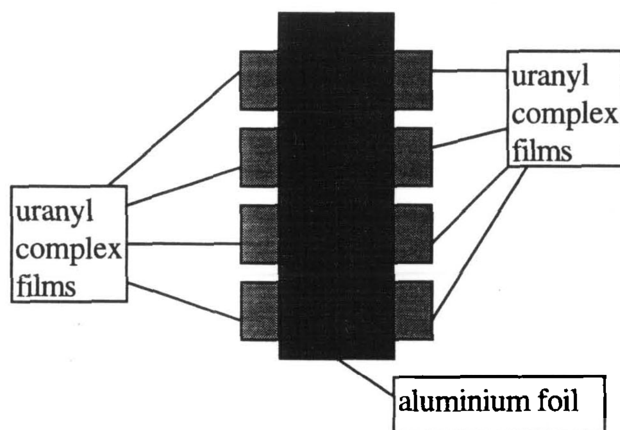

Figure 4-6

4.5.2 Electron beam lithography

An ETEC Corp. autoscan U1 SEM was used to provide the electron beam for lithography and also to image the lithographic patterns.

Electron beam lithography of $UO_2(OOCC_5H_{11})_2$ was conducted in the following way. A film of $UO_2(OOCC_5H_{11})_2$ was prepared on a 1.0x1.0 cm Si chip by spin-coating. The Si substrate used in the experiments had a resistivity in the range of 0-0.021Ω cm. The sample was then mounted on a SEM sample holder and transferred to the SEM vacuum chamber. The film was exposed with a focused 20 kv electron beam for 1 or 2 minutes. The sample was shifted and exposed again. This was repeated for several times. The patterns generated from exposure were then imaged by SEM.

Same procedure was used for the electron beam lithography of $UO_2(OOCCH_2OC_2H_5)_2$, $UO_2(OOCC_2H_4OC_2H_5)_2$, and $UO_2(OH_2)$(t-butylacac)$_2$.

References

1. R. W. Berry, P. M. Hall and M. T. Harris, "Thin Film Technology", D. Van Nostrand Company, Inc., New York, 1968, p2.
2. C. E. Morosanu, "Thin Films by Chemical Vapour Deposition", Elsevier, New York, 1990, Ch.1.
3. J. L. Vossen and W. Kern, "Thin Film Processes II", Academic Press, Inc., New York, 1991, Ch. III-1.
4. C. E. Morosanu, "Thin Films by Chemical Vapour Deposition", Elsevier, New York, 1990, Ch.2.
5. K. R. Lawless, *Phys Thin Films*, **4** (1967) 191.
6. F. A. Lowenheim, "Thin Film Processes", Academic Press, New York, 1978, Ch.3.
7. G. L. Schnable and P. F. Schmidt, *J. Electrochem. Soc.*, **123** (1976) 310.
8. C. J. Dell'oca, D. L. Pulfrey and L. Young, *Phys Thin Films*, **6** (1971) 1.
9. R. Glang, "Hand Book of Thin Film Technology", McGrawHill, New York, 1970 Ch.1
10 J. M. E. Harper, "Thin Film Processes", Academic Press, New York, 1978, Ch.2.
11. J. Amano and R. P. W. Lawson, *J. Vac. Sci. Technol.,* **14** (1977) 831, **15** (1978) 118.
12. E. H. C. Parker, "The Technology and Physics of MBE", Plenum, New York, 1985.
13. L. Maissel, "Hand Book of Thin Film Technology", McGrawHill, New York, 1970, p61.
14. J. E. Curran, *J. Vac. Sci. Technol.,***14** (1977) 108.
15. D. M. Mattox, *J. Vac. Sci. Technol.,***10** (1973) 47.
16. V. Hoffman, *Solid State Technol.,* **10**(12) (1973) 93.

17. J. J. Hsieh, "Materials, Properties and Preparation", Vol. 3, North-Holland, Amsterdam, 1980, p415.

18. R. Pretorius, Z. L. Liau, S. S. Lau, and M. A. Nicolet, *Appl. Phys. Lett.,* **19** (1976) 598.

19. J. A. Nemetz and R. E. Tressler, *Solid State Technol.,* **26**(1) (1983) 79; **26**(9) (1983) 209.

20. A. S. Grove, "Physics and Technology of Semiconductor Devices", Wiley, New York, 1967.

21. T. Sugano, *Thin Solid Films,* **72** (1980) 9.

22. R. V. Giridhar and K. Rose, *Appl. Phys. Lett.,* **45** (1984) 578.

23. T. E. Orlowski and H. Richter, *Appl. Phys. Lett.,* **45** (1984) 241.

24. T. Sugii, T. Ito, and H. Ishikawa, *Appl. Phys. Lett.*, **45** (1984) 966.

25. K. Sugiyama, K. Kinbara and H. Iton, *Thin Solid Films,* **112** (1984) 257.

26. B. Gorowitz, T. B. Gorczyca and R. J. Saia, *Solid State Technol.,* **28**(6) (1985) 197.

27. J. Y. Chen, R. C. Henderson, J. T. Hall and J. W. Peters, *J. Electrochem. Soc.,* **131** (1984) 2146.

28. A. Sawabe and T. Inuzuka, *Appl. Phys. Lett.,* **46** (1985) 146.

29. I. P. Herman, *Chem. Rev.*, **89** (1989) 1323.

30. R. B. Jackman and J. S. Foord, *Appl. Phys. Lett.,* **49** (1986) 196.

31. G. M. Shedd, H. Lezec, A. D. Dubner and J. Melngailis, *Appl. Phys. Lett.,* **49** (1986) 1584.

32. V. Balzani & V. Carassiti, "Photochemistry of Coordination Compounds", Academic Press, London and New York, 1970, Ch.2.

33. J. G. Calvert, J. N. Pitts, Jr., "Photochemistry", John Wiley & Sons Inc., New York, 1966, Ch.1.

34. A. W. Czanderna, "Methods of Surface Analysis", Elsevier Scientific Publishing Company, New York, 1975, Ch.5.

35. P. W. Palmberg, *Analytical Chem.,* **45**(6) (1973) 549A.

36. T. W. H. Ho, S. L. Blair, R. H. Hill and D. G. Bickley, *J.of Photochem. Photobiol. A:Chem.*, **69** (1992) 229.

37. A. A. Avey and R. H. Hill, "6th Canadian Materials Science Conference", Kingston, 1994.

38. B. J. Palmer, A. Becalska, T. W. H. Ho and R. H. Hill, *J. Mater.Sci.*, **28** (1993) 6013.

39. S. L. Blair, J.Hutchins, R. H. Hill and D. G. Bickley, *J. Mater.Sci.*, **29** (1994) 2143.

40. W. C. Chu and R. H. Hill, "The 1994 International Conference on Electronic Materials", Taiwan, 1994.

41. C. E. Morosanu, "Thin Films by Chemical Vapour Deposition", Elsevier, New York, 1990, Ch.15.

42. J. M. Doyle, "Thin-Film and Semiconductor Integrated Circuitry", McGraw-Hill Book Company, Toronto, 1966, Ch.2.

43. I. W. Boyd, R. B. Jackman, "Photochemical Processing of Electronic Materials", Academic Press Limited, Toronto, 1992, Ch.4.

44. D. M. Tennant, L. A. Fetter, L. R. Harriott, A. A. MacDowell, P.P. Mulgrew, W. K. Waskiewicz, D. L. Windt and O. R. Wood II, *J. Vac. Sci. Technol.*, **B10**(6) (1992) 3134.

45. R. C. Weast, D. R. Lide, M. J. Astle and W. H. Beyer, "CRC Handbook of Chemistry and Physics", 70th Ed., CRC Press, Boca Raton, Florida, 1989-1990, E-151.

46. R. A. Serway, "Physics for Scientists & Engineers", Saunders College Publishing, 2nd Ed., New York, 1986.

47. W. B. Chou, M. N. Azer, J. J. Mazumder, *J. Appl. Phys.*, **66** (1989) 191.

48. H. H. Gilgen, T. Cacouris, P. S. Shaw, R. R. Krchnavek and R. M. Osgood, *Appl. Phys.*, **B42** (1987) 55.

49. V. A. C. Hanappel, D. van der Vendel, H. D. van Corbach, T. Fransen and P. J. Gellings, *Thin Solid Films*, **256** (1995) 8.

50. J. Ma, F. Ji, H. Ma and S. Li, *J. Vac. Technol.*, **A13** (1995) 92.

51. P. R. Willmott, P. Felder, M. Lingenauer, J. R. Huber, *J. Vac. Technol.*, **A13** (1995) 248.

52. S. Kim, Y. Kang, and S. Baik, *Thin Solid Films*, **256** (1995) 240.

53. L. X. Cao, Z. C. Feng, Y. Liang, W. L. Hou, B. C. Zhang, Y. Q. Wang and L. Li, *Thin Solid Films*, **257** (1995) 7.

54. D. C. Sun, E. Y. Jiang, H. L. Ming and C. Lin, *J. Phys. D: Appl. Phys.*, **28** (1995) 4.

55. H. E. Fisher, D. J. Larkin and L. V. Interrante, *MRS Bull.*, **16** (1991) 59.

56. C. Miyake, Y. Yoneda, M. Matsumura, T. Iida and Ki Taniguchi, *J. of Nucl. Sci. and Tech.*, **21** (1990) 382.

57. E. H. P. Cordfunke, "The Chemistry of Uranium", Elsevier Scientific Publishing Company, 1969, p22.

58. F. A. Cotton and G. Wilkinson, "Advanced Inorganic Chemistry", Interscience Publishers, 2nd Ed., 1966, p1094.

59. D. R. Lide, "CRC Handbook of Chemistry and Physics", 75th Ed., CRC Press, Boca Raton, Florida, 1994-1995, p10-282.

60. L. Goetting, B. J. Palmer, M. Gao, R. H. Hill, *J. Mater.Sci.*, **29** (1994) 6147.

61. A. W. Adamson and P. D. Fleischaner, "Concepts of Inorganic Photochemistry", Robert E. Krieger Publishing Company, Malabar, Florida, 1984, p258.

62. A. E. Comyns, B. M. Gatehouse and E. Wait, *J. Chem. Soc.*, (1958) 4655.

63. Y. Yokoyama, A. Inaba, H. Hara, T. Yamazaki, H. Tamura and Y. Kushi, *Chem. Lett.*, (1990) 671.

64. A. A. Belyaeva, V. N. Bukhmarina, R. B. Dushin, G. V. Sidorenko, D. N. Suglobov, *Radiokhimiya*, **24** (1982) 57.

65. A. Kiss, and J. Csaszar, *Acta. Chim. Acad. Sci. Hung.*, **13** (1957) 49.

66. H. F. Holtzclaw, Jr. and J. P. Collman, *J. Amer. Chem. Soc.*, **79** (1957) 3318.

67. R. West and R. Riley, *J. Inorg. Nucl. Chem.*, **5** (1958) 295.

68. D. A. Skoog, D. M. West, F. J. Holler, "Fundaments of Analytical Chemistry", 4th Ed., Saunders College Publishing, Toronto, 1982, p466.

69. B. Marciniak and G. E. Buono-Core, *J.of Photochem. Photobiol. A:Chem.*, **52** (1990) 1.

70. L. Sacconi and G. Giannoni, *J. Chem. Soc.*, (1954) 2751.

71. C. N. R. Rao, "Ultra-Violet and Visible Spectroscopy", Plenum Press, New York, 1967, p17.

72. G. B. Deacon and R. J. Phillips, *Coord. Chem. Rev.*, **33** (1980) 227.

73. H. D. Burrows and T. J. Kemp, *Chem. Soc. Rev.*, **3** (1974) 139.

74. S. S. Sandhu, R. J. Singh and S. K. Chawla, *J.of Photochem. Photobiol. A:Chem.*, **52** (1990) 65.

75. L. Doub and J. M. Vandenbelt, *J. Amer. Chem. Soc.*, **69** (1947) 2714, **71** (1949) 2414.

76. J. H. Lai, *Polymer Engineering and Science,* **15** (1979) 1117.

77. W. W. Flack, D. S. Soong, A. T. Bell and D. W. Hess, *J. Appl. Phys.*, **56**(4) (1984) 15.

78. H. R. Hoekstra, & S. Siegel, *J. Inorg. Nucl. Chem.*, **18** (1961) 154.

79. L. I. Maissel and R. Glang,"Handbook of Thin Film Technology", McGraw-Hill Book Company, Toronto, 1970, p12-6.

80. J. A. Hearne and A. G. White, *J. Chem. Soc.*, (1957) 2168.

81. Uses 19 Å^3 times the number of non-hydrogen atoms in the molecule.

82. L. I. Maissel and R. Glang, "Handbook of Thin Film Technology", McGraw-Hill Book Company, Toronto, 1970, p11-10.

83. B. J. Palmer, PhD thesis, Simon Fraser Univ., 1992, Ch.1.

84. A. W. Adamson and P. D. Fleischaner, "Concepts of Inorganic Photochemistry", Robert E. Krieger Publishing Company, Malabar, Florida, 1984, Ch.9.

85. E. Etledgni, K. T. Park, T. Cao and M. W. Ruckman, *J. Appl. Phys.*, **74**(4) (1993) 1781.

86. R. Fix, R. G. Gordon and D. M. Hoffman, *Chem. Mater.*, **5** (1993) 614.

87. P. O'Brien, J. R. Walsh, A. C. Jones, S. A. Rushworth and C. Meaton, *J Mater. Chem.,* **3** (1993) 739.

88. R. Laiho and A. Pavlov, *Thin Solid Films,* **255** (1995) 9.

89. S. R. Heller and G. W. A. Milne, "EPA/NIH Mass Spectral Data Base", U. S. Government Printing Office, 1978, p5492.

90. R. M. Silverstein, G. C. Bassler, T. C. Morrill, "Spectrometric Indentification of Organic Compounds", 4th Ed., John Wiley & Sons, Inc., Toronto, 1981.

91. T. W. Graham Solomons, "Organic Chemistry", 4th Ed., John Wiley & Sons, Inc. Toronto, 1978, p345.

92. F. W. McLafferty, "Interpretation of Mass Spectra", 2nd Ed, W. A. Benjamin, New York, 1973.

93. J. K. Kochi, "Free Radicals", Vol. 1, John Wiley & Sons, Inc., Toronto, 1973, p100.

94. W. Horspool and D. Armesto, "Organic Photochemistry", Ellis Horwood, Toronto, 1992, p195.

95. T. H. Lowry, "Mechanism and Theory in Organic Chemistry", 2nd Ed., Harper & Row Publishers, New York, 1981, p7.

96. J. K. Kochi, "Free Radicals", Vol. 1, John Wiley & Sons, Inc., Toronto, 1973, p413.

97. T. H. Lowry, "Mechanism and Theory in Organic Chemistry", 2nd Ed., Harper & Row Publishers, New York, 1981, p696.

98. J. G. Calvert, J. N. Pitts, Jr., "Photochemistry", John Wiley & Sons Inc., New York, 1966, p20.

99. E. Rabinowitch and R. L. Belford, "Spectroscopy and Photochemistry of Uranyl Compounds", The MacMillan Company, New York, 1964, Ch.4.

100. A. S. Hornby, "Oxford Advanced Learner's Dictionary", 4th Ed., Oxford University Press, 1989, p728

101. W. M. Morean, " Semiconductor Lithography", Plenum Press, New York, 1988, P1.

102. L. F. Thompson, C. G. Willson and M. J. Bowden, "Introduction to Microlithography", ACS, Washington, DC, 1994, Ch.1.

103. P. Singer, *Semiconductor International*, **18**(1) (1995) 46.

104. T. W. H. Ho, S. L. Blair, R. H. Hill and D. G. Bickley, *J.of Photochem. Photobiol. A:Chem.*, **69**,229(1992).

105. L. F. Thompson, C. G. Willson and M. J. Bowden, "Introduction to Microlithography", ACS, Washington, DC, 1994, p59.

106. L. F. Thompson, C. G. Willson and M. J. Bowden,"Introduction to Microlithography", ACS, Washington, DC, 1994, p10.

107. L. F. Thompson, C. G. Willson and M. J. Bowden, "Introduction to Microlithography", ACS, Washington, DC, 1994, Ch.1.

108. W. Chu, H. I. Smith, S. A. Rishton, D. P. Kern and M. L. Schattenburg, *J. Vac. Sci. Technol.*, **B10**(1) 1992) 118.

109. C. N. Archie, J. I. Garanlund, R. W. Hill and A. D. Wilson, *J. Vac. Sci., Technol.*, **B10**(6) (1992) 3224.